THE DESIGN AND PRACTICAL IMPLEMENTATION OF A SIX-PHASE INDUCTION MOTOR

THESIS

SUBMITTED IN PARTIAL FULFILMENT OF THE REQUIREMENTS FOR THE AWARD OF THE DEGREE OF

MASTER OF ENGINEERING
IN
POWER AND MACHINES ENGINEERING

BY

Samuel E. Iduh [a], Silas E. Omugbe [b]
(*PG/ENG9200692*)   (*PG/ENG1410538*)

Under the Supervision of

Engr. Prof. E. U. Ubeku
Professor of Electrical Power Systems

DEPARTMENT OF ELECTRICAL/ELECTRONIC ENGINEERING
FACULTY OF ENGINEERING
UNIVERSITY OF BENIN, BENIN CITY, NIGERIA

JUNE 2017

[a] e-mail: iduhsamuel@gmail.com [b] e-mail: dexterevi@gmail.com

CERTIFICATION

This is to certify that the Master of Engineering thesis titled "The Design and Practical Implementation of a Six-Phase Induction Motor" submitted by Samuel Iduh with Matriculation number: PG/ENG9200692 and Omugbe Silas with Matriculation number: PG/ENG1410538 in the fulfilment of the requirements of the degree of "Master of Engineering" in Electrical Engineering is a bonafide record of investigations carried out by them in the Department of Electrical/Electronic Engineering, Faculty of Engineering, University of Benin, Benin City under my guidance and supervision. In my opinion, this has attained the standard fulfilling the requirements of the M.Eng. degree as prescribed in the regulation of the University.

Engr. Prof. E. U. Ubeku
Supervisor

Engr. Prof. S. O. Igbinovia
Head of Department

ACKNOWLEGEMENT

ABSTRACT

This thesis presents a re-designed conventional three phase 5-hp squirrel cage, 4-pole, 48 slots induction motor to a six-phase induction motor (SPIM). It also presents the in-depth of a single layer winding of a three-phase motor that was re-design to the six-phase split winding layout which was practically explained to the understanding of both the engineers and the technicians who normally find it difficult with windings of electrical machines.

The optimized re-designed SPIM is presented in the MATLAB/Simulink environment to perform a comparative assessment of the different phase loss scenarios of the six-phase configuration with respect to the six-phase healthy case and its conventional three-phase induction motor.

The result shows a comparative benefit of the six-phase induction motor over the three-phase induction motor; in such that in the near future because of its effective way to provide a higher reliability and sustainability under the loss of phase/phases condition it will be practically applied in the power driven devices/machines like in the area of Electric Vehicles, etc.

CONTENTS

SYMBOLS AND NOTATIONS

A	Area
AC	Alternating current
B	Magnetic flux
D, d	Diameter
DE	Differential evolution
D_r	Dimensions of the rotor
EAs	Evolutionary algorithms
EMF	Electromotive force
F	Force
GA	Genetic algorithm
mmf	Magneto motive force
RMF	Rotating magnetic field
SPIM	Six-phase induction motor
THD	Total Harmonic Distortion

Symbols

$α$	Per slot angle
$ω$	speed
D	Diameter
L	Inductance
R	Resistance,
f	Frequency
$η$	Efficiency
$ρ$	Resistivity
$τ$	Full span or pole pitch
$\emptyset_{sr}$	Flux per pole
$\emptyset$	Flux
B_{sr}	Maximum flux density per pole
$°e$	Electrical degrees
$d{-}q$	Direct-quadrature
$d{-}q{-}0$	Direct-quadrature-zero transformation
$F_{s\,max}$	Maximum stator Magneto motive force
g	Height of the air gap
hp	Horse power
I	Rated current
I_{ph}	Current per phase
J	Current density
K_d	Distribution factor
K_p	Pitch factor
K_w	Winding factor

l	Length of the wire
m	Number of phase
N_{ph}	Number of turns per phase
n_s	Synchronous speed
N_s	Number of slot
P	Number of pair of poles
p	Number of poles
P_f	Power factor
P_{in}	Input power
P_{out}	Output power
q	Number of slots per pole per phase
S	slot
V	Voltage
v	Velocity of the wire
V_{ph}	Induced voltage per phase
W_m	Weight of material

LIST OF FIGURES

LIST OF TABLES

CHAPTER ONE
INTRODUCTION

1.1. Background to the Study

Induction motors are rotating machines; also referred to as transducers capable of converting electrical energy to kinetic energy. They are widely found not limited only to the industries but the transportation system and other modern life application because of simple reasons ranging from low cost effectiveness, high reliability, robustness, higher torque and low maintenance when compared to other rotating machines. So, over the years back the conventional three-phase induction motors have been seen as a standard for electrical alternating current drives for the industries even though they have inherent setback with respect to performance as regards the loss of phase conditions (Mandal, 2015). Under this loss of phase condition the three-phase induction motor does not offer the adequate operation such as output power and torque as required in electric traction and other applications. Also, they can be utilized in hazardous environments such as mining, pumping and blowing operations (Kadaba, 2008). And there is need to move a little forward away from the normal single-phase or three-phase induction motor; this forms the context of this research/study.

And this aspect in induction motor has been investigated over the last two/three decades where the number of stator phases is more than three (Nanoty & Chudasama, 2012). An induction motor with two set of three-phase windings in a stator (single frame) of an induction motor to form a single six-phase machine is said to a six-phase induction motor (SPIM) (Tir et al., 2016). This poly-phase system having a dual 3-phase induction motor have two stator windings sets spatially shifted by 30˚ electrical (e) with separated neutrals as for a star configuration. Therefore, this is one of the means to over-come the inherent setbacks as highlighted as regards the loss of phase conditions in induction motors (Kadaba, 2008). They can function with an asymmetrical winding structure when there is loss of the machine phase(s) thus making them fault tolerant (Jimoh et al., 2014). These multi-phases have numerous advantages over the usual three-phase system as it reduces the amplitude and increases the frequency of torque pulsation, reduce stator harmonic currents, reduce the current per phase without enhancing the voltage per phase, lower the direct current link harmonics, increases power and reliability (Tir et al., 2016). These machines are utilized in high-current /high-power usage such as in electric ship propulsion, locomotive traction, aero plane application and electric/ hybrid electric vehicles (Nanoty & Chudasama, 2012).

This research focuses on the design and the practical implementation of a SPIM. The goal is to develop an exceptional design for the induction motor that can operate in a six-phase mode. The SPIM will be able to prove a reliable operation in the case of loss of phase(s).

1.2. Problem Statement

The current per phase in a six-phase induction motor with two set of three-phase windings (sheltered in the same stator) is reduced. In addition, the three-phase windings are phase displaced by 30˚e. However, each of the three-phase stator windings of the motor (SPIM) considered in this study is excited by a three-phase inverter, thereby, the total power rating of the motor is theoretically doubled (Darkoju, 2016). In addition, since each set of winding is being excited by a three-phase source, the system reliability is improved. With these developments, the SPIM have shown they have several gains over the traditional three-phase induction motors. As SPIM are finding their applications in the areas that require high reliability as well as high power

density and efficiency, some of which are for electric ship propulsion, locomotives traction, electric aircraft and aerospace application, in recent surveys and researches the emphasis has been shifted to vector (field-oriented) and direct torque control of induction motors (Nanoty & Chudasama, 2012).

As in early time, induction motors have two-phase, but the three-phase system later replaced it and it eliminates the third harmonic problem posed by the two-phase motor and this motor (three-phase machine) have since being widely accepted and used in homes and industries (Mandal, 2015). Recent survey/observations carried out suggest increasing interest in the six-phase induction motor. After much literature review it is observed that more research efforts have not been applied in this new area in terms of the design and practical implementation of a SPIM (Mandal, 2015).

For the six-phase induction motors, the generation of the 5th and 7th current harmonics is one of the setbacks in this poly-phase induction motor (Nanoty & Chudasama, 2012). This makes the motor size to be increased and the cost also, as to take care of additional losses but still have advantages which may worth it in some areas of application.

1.3.   Aim and Objectives

This project is aim at carrying out the design and practical implementation of a SPIM.

The objectives of this project are set out as follows;

(a) To design a practical SPIM using an existing three-phase induction motor frame-project/work.

(b) To model mathematically a SPIM in MATLAB environment.

(c) To carry out simulation of the SPIM in MATLAB.

(d) To test the designed/developed SPIM motor using three-phase supply and two set of three-phase supply system if possible.

(e) To examine the effect of different phase loss conditions on the performance of SPIM.

1.4.   Methodology

This study focuses on the design and the practical implementation of a SPIM. To achieve the set objectives for this study the following was worked out;

(a) The six-phase induction motor was developed and redesigned from an existing three-phase induction motor frame project/work. The stator windings was a star configuration

(b) The mathematical model and direct quadrature-zero transformation ($d–q–0$) model for the SPIM was developed; and the simulation of the developed mathematical model was carried out.

(c) The designed package for six-phase induction motor underwent optimization process using the genetic algorithm. And this procedure was based on the weight factor equations.

(d) The testing of the SPIM was carried out first with a three-phase power supply and then with the same three-phase power on the two set of three-phase windings.

(e) Examine the effects of various phase loss conditions on the operating conditions of the SPIM.

1.5.   Scope of the Research

This study was limited to the re-configuration of the existing three-phase induction motor into six-phase induction motor, design of the re-configured SPIM, testing of the designed SPIM, simulation of the SPIM in a MATLAB/Simulink and the analysis/verification of experimental results with regards to the practical implementation of the designed SPIM in contrast to the typical three-phase induction motor.

1.6.   Expected Results and Delivery

By the end of the project, a SPIM was designed and implemented practically from an existing three-phase scheme. The method entails reconfiguring the existing 3-phase into a 6-phase induction machine winding design with the same structure of the stator core lamination. Its delivery period was more four (4) months since it would involve research and practical implementation of the SPIM. Also, a model describing in details the simulation of a SPIM in a MATLAB/Simulink environment was presented. A paper shall be published in peer reviewed journal.

1.7.   Study Organization

The study includes an introductory chapter with the next chapter focusing on literature review.

Chapter 3 elaborates the design procedures of a normal three-phase induction motor; dwelling on the design layout of the existing three-phase of the 5 hp, 4-pole, 48 slots induction motor and also discussing the SPIM in detail. The re-configuration procedure of the existing three-phase into six-phase induction motor are explained in details; starting from the basic three-phase induction motor design to the complete design of the re-configured SPIM. Also, the fundamentals of simulation in MATLAB carried out on the SPIM was compared to the equivalent three-phase induction motor.

Chapter 4 covers the testing of the designed SPIM; and the challenges faced during the development and the testing of the machine and various ways employed to overcome the difficulties was focused; and the analysis and verification of experimental results with regards to the practical implementation of the designed six-phase induction motor were also examined.

Chapter 5 concludes the study from which recommendations were given and future study presented.

CHAPTER TWO
LITERATURE REVIEW

2.1. Introduction

Motors are generally categorized by their type and the electrical supply requirement. Essentially, there are two extensive classes of alternating current (AC) machines. In poly-phase synchronous motors, the magnetic field linked with the rotor results from a rotor winding excited by direct current through slip rings or brushless exciter from permanent magnets on the rotor structure. Conversely, the rotor magnetic field is created by electromagnetic induction effects in the single-phase induction machine.

Multi-phase machines are AC type categorized by a stator winding composed of generic number of phases. The initial attention of the multiphase machines was triggered by the likelihood of lowering the torque ripple in inverter fed drives, compared to the three-phase case. The modern day generation technology and electric drive multiphase machines have numerous benefits over the customary three-phase machine such as high fault tolerance, higher reliability, increasing the frequency of torque pulsation, reducing the amplitude and reducing the rotor harmonic current per phase without increasing the voltage per phase, lowering the dc-link current harmonics. The enhanced reliability as a result of fault tolerance, is perhaps, one of the leading reasons of the utilization of six-phase induction motor drives in locomotives (Nanoty & Chudasama, 2012).

2.2. Multi-Phase Induction Motor

Different efforts have been made in the literature to show the comparative gains of the multi-phase induction motors over the normal three-phase induction counterpart. Lipo and Nelson as reported in Nelson et al. (1969) carried out stability analysis of symmetrical induction motors. Zhao and Lipo (1995) used the vector space decomposition method to model a six-phase induction machine. Two distinct models were utilized to investigate the dynamic behavior of machines excitation as a result of open circuit but did not analyze the unbalanced condition triggered by the short circuit at stator terminals. This same approach was used by Hadiouche et al. (2000). The technique turns the six-dimensional space of the machine into three orthogonal subspaces of two dimensions. Zhao & Lipo (1996) also presented another model to represent the dynamic behavior of the machine under unbalanced conditions.

The derivation of voltage models in phase variables as well as the conversion to the direct-quadrature-zero transformation ($d–q–0$) reference frame of a multi-phase machine with unsymmetrical phase shift was reported by Nelson and Krause (1974). A *d-q-o* model for SPIM comprising leakage inductance coupling was presented by Lipo (1980). The $d–q$ model of the multi-phase machine was developed by Singh (2002). A similar study was performed using Matlab/Simulink by Shan et al. (2010). Hamdani et al. (2008) presented a generalized two axis (d-q) model of squirrel cage induction motor used for rotor faults diagnosis. Conversely, Mohapatra et al. (2002) presented a different scheme of SPIM control with open end. The conclusion drawn is, substantial generation of the 5th and 7th current harmonics is one of the main drawbacks of multiphase induction motor. These harmonics cause additional losses in the motor. This will lead to increased size and cost of motor and inverter. Moreover, the problem of 3rd and 7th harmonics is an issue for any phase number higher than three, the exception being asymmetrical SPIM.

Various methods for electric drives are described by Romeral (2002). The concept of multiphase multi motor drives control when fed from single voltage source inverter is

given by Krishna et al. (2005) and Toliyat (1996). Sensor less field oriented control of SPIM was explained in detail and it is more economical for high power applications (Dejan et al., 2006; Markadah et al., 2009; Perng et al., 1998). Kaneyuki & Koyama (1997) presented application of multiphase motors in electric vehicles in a Mitsubishi Electric Advance -Technical report on electric drives for electric vehicles. Vector control of induction motor is explained in detail (Nanoty & Chudasama 2012). Split-phase induction motor consists of two identical stator windings sharing the same magnetic circuit. These motors help in extending the power range of solid-state based drives (Shi et al., 1999).

The six-phase machine modeling under normal and fault conditions was reported in several papers. The modeling is presented didactically in (White & Woodson, 1959). The analysis can be done similarly to the three-phase case, i.e. the phase variable model is transformed into another reference with new variables using a real or complex matrix. Levi (2006) and Levi et al. (2007) surveyed the contemporary advances in the operation of the multiphase induction motor drives. In addition, series connected multiphase induction motors both five phase and six phase are discussed. Asymmetrical six phase induction motors are found to be more suitable. These studies suggest a growing pursuit for multiphase machines. A direct control method for five phase voltage source inverter Induction Motor drives investigation leads to conclusion that fast torque response with low ripple torque can be obtained (Jones et al., 2005). Singh (2002) as well as Singh & Lim (2005) have given extended research on multiphase machines. Using two current sensors the torque can be improved in six phase induction motor (Bojoi et al., 2005). Also, the SPIM torque can be improved by injecting third harmonic current externally (Gregor et al., 2008). Torque Density Improvement in a six-phase induction motor was carried out with third harmonic current injection in Lyra & Lipo (2002). The conclusion, drawn from the research done is that by injecting third harmonic current, the production of electromagnetic torque can be improved.

Most of the researchers have used multiphase inverter for multiphase motor, i.e. six-phase inverter for six-phase induction motor (Dejan et al., 2006). Nanoty & Chudasama (2012) centered their study on the developmental design and testing of a six-phase induction motor with emphasis on the control scheme. Nevertheless, little research have been applied in practical design and development the six-phase induction motor free from third harmonic current injection for torque improvement.

CHAPTER THREE
THE DESIGN

3.1. Design of M-Phase Induction Machine

Three phase induction motors are invariably utilized in several residential, industrial, commercial and utility applications thanks to low price, reliable operation, strong operation and low maintenance, poly-phase motor drives with phase number more than 3 (three) results in associate improvement within the medium to high power drives application. The poly-phase induction motor notice application in special and demanding space/area wherever high reliability is needed like electrical vehicles/Hybrid electrical vehicles and in high power utilizations (Aher & Thosar, 2016)

A higher degree of freedom will be achieved in an electrical drive system once the machine is modified for an additional with variety of phases more than 3 (three). For applications wherever reliability is incredibly vital, the employment of poly-phase systems has emerged as an awfully possible choice; especially, with the loss of a single or a lot of stator coil phases, a poly-phase induction machine will still be driven with associate acceptable post-fault strategy (Miranda & Gomes, 2012)

3.2   Presentation of the Three Phase Induction Machine

3.2.1 The Structure

The stator of an induction machine comprise three set of windings as shown in Fig. 3.1, coupled in delta (or in star). The rotor can be considered to aid a winding comparable to that of a stator, i.e., a three-phase winding with equal number of poles as in the stator (Benoît et al., 2012).
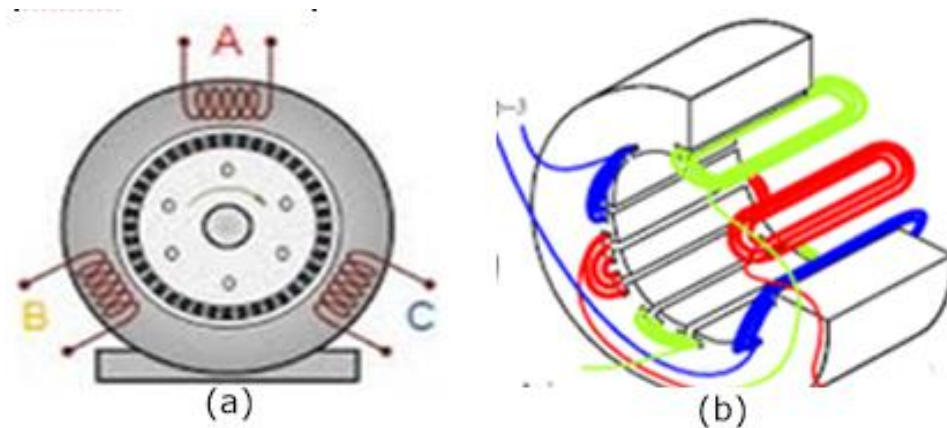
Fig. 3.1 The stator of a three-phase machine (a) one set of winding per phase
(b) two sets of winding per phase
Source: Benoit et al. (2012)

As shown in Fig. 3.2, the "coiled rotor" technology comprises a three-phase windings liken to the stators coupled in star for which each winding free bound is connected to a rotating ring by the rotor tree. The brushes create contacts on this ring and permit an external linking to the rotor, which could be a link to resistors or a short circuit, hence, some of the machine's characteristics are altered. Also, the connection can permit a peripheral supply, which could adjust the rotor capacities. This phenomenon is called

''Doubly-Fed Induction Machine''. The result looks like a squirrel cage and this suggests the current name of ''cage machine'', which operates like a coiled rotor (Benoît et al., 2012).

Fig. 3.2 The rotor of an AC machine (a) coiled rotor (b) squirrel cage rotor
Source: Benoit et al. (2012)

3.2.2. Operational Principle

When an alternating current is applied to a stator armature it produces a flux in the magnetic circuit of the stator. This flux induces an EMF in the conducting bars of rotor as they are "cut" by the flux while the magnet is being moved ($= BvL$ (Faraday's Law), where B is the magnetic flux v is the velocity of the wire, and l is the length of the wire) (Karady & Holbert, 2013). A current (I) flow in the rotor circuit as a result of the induced EMF that in turn produces a force, ($F = BIl$) can be converted to the torque as output as shown in Fig. 3.3.
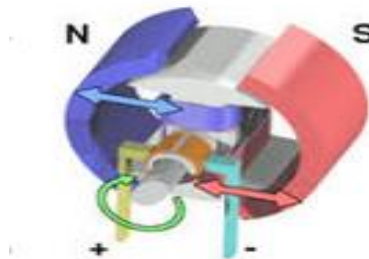
Fig. 3.3 Illustration of Faraday's law
Source: Benoit et al. (2012)

The three-phase currents, I_a, I_b and I_c, in a three-phase induction motor, are each of equal magnitude, but with phase shift of 120°. The total flux, which is the summation of the three ac fluxes in the machine, results in a rotating magnetic field (RMF) that turns with constant speed and has constant amplitude. The interfacing of the rotor current and the rotating flux generates a driving force, and then a torque, which is proportional to the rotor bar current and the flux density ($F = BIl$). The direction of rotation of the rotor is identical to that of the rotation of a revolving magnetic field in the air gap. Nevertheless, for the currents to be induced, the speed of the rotating magnetic field in the stator and the speed of the physical rotor must be different, otherwise the magnetic field will not move relative to the rotor conductors; hence, current will not be induced.

Similar to the working of three-phase induction motor, the six-phase induction motor works on the application of Faraday's law and Lorentz force on conductor. When six phase ac supply is applied to the stator winding which are spatially and time displaced by 60 °the rotating magnetic field is produce, which rotates at synchronous speed.

When short circuited rotor (squirrel cage) is placed in rotating magnetic field an EMF is induced in the rotor conductor due to electromagnetic induction. Due to this EMF, current starts flowing in the rotor conductor and sets up its own magnetic field. Due to interaction of these two magnetic fields, a torque is produced and conductor tends to move (Aher & Thosar, 2016).

3.3. The Six-Phase Induction Machine
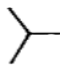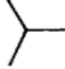
A system with more than three stator phases can be referred to as multi-phase system. A classic example includes the six-phase induction motor derived from dual 3-phase induction motor having two set of stators windings spatially shifted by 30 electrical degrees with separated neutral. Compared to the typical 3-phase motor, the dual-3-phase systems generate a higher torque; hence, they are preferred in high power (or current) applications, such as electric / hybrid vehicles, aerospace, and ship propulsion applications. Similarly, the six-phase synchronous motor can be utilized for high power applications but has higher weight compared to of six phase induction motor with similar rating (Taheri, 2013).

For any split-phase motor configuration the phase belt of the three phases are split into two halves with the N sets of 3-phase windings are spatially phase shifted by 60°/N electrical degrees. The dual 3-phase induction machine is a six-dimensional system. To lessen the difficulty in the modeling and control of the dual three-phase induction machine, the following are assumptions made;

1. Magnetic saturation, core losses and mutual leakage inductances are negligible
2. Distribution of rotor and stator windings are sinusoidal.

Table 3.1 shows the different multiple phases and in relation to the phase belt angle and the minimum number of stator leads required for them (Yadav et al., 2014).

Table 3.1 Multi phase machines having the multiple of three phase system

Belt Angle	120	60	60	40	30	30	20	20
No of Phase belt per pole	1.5	3	3	4.5	6	6	9	9
No. of stator terminals	3	3	6	9	6	12	9	18
Connection Name	3 phase	Semi-6 phase	6 phase symmetric	9 phase symmetric	6 phase asymmetric	12 phase	9 phase asymmetric	18 phase
Schematic connections								

Source: Yadav et al. (2014)

3.4   Design Equations

3.4.1 General Output Equation

The conventional design starts with the well-known output equation as derived to suite the six-phase induction motor. Generally, the output equation can be derived from the following expressions (Sawhney, 2001):

$$P_{in} = m \, V_{ph} \, I_{ph} \times 10^{-3} \tag{3.1}$$

Where P_{in} is the input power, m is the number of phase, V_{ph} is the induced emf per phase and I_{ph} is the current per phase and

$$V_{ph} = 4.44\, f\, \emptyset\, N_{ph}\, K_w \tag{3.2}$$

Where, N_{ph} is the number of turns, K_w is the winding factor, f is the frequency, and $\emptyset$ is the flux. Substituting Eq. (3.2) into Eq. (3.1), the equation (3.1) can be written as

$$P_{in} = m\, 4.44\, f\, \emptyset\, N_{ph}\, K_w\, I_{ph} \times 10^{-3} \tag{3.3}$$

Also, $f = p\, n_s\, /2$; where p is the number of poles, and n_s is the synchronous speed. Hence, Eq. (3.3) becomes

$$P = P_{in} = 2m \times 2.22\, (pn_s/2)\, \emptyset\, N_{ph}\, K_w\, I_{ph} * 10^{-3} \tag{3.4}$$

Re-arrange equation (3.4), gives

$$P_{in} = 1.11 \times (\emptyset\, p) \times (2m\, I_{ph}\, N_{ph}) \times n_s K_w \times 10^{-3} \tag{3.5}$$

Where $(\emptyset\, p)$ is the magnetic loading and $(2m\, I_{ph}\, N_{ph})$ is the total electric loading. But the total electric loading of an AC machine is nQD, as the total magnetic loading of an AC machine is $nDLB_{av}$. Therefore;

$$P_{in} = 1.11 \times nDLB_{av} \times nQD \times n_s K_w \times 10^{-3} \tag{3.6}$$

$$P_{in} = 1.11 \times n^2\, B_{av}\, Q\, K_w\, D^2 L\, n_s \times 10^{-3} \tag{3.7}$$

$$P_{in} = C_o\, D^2 L\, n_s \tag{3.8}$$

where

$$C_o = 1.11 \times n^2\, B_{av}\, Q\, K_w \times 10^{-3} \tag{3.9}$$

And

$$P_{in} = P_{out}/\eta\, P_f \tag{3.10}$$

$$P_{in} = P_{out} + \text{Losses} \tag{3.11}$$

Also,

$$K = L/T \tag{3.12}$$

$$T = nD/p \tag{3.13}$$

Where P_{out} is the output power, P_f is the power factor, η is the efficiency, T is the pole pitch, n is the pie, p is the number of poles and D is the bore diameter.

3.5. Computation of Torque in Closed Form

The induced voltage is as given:

$$V_{ph} = 4.44\, f\, \emptyset\, N_{ph}\, K_w \tag{3.14}$$

Where, all parameters are as previously defined.

3.5.1. Calculation of the Winding Factor

(i) Coil Pitch or Coil Span $= \dfrac{No\ of\ Slots}{No\ of\ Poles} \qquad = \dfrac{48}{4} = 12$ $\tag{3.15}$

(ii) The concentric layer $K = 4$; Here, $K = 1, 2, 3, 4$ and $h = 1, 3, 5, 7$ (Odd Harmonics)

(iii) Slot Angle, $\alpha = \dfrac{360^o}{No\ of\ Slots} = \dfrac{360^o}{48} = 7.5$ $\tag{3.16}$

(iv) Span Angle, $\dfrac{\beta_k}{2} = \dfrac{180^o - \alpha h}{2}$ $\tag{3.17}$

Hence, $\dfrac{\beta_1}{2} = \dfrac{180^o - 7.5(1)}{2} = 86.25^o$; $\dfrac{\beta_2}{2} = \dfrac{180^o - 7.5(3)}{2} = 78.75^o$; $\dfrac{\beta_3}{2} = \dfrac{180^o - 7.5(5)}{2} = 71.25^o$; and $\dfrac{\beta_4}{2} = \dfrac{180^o - 7.5(7)}{2} = 63.75^o$.

(v) The winding factor, $K_w = \dfrac{\left(\sin\frac{\beta_1}{2}\right)^2+\left(\sin\frac{\beta_2}{2}\right)^2+\left(\sin\frac{\beta_3}{2}\right)^2+\left(\sin\frac{\beta_4}{2}\right)^2}{\sin\frac{\beta_1}{2}+\sin\frac{\beta_2}{2}+\sin\frac{\beta_3}{2}+\sin\frac{\beta_4}{2}}$ (3.18)

$$K_w = \frac{(\sin 86.25)^2+(\sin 78.75)^2+(\sin 71.25)^2+(\sin 63.75)^2}{\sin 86.25+\sin 78.75+\sin 71.25+\sin 63.75}$$

$$K_w = \frac{0.9957+0.9619+0.8967+0.8043}{0.9979+0.9808+0.9469+8969} = \frac{3.6587}{3.8225} = 0.9571$$

Therefore Eq. (3.14) becomes

$$E_{ph} = 4.44f\emptyset_{sr}N_{ph} \times 0.9571 \tag{3.19}$$

Also,

$$E_{ph} = \frac{V_{L-L}}{\sqrt{3}} = \frac{415}{\sqrt{3}} = 265\ V \tag{3.20}$$

Combining Eq. (3.19) and Eq. (3.20), the flux per pole can be deduced as follow:

$$\phi_{sr} = \frac{E_{ph}}{4.44fN_{ph} \times 0.9571} = \frac{239.6}{4.44 \times 50 \times 504 \times 0.9571} = 0.00224\ Wb$$

Flux per pole is given as: $\emptyset_{sr} = \frac{2}{\pi}\tau_p LB_{sr}$, hence, the maximum flux density per pole, B_{sr} is stated as follow:

$$B_{sr} = \frac{\pi \times \emptyset_{sr}}{2 \times \tau_p \times L} \tag{3.21}$$

Where the pole-pitch, τ_p, is given as:

$$\tau_p = \frac{\pi \times D}{P} = \frac{\pi \times 9.05}{4} \quad = 0.0710\ m \tag{3.22}$$

The maximum flux density per pole, B_{sr}, deduced as follow:

$$B_{sr} = \frac{\pi \times 0.00224}{2 \times 0.0710 \times 0.146} = 0.339\ \text{Wb/m}^2 \tag{3.23}$$

The maximum value of the stator Magnetomotive force (mmf) $F_{s\,max}$, can be expressed as follows

$$F_{s\,max} = \frac{4 \times K_w \times N_{ph} \times I \times \sqrt{2}}{\pi \times P} = \frac{4 \times 0.9571 \times 504 \times 8.9 \times \sqrt{2}}{\pi \times 4} = 1932.6\ AT/pole \tag{3.24}$$

In a balanced 3-phase induction motor, the amplitude of the resultant Stator MMF, F_s is given as:

$$F_s = \frac{3}{2} \times F_{s\,max} = \frac{3}{2} \times 1932.60 = 2898 AT/Pole \tag{3.25}$$

The expression of the minimum value of the electromechanical torque established is given as

$$T_{max} = \frac{\pi}{2} \times \left(\frac{P}{2}\right)^2 \times \emptyset_{sr} \times F_s \tag{3.26}$$

$$T_{max} = \frac{\pi}{2} \times \left(\frac{4}{2}\right)^2 \times 0.00224 \times 2898.907 = 40.8\ Nm$$

3.6. Computation of Number of Turns per Phase

The amplitude resultant flux density at mid-gap level, $B_{sr\,6\,phase}$ for the new six phase design using Eq. (3.21) is as follows:

$$B_{sr} = \frac{\pi \times 0.00224}{2 \times 0.07170 \times 0.146} = 0.339 \text{ Wb/m}^2 \tag{3.27}$$

Where $\tau_p = 0.07107\,m$ and $L = 0.146\,m$ are the same as in the 3 phase original design.

Also, the maximum torque for the six-phase design can be written on the basis of Eq. (3.26) as $T_{\max\,6\,phase} = \frac{\pi}{2} \times \left(\frac{4}{2}\right)^2 \times 0.0224 \times 2898.907 = 40.8\,Nm$, which is the same value given in Eq. (3.26).

Also, it follows from Eq. (3.26) that:

$$F_{s\,6\,phase} = \frac{T_{\max 6\,phase} \times 8}{P^2 \times \emptyset_{sr6phase}} = \frac{40.8 \times 8}{4^2 \times 0.00224} = 9107\,AT/Pole \tag{3.28}$$

The $F_{s\,max}$ in a balanced 6-phase machine, is related to the total stator mmf per pole, $F_{s\,6\,phase}$, expression as;

$$F_{s\,6\,phase} = \frac{6}{2} \times F_{s\,max\,6\,phase}$$

Therefore,

$$F_{s\,max\,6\,phase} = \frac{2}{6} \times F_{s\,6\,phase} = \frac{2}{6} \times 2898.907 = 966.3\,AT$$

However, from Eq. (3.24) $F_{s\,max}$ is also equal to,

$$F_{s\,max\,6\,phase} = \frac{4 \times K_w \times N_{ph} \times I \times \sqrt{2}}{\pi \times P} = 966.3\,AT \tag{3.29}$$

From Eq. (3.29), the product of $K_w \times N_{ph}$ is found to be,

$$K_w \times N_{ph\,6\,phase} = \frac{\pi \times P \times F_{s\,max\,6\,phase}}{4 \times I \times \sqrt{2}} = \frac{\pi \times 6 \times 966.3}{4 \times 8.9 \times \sqrt{2}} = 361.78 \tag{3.30}$$

3.6.1 Computation of New K_w

(i) The concentric layer, $K = 2$; Here $K = 1,2$; $h = 1,3$ (Odd Harmonics)

(ii) Slot Angle, $\alpha = \dfrac{360^o}{No\;of\;Slots} = \dfrac{360^o}{48} = 7.5$

(iii) Span Angles, $\dfrac{\beta_k}{2} = \dfrac{180^o - \alpha h}{2}$; $\dfrac{\beta_1}{2} = \dfrac{180^o - 7.5(1)}{2} = 86.25^o$; $\dfrac{\beta_2}{2} = \dfrac{180^o - 7.5(3)}{2} = 78.75^o$

The winding, $K_w = \dfrac{\left(\sin\frac{\beta_1}{2}\right)^2 + \left(\sin\frac{\beta_2}{2}\right)^2}{\sin\frac{\beta_1}{2} + \sin\frac{\beta_2}{2}} = \dfrac{(\sin 86.25)^2 + (\sin 78.75)^2}{\sin 86.25 + \sin 78.75} = \dfrac{0.9957 + 0.9619}{0.9979 + 0.9808} = 0.9893$

Then $N_{ph6-\phi} = \dfrac{361.78}{0.9893} \cong 366$

3.7. Computation of Voltage rating of the Six-Phase Motor

In order to sustain the same power rating for both the three-phase and the six-phase machines, then the following equation was assumed:

$$3 \times V_{ph\,3\,phase} \times I_{ph\,3\,phase} = 6 \times V_{ph\,6\,phase} \times I_{ph\,6\,phase} \tag{3.31}$$

If $V_{ph\,3\,phase} = 240$ V and $I_{ph\,3\,phase} = 8.9$ A; from Eq. (3.31), $V_{ph\,6\,phase} = 120$ V

3.8.   Winding Design

The connection technique and the vector of bipolar binary six-phase 30º winding are illustrated in Fig. 3.4 and Fig. 3.5.
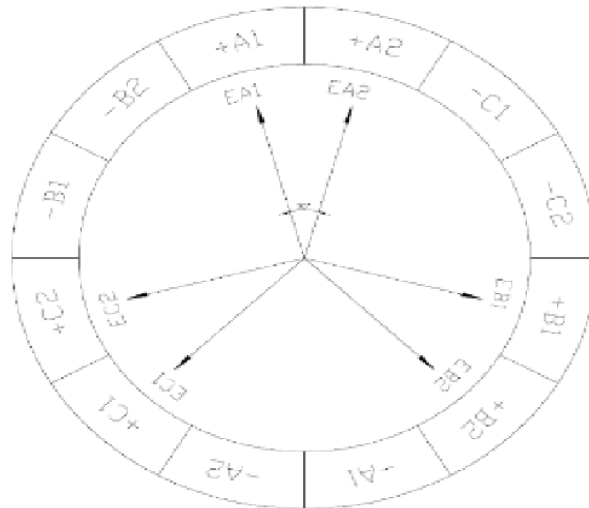
Fig. 3.4 Winding structure of six-phase induction motor
Source: Tuo (2012)
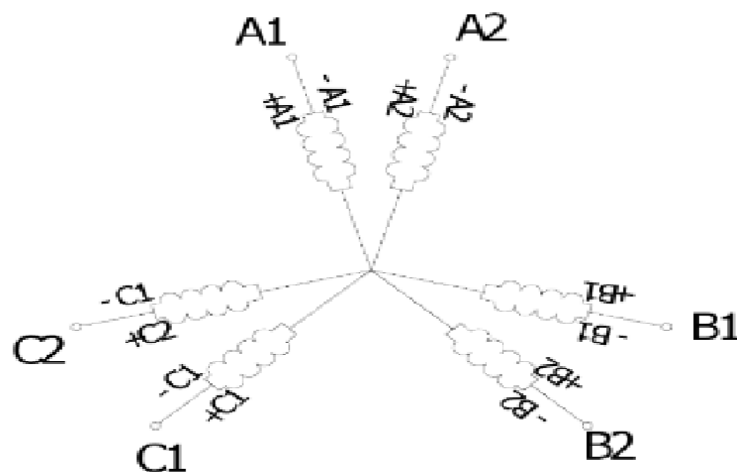
Fig. 3.5 Wiring diagram of six-phase induction motor
Source: Tuo (2012)

The distribution of the 12-phase belts observed along the circumference of the stator (Fig. 3.4) can be viewed as the real position of the upper coil on the border edge and this depends on the coil pitch. Conversely, the double Y connection approach, shown in Fig. 3.5, comprised six-phase and two parallel slips has each phase (Tuo, 2012). Since the design of a three-phase ac machine is always the point of contraction here, explanation to elaborate its design in details then, move over to its compact ability with a six-phase system.

3.8.1. Three Phase System

A three-phase AC machine with 2 pole (Khan et al., 2010): the phase angle between two consecutive phases is given as follow

$$\emptyset = 360°/3 \text{ (electrical)} = 120° \text{ electrical} = 120° \text{ (mechanical)} \qquad (3.32)$$

Table 3.2 shows the number of slots and its allocation for a 3-phase, two pole induction motor.

Table 3.2 Three-phase two pole induction motor stator slot allocation

Number of slot	Pole - 1			Pole – 2		
	R	B	Y	R	B	Y
6	1	1	1	1	1	1
9	2	1	2	1	2	1
12	2	2	2	2	2	2
15	3	2	3	2	3	2
18	3	3	3	3	3	3
21	4	3	4	3	4	3

The R, Y, B represent the three phases and are under each pole. The minimum number of slots required for such a design is 6 as shown in the Table 3.2. The increment in the slot is in 3. The number of slots per phase is always the same for all the phases and so the minimum number of slot is given as

$$S = m \text{ (phase)} \times p \text{ (poles)} \qquad (3.34)$$

S is the minimum number of slot, *m* is the number of phase, and *p* is number of poles.

Generally, the numbers of slots needed are;

$$(6 + 3K) = 3(2 + K) \qquad (3.35)$$

K = 0, 1, 2, 3, ...

The per slot angle (α) becomes

$$\alpha = 360°/3(2 + K) = 120/(2 + K) \text{ (mech)} \qquad (3.36)$$

The phase angle required between any consecutive phase in terms of slots

$$= 120/\text{slot angle} = 120 / (120/(2 + K)) \text{slot angle} = (2 + K) \text{ slot} \qquad (3.37)$$

Equation (3.37) suggests as shown in Table 3.2 that each phase has a minimum number of slot to be 2 for K = 0 and progresses to 3 for the value of K = 1 and so on. If phase *R* begins from the slot number 1 then phase Y will start from $(2 + K)^{th}$ number of slot and phase B from $2(2 + K)^{th}$ number of slot.

A three phase four pole AC machine: the phase angle between any consecutive phases is expressed as

$$\emptyset = 360°/3 \text{ (electrical)} = 120° \text{ (electrical)} = 60° \text{ (mechanical)} \qquad (3.38)$$

Also, the winding disposition and number of slots required for three phase four pole AC machine can be found.

The number of slot required, typically, is:

$$(12 + 6K) = 6(2 + K) \qquad (3.39)$$

Where K = 0, 1, 2, 3. This gives rise to Table 3.3 with a minimum number of slot to be 12. Therefore, per slot angle (α) becomes

$$\alpha = 360°/6(2 + K) = 60° / (2 + K) \text{ (mechanical)} \qquad (3.40)$$

The required phase angle between any consecutive phases in terms of slots

$$= 60°/ \text{ slot angle} = 60°/ (60° / (2 + K) = (2 + K) \text{ slots} \qquad (3.41)$$

Table 3.3 Three phase four pole induction motor slot allocation

No. of slot	Pole - 1			Pole - 2			Pole - 3			Pole - 4		
	R	B	Y	R	B	Y	R	B	Y	R	B	Y
12	1	1	1	1	1	1	1	1	1	1	1	1
20	2	1	2	1	2	1	1	2	1	2	1	2
24	2	2	2	2	2	2	2	2	2	2	2	2
32	3	2	3	2	3	2	3	2	3	2	3	2
36	3	3	3	3	3	3	3	3	3	3	3	3
44	4	3	4	3	4	3	4	3	4	3	4	3
48	4	4	4	4	4	4	4	4	4	4	4	4

If phase *R* begins from slot number 1 then phase *Y* will start from $(2 + K)^{th}$ slot and phase B from $2(2 +K)^{th}$ slot. Generally, for *P* number of pole, *m* number of phases of the machine, the number of slot N_s required is given as:

$$N_S = (m/2)P(2 + K) \text{ slot} \qquad (3.42)$$

Where K = 0, 1, 2, 3, …

3.8.2. Six Phase System

A six–phase AC machine with two pole: The phase angle between any consecutive phases is expressed as:

$$\emptyset = 360°/6 \text{ (electrical)} = 60° \text{ (electrical)} = 60° \text{ (mechanical)} \qquad (3.43)$$

Table 3.4 shows the number of slots and its allocation for a six-phase, two pole induction motor.

Table 3.4 Six-phase two pole induction machine stator slot allocation

No. of slot	Pole – 1						Pole - 2					
	A	C	B	D	F	E	A	C	B	D	F	E
12	1	1	1	1	1	1	1	1	1	1	1	1
18	1	2	1	1	2	1	2	1	2	2	1	2
24	2	2	2	2	2	2	2	2	2	2	2	2
30	2	3	2	2	3	2	3	2	3	3	2	3
36	3	3	3	3	3	3	3	3	3	3	3	3
42	3	4	3	3	4	3	4	3	4	4	3	4
48	4	4	4	4	4	4	4	4	4	4	4	4

Typically, the number of slot N_s needed are:

$$N_s = 6(2 + K) \qquad (3.44)$$

K = 0, 1, 2, 3, …

The per slot angle (ą) becomes

$$ą = 360°/6(2 + K) = 60°/(2 +K) \text{ (mechanical)} \qquad (3.45)$$

And the needed phase angle between any consecutive phases in terms of slots

$$= 60/\text{slot angle} = 60°/(60°/(2 +K)) = (2 +K) \text{ slot} \qquad (3.46)$$

If phase *A* starts from slot number 1 then phase *B* will starts from $(2 +K)^{th}$ slot, phase *C* starts from $2(2 +K)^{th}$ slot, phase *D* starts from $3(2 +K)^{th}$ slot, phase *E* starts from $4(2 +K)^{th}$ slot and phase *F* starts from $5(2 +K)^{th}$ slot.

A six-phase AC machine with four pole (P = 4): the phase angle between any consecutive phase is given as:

$$\emptyset = 360°/6 \text{ (electrical)} = 60° \text{ (electrical)} = 30° \text{ (mechanical)} \qquad (3.47)$$

Table 3.5 shows the number of slot and its allocation for a six-phase, four pole induction motor. Here the number of slot N_s required are:

$$N_s = 12(2 +K) \qquad (3.48)$$

where K = 0, 1, 2, 3, …

Table 3.5 Six-phase four pole induction motor stator slot allocation

No. of	Pole - 1						Pole - 2						Pole - 3						Pole - 4					
slot	A	C	B	D	F	E	A	C	B	D	F	E	A	C	B	D	F	E	A	C	B	D	F	E
24	1	1	1	1	1	1	1	1	1	1	1	1	1	1	1	1	1	1	1	1	1	1	1	1
36	1	2	1	1	2	1	2	1	2	2	1	2	1	2	1	1	2	1	2	1	2	2	1	2
48	2	2	2	2	2	2	2	2	2	2	2	2	2	2	2	2	2	2	2	2	2	2	2	2
60	3	2	3	3	2	3	2	3	2	2	3	2	3	2	3	3	2	3	2	3	2	2	3	2
72	3	3	3	3	3	3	3	3	3	3	3	3	3	3	3	3	3	3	3	3	3	3	3	3

The basic rules for designing AC windings are described Kadaba et al. (2011).

3.9. Windings Design Formulations and Layout: Case-Study of 5-hp 3-Phase Induction Motor

Table 3.6 shows the workable combinations of slot for a 3-phase induction motors that can be instantly reconfigured into 6-phase induction motors (Kadaba, 2008). As suggested, a fractional slots value per pole per phase should be discouraged. Hence, the case under study is 48 slots with 4 poles (see Table 3.6).

Table 3.6 Permissible slot combinations of 3-phase induction motors that can be readily reconfigured to 6- phase induction motors

Number of slot, Ns	Number of pole, p	M, phases / No. of slots per pole per phase, q	M, phases / No. of slots per pole per phase, q
12	2	3 / 2	6 / 1
	4	3 / 1	6 / Fraction ½ NA
	6	3 / Fraction 2/3	6 / Fraction 1/3 NA
24	2	3 / 4	6 / 2
	4	3 / 2	6 / 1
	6	3 / Fraction 4/3 NA	6 / Fraction 2/3 NA
36	2	3 / 6	6 / 3
	4	3 / 3	6 / Fraction 3/2 NA
	6	3 / 2	6 / 1
48	2	3 / 8	6 / 4
	4	3 / 4	6 / 2
	6	3 / Fraction 8/3 NA	6 / Fraction 4/3 NA
60	2	3 / 10	6 / 5
	4	3 / 5	6 / Fraction 5/2 NA
	6	3 / Fraction 10/3 NA	6 / Fraction 5/3 NA
72	2	3 / 12	6 / 6
	4	3 / 6	6 / 3
	6	3 / 4	6 / 2

** NA – Not Applicable   **Source:** Kadaba (2008)

3.10. Characteristics of the Induction Motor under Study

This section centers on the complete design and testing of prototype six phase induction motor. The design of six phase induction motor is done as per three phase induction motor initially with a case-study of 48-slot, 4-pole, 5-hp squirrel cage induction motor at rated 415 V (line-to-line voltage) with 6.8 A per phase with speed of 1430rpm. The inner diameter of the stator bore, D = 9.05 cm. The stator length, l = 14.6cm. The stator has a concentric winding with 21 turns per coil and 8 coils per phase. Hence, N_{ph} = 168. Here, q = 4 slots per pole per phase and D_r (dimensions of the rotor) is 8.9cm. Stator winding is considered to be m–phase (either odd or even) that is sinusoidally distributed, and this removes (6n +1) order harmonics, where n =

1, 3, 5, …, (Levi, 2006). In this study, a three-phase, 48-slots induction machine with 4-poles was chosen.

3.10.1.   Some Terminologies

   Armature windings of a machine is defined as an layout of conductors constructed to produce emfs by relative motion in a hetero-polar magnetic field, and these group of conductors are spread in slots over the periphery of the stator (armature), either are joined in series to boost the voltage rating or parallel so as to increase the current rating.

   Turn consists of two conductors separated from each other by a pole pitch or nearly so and connected in series.

   Coil pitch or ***Coil span*** is the space between the two coil-sides of a coil, typically measured in terms of electrical degrees.

   Phase belt or ***Phase band*** is the collection of adjoining slots fitting to one phase under a pole-pair.

   Conductors are the active length of wire or strip in the slot of the stator.

   Pole pitch is the tangential space between the same points on two adjacent pole.

   Coil consists of single turn or several turns sited in virtually the same magnetic position.

   Coil group is the group of coils having the same center.

3.10.2. Windings of the stator

   The design of the SPIM is done on a 3-phase induction motor frame. Thus a 5-hp, 4 pole, 48 slots six phase induction motor is developed. A six-phase machine can be built by dividing the 60° phase belt into portions each spanning 30°. Also, considering Tables 3.1, 3.3 and 3.5 the corresponding column for 48 slots will be the basis of the construction/design of the new winding formation for the new SPIM. But the initial or the former winding formation for the three-phase induction motor is shown in Fig. 3.6. Fig. 3.7 to Fig. 3.9 show the winding formation of the R phase, Y phase and the B phase of the 3-phase induction motor, respectively.

3.10.3. Design of the Stator Winding for the Six Phase Machine

   On the basis of the windings design rules described by Nanoty & Chudasama (2012) it follows that the number of slots per pole per phase, $q = 2$, from $q = \frac{Ns}{m*p}$. In the case of a motor with 48-slot, 4 poles and 6-phases, then, $Ns = 2$. Besides, each coil has approximately 361 turns.
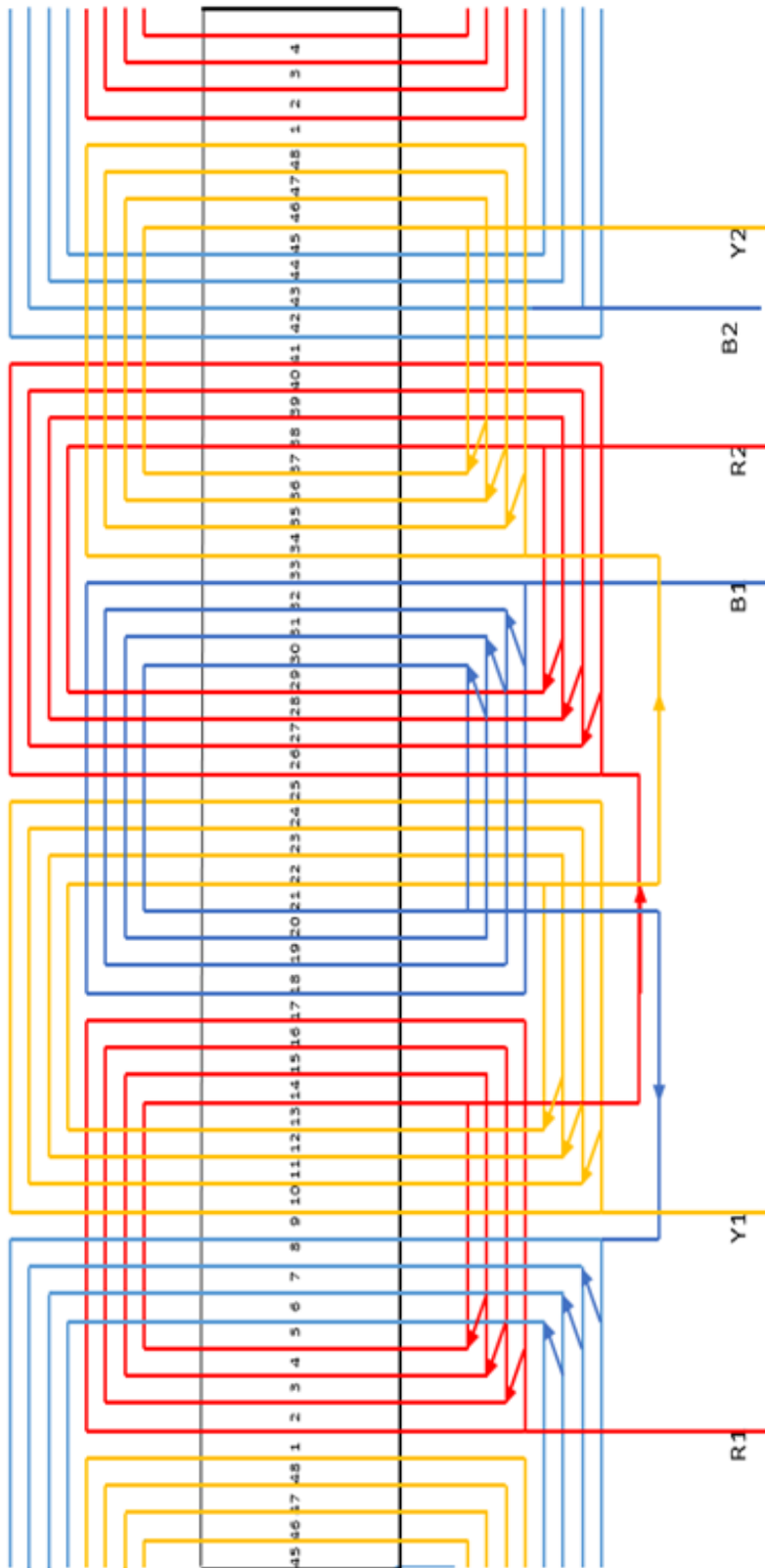
Fig. 3.6 Winding formation of the three phase induction motor
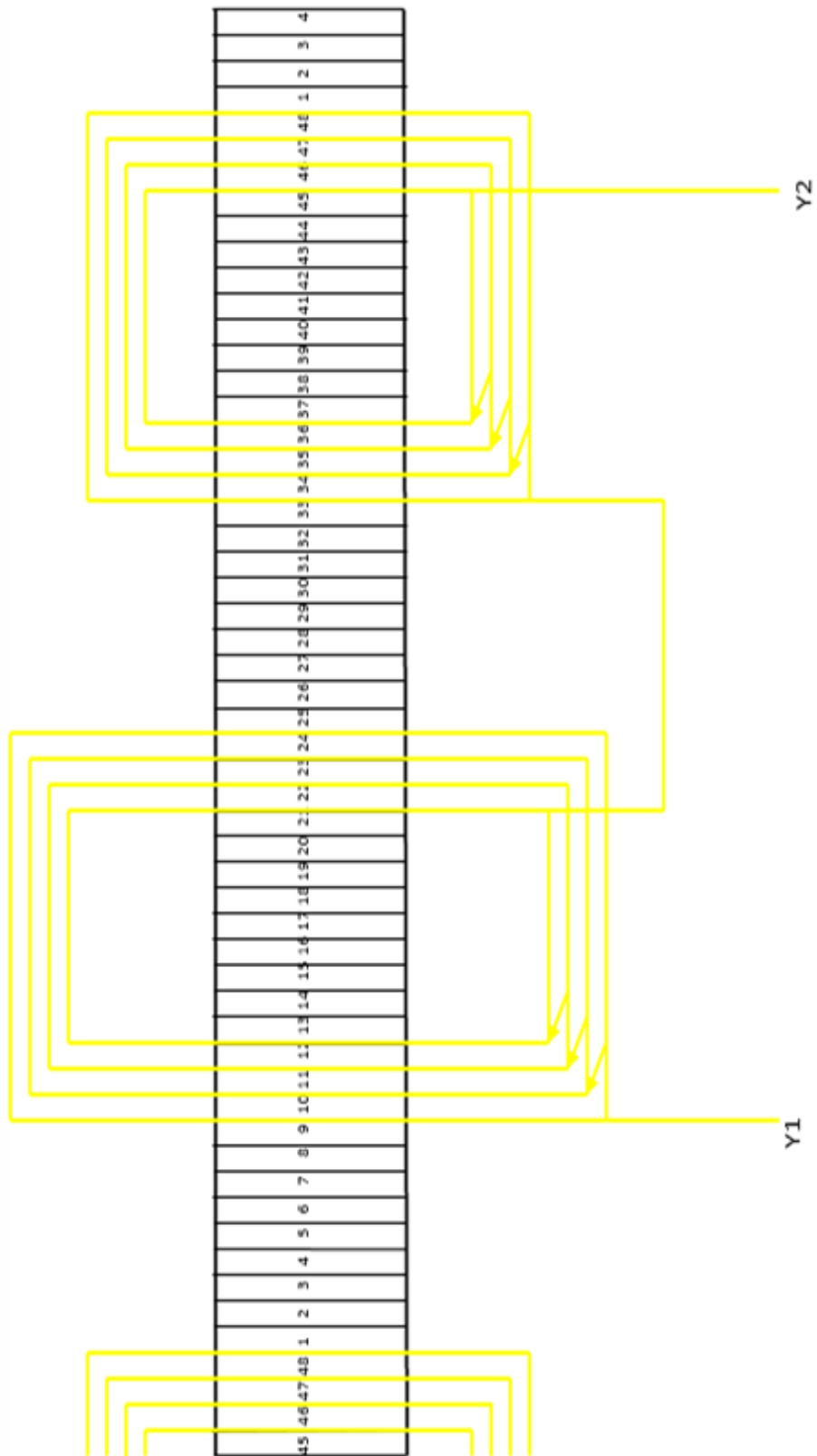
Fig. 3.7 Winding formation of the R phase of the three phase induction motor

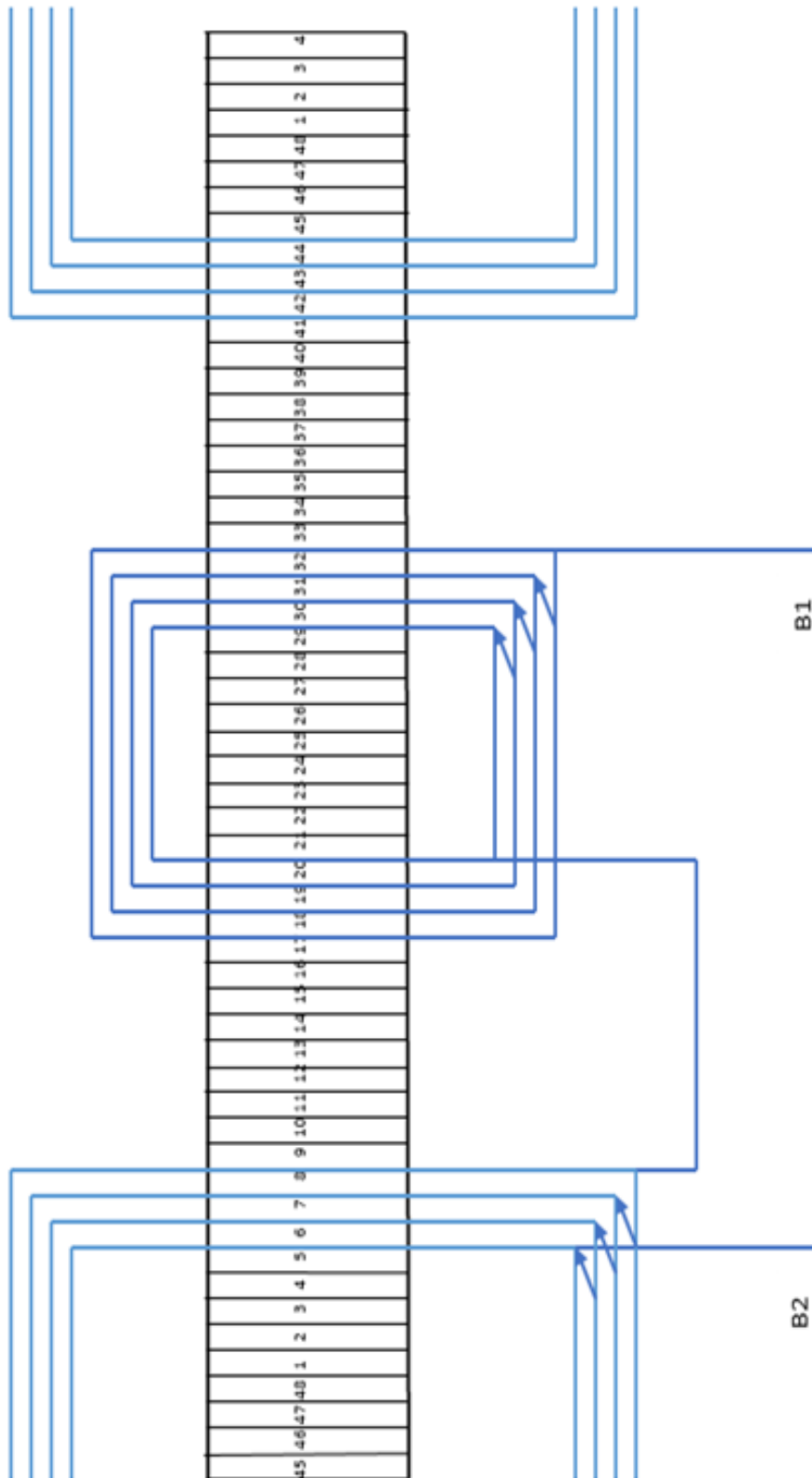**Fig. 3.8** Winding formation of the Y phase of the three phase induction motor

Fig. 3.9 Winding formation of the B phase of the three phase induction motor

The slot pitch angle for the 6-phase machine is deduced as:

$$\text{slot pitch} = \frac{360^0}{Ns} = \frac{360}{48} = 7.5^0 \text{ mechanical} \qquad (3.49)$$

and

$$\theta°m = 2\,\frac{\theta°e}{p} \qquad (3.50)$$

Therefore,

$$\theta°m = 2 \times {}^{30}\!/_4 = 15° \text{ mechanical} \qquad (3.51)$$

The six-phase is built such that one set of the three-phase is displaced from the other by $30°e$ with a resulting asymmetrical six-phase machine. Thus, the $30°e$ displacement correspond to $15°/7.5° = 2\ slots$. Here, both set of the three phase windings have 2 slots per pole per phase. The two set of three-phase is "ABC" and the second set of three-phase is "XYZ".

Concentric windings are divided into two type viz. (a) un-bifurcated winding and (b) bifurcated winding. In un-bifurcated winding, a pair of adjacent pole phase groups forms a concentric coil, whereas in bifurcated winding, each pole-phase group is divided into two sets of concentric coils sharing its return coil sides with another such group. If the number of pole pairs is even, the overhang can be accommodated in two planes. If the number of pole pair is multiple of three, then a three–plane overhang can be used. The full span or pole pitch, $\tau = Z/2P$; where P is the number of pair of poles.

In un-bifurcated concentric windings, the first of the q (number of slots per pole per phase) coils being the smallest is thrown from the qth slot having coil-span, y (coil span) = $(\tau - q + 1)$. The second coil that is larger than the first coil will be thrown from the second slot to its coil-span, y = $(\tau - q + 2)$. As q = 2, the second coil being the largest coil will be thrown from first slot having its coil-span, y = $(\tau - q + 2)$. Fig. 3.6 shows the single layer concentric winding diagram of stator (armature) with 48 slots and four poles. Then q = 48 / (4X6) = $2.\tau$ = 48/4 = 12. The inner coil is thrown from the second slot having coil-span, y = $(\tau - q + 1)$ = 12 – 2 + 1 =11 to (2+11) = 13th slot. The outer coil, which is larger than the inner coil is thrown from the first slot having coil-span, y = $(\tau - q + 2)$ = 12 – 2 +2= 12 to (2+12) = 14th slot. The other coils are arranged in the same manner. Fig. 3.7 displays the connections of two coils that form the coil group of a phase of the winding. Fig. 3.10 to Fig. 3.12 show the slot allocation for the physical formation of the coil/coil group being single layer for phase A, B and C respectively while Figs. 3.13 – 3.15 show the slot allocation for the physical formation of the coil/coil group being single layer for phase X, Y and Z respectively.
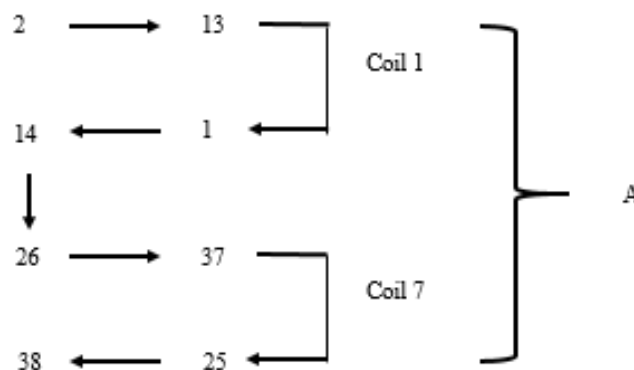

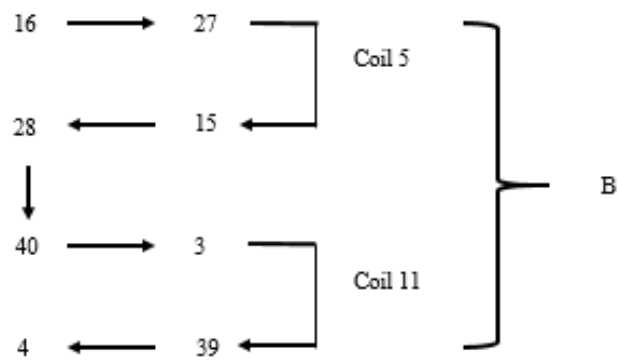**Fig. 3.10** Schematics connection for phase A
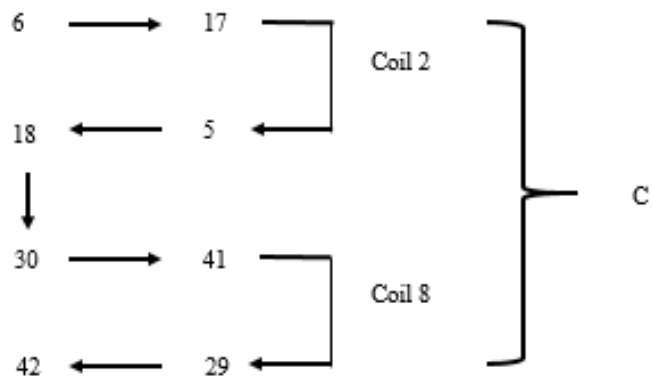
Fig. 3.11 Schematics connection for phase B

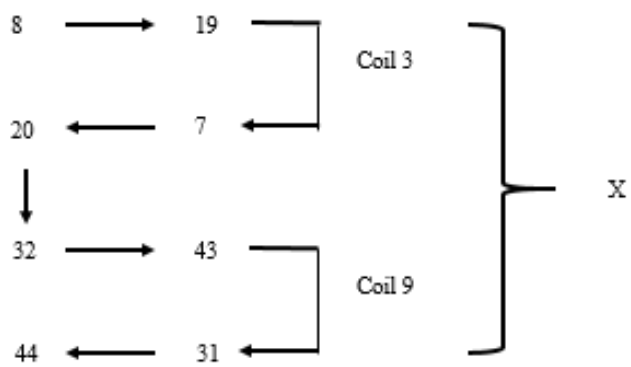**Fig. 3.12** Schematics connection for phase C

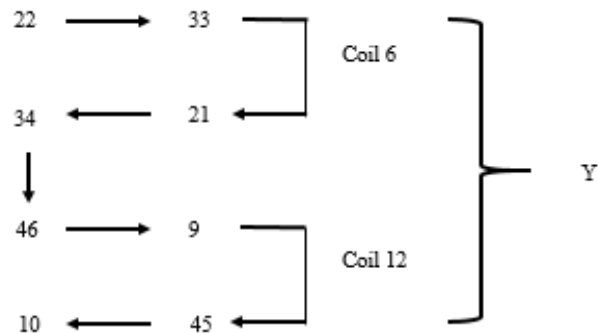**Fig. 3.13** Schematics connection for phase X

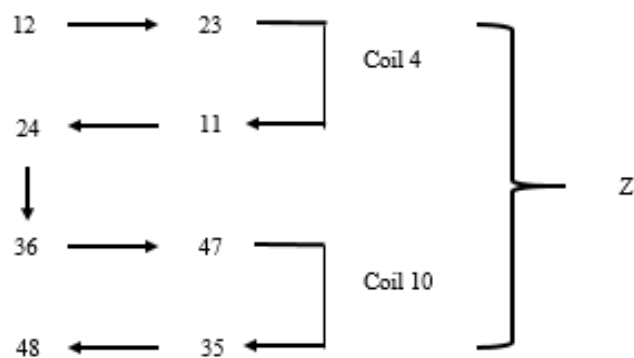**Fig. 3.14** Schematics connection for phase Y

Fig. 3.15 Schematics connection for phase Z

From the foregoing diagrams (Fig. 3.10 to Fig. 3.15) showing the schematics connections for the various phases the following can be deduced as shown in Fig. 3.16:

1   The start of coil 3 is a terminal point to receive power supply as the finish is connected to the start of coil 9 and its finish is a star connection point.
2   Also, the start of coil 2 is a terminal point to receive power supply as the finish is connected to the start of coil 8 and its finish is a star connection point.
3   The start of coil 5 is a live terminal point as the finish is connected to the start of coil 11 and its finish is a star connection point.
4   The start of coil 3 is a live terminal point to receive power supply as the finish is connected to the start of coil 9 and its finish is a star connection point.
5   The start of coil 4 is a live terminal point to receive power supply as the finish is connected to the start of coil 10 and its finish is a star connection point.
6   The start of coil 6 is a live terminal point to receive power as the finish is connected the start of coil 12 as its finish is a star connection point.
7   Also, the finish terminals of coil 7, coil 8 and coil 11 at slot number 38, 42 and 4 respectively form the neutral, i.e., star connection point for the ABC set of three phase winding; while the finish terminals of coil 9, coil 10 and coil 12 at slot number 44, 48 and 10 respectively form the second star connection point for the XYZ set of the other three phase. And these two-star connection points (i.e., neutral points) must be kept separate.

3.10.4. Connection Diagrams for the 6-Phase Operation

The schematic connections for the six phase induction motor are illustrated in Fig. 3.16 to Fig. 3.23. Pictorial views of the developed six phase induction motor are shown in Fig. 3.24 to Fig. 3.28 while Fig. 3.29 shows the pictorial view of the new induction motor with its manufacturer's name.
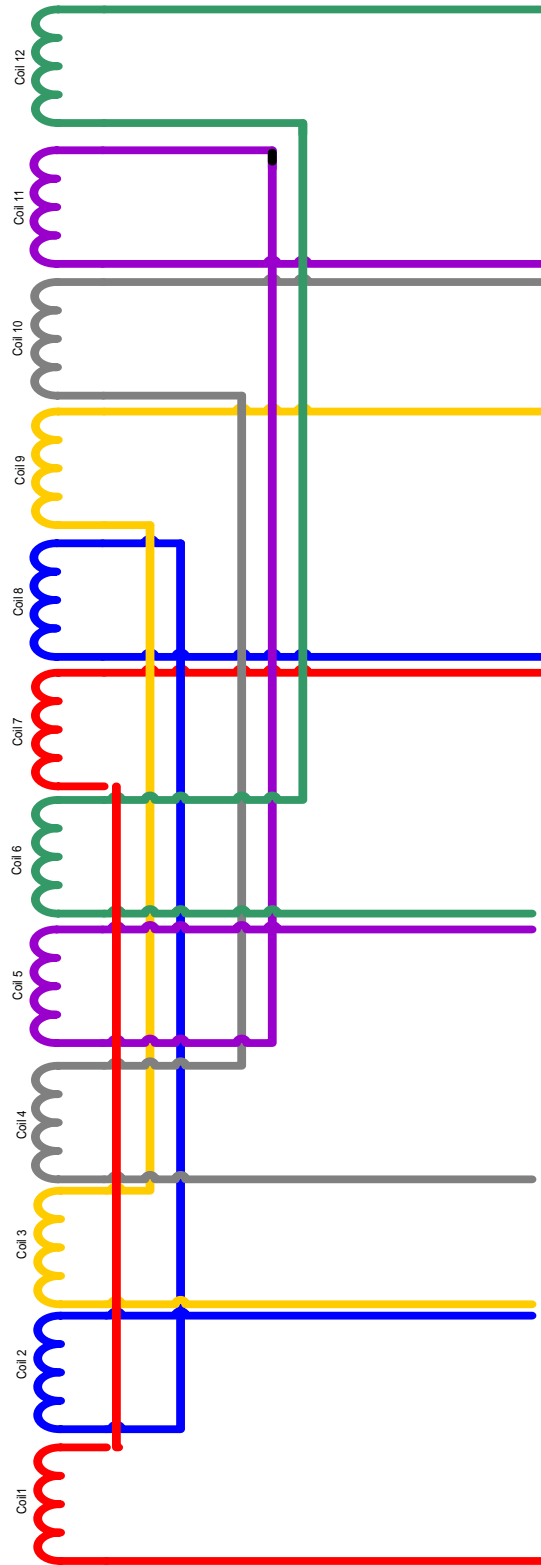
Fig. 3.16 Schematic connection for all the phases for the six phase induction motor
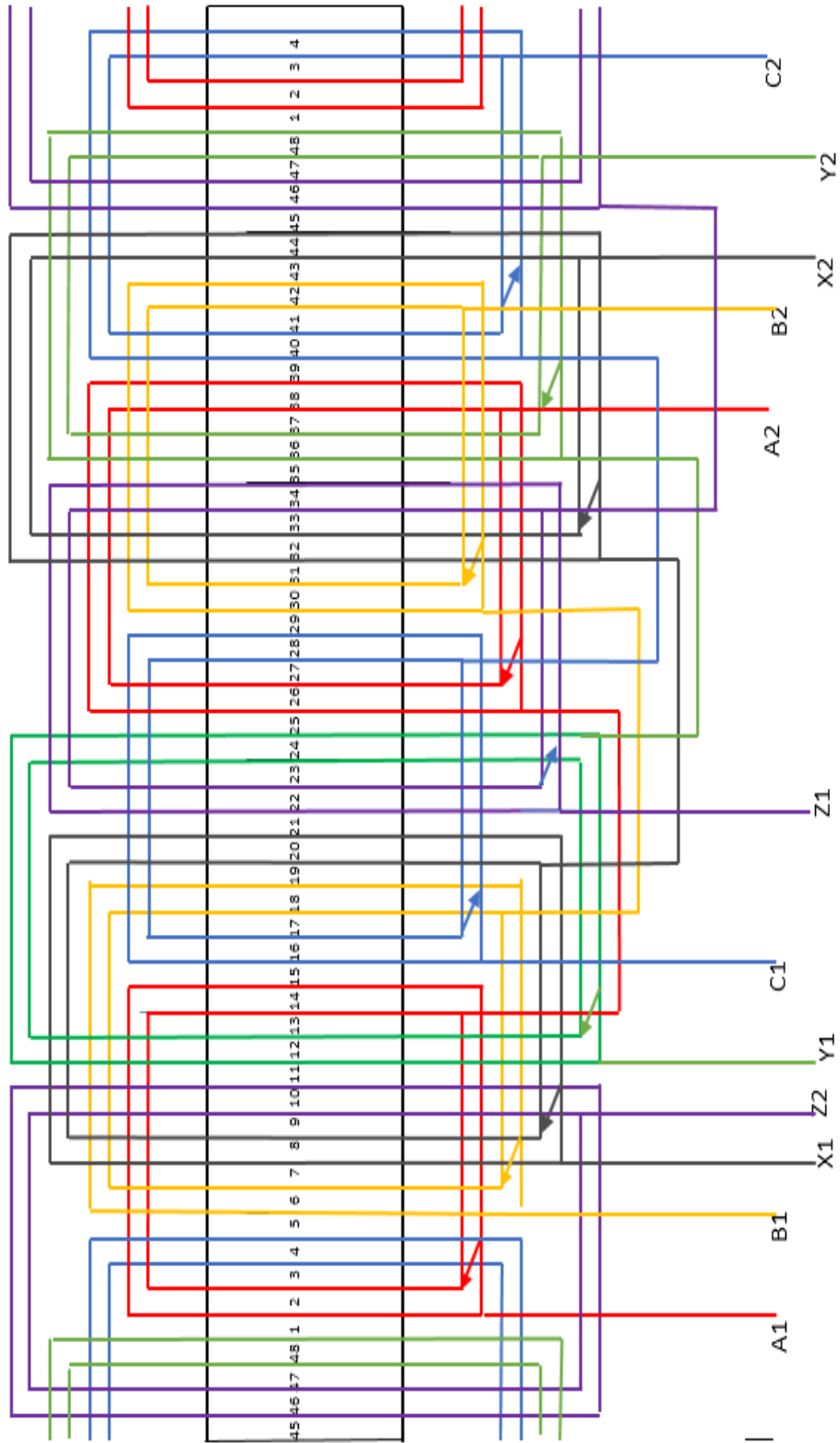
Fig. 3.17 Winding formation of the phases of the six phase induction motor
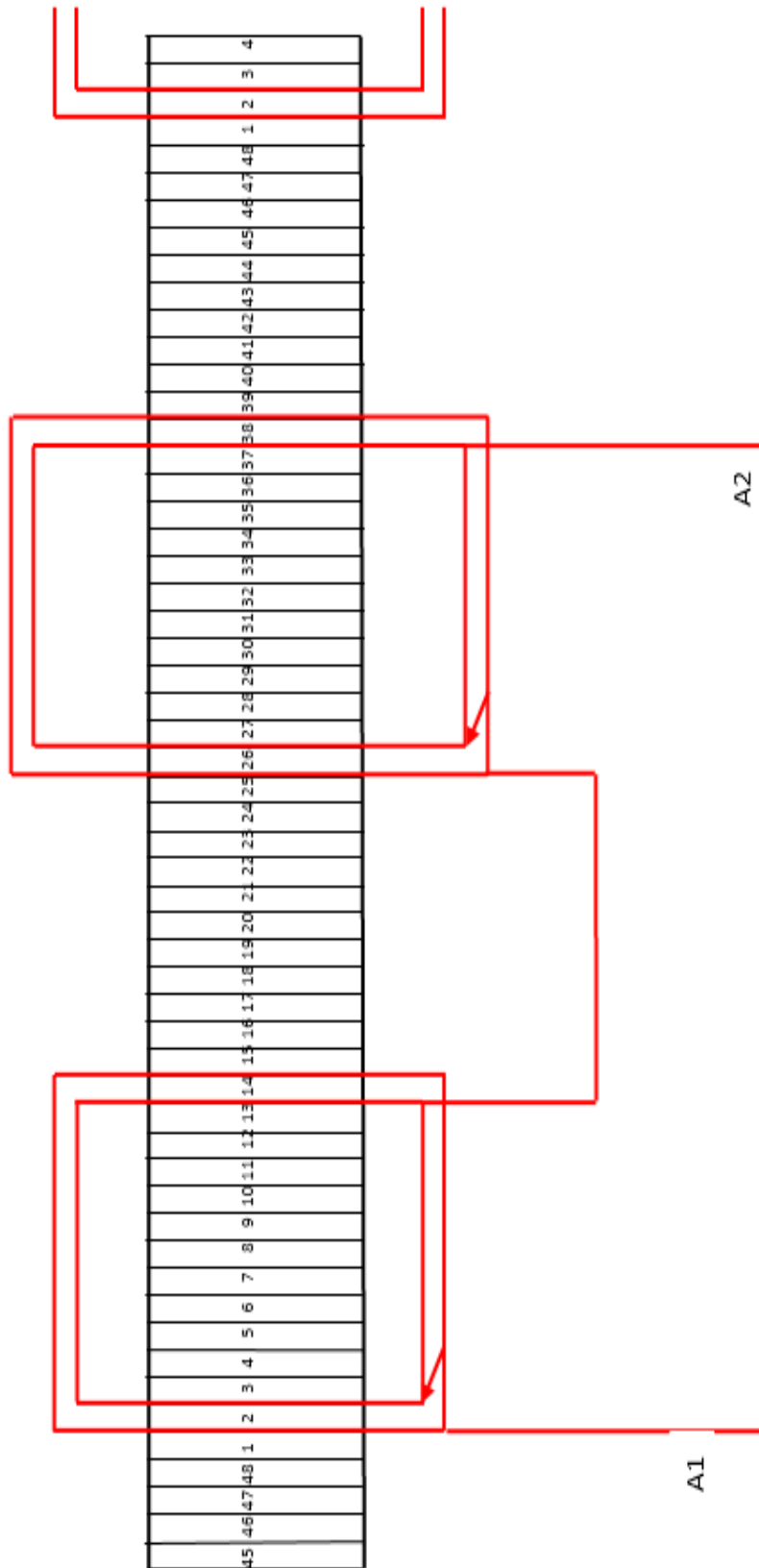
Fig. 3.18 Winding formation of the A phase of the six phase induction motor
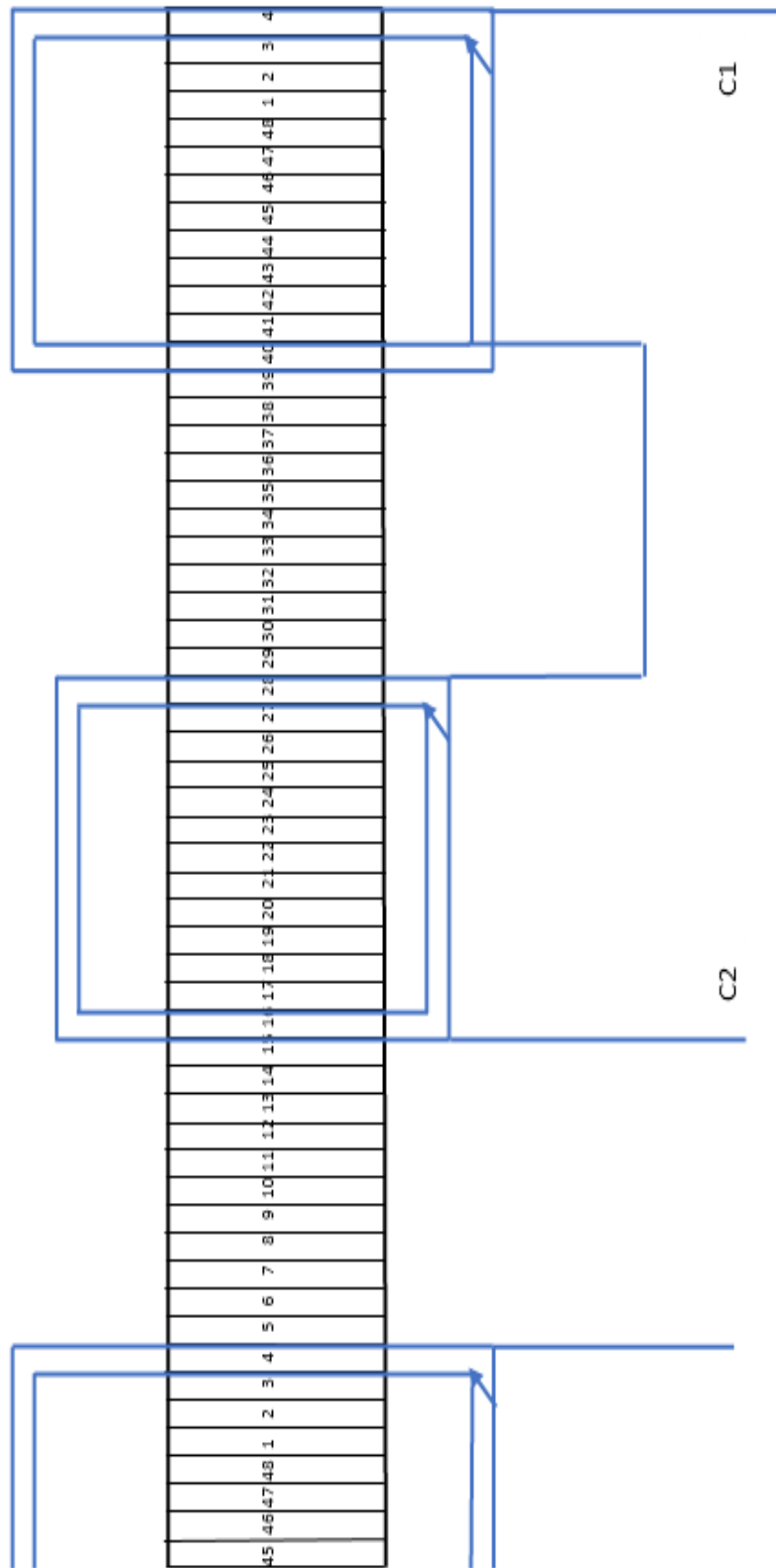
Fig. 3.19 Winding formation of the C phase of the three phase induction motor
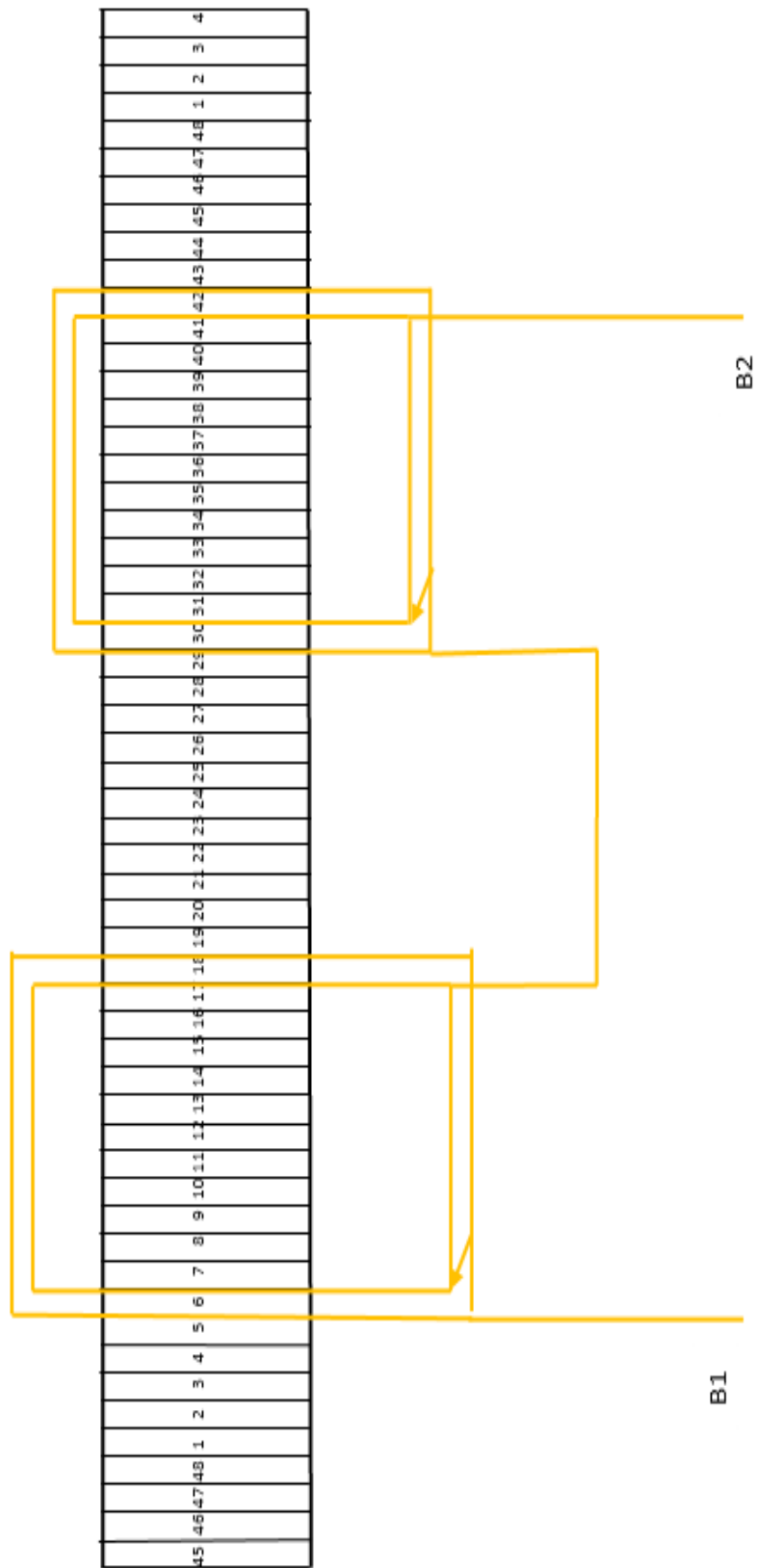
Fig. 3.20 Winding formation of the B phase of the six phase induction motor
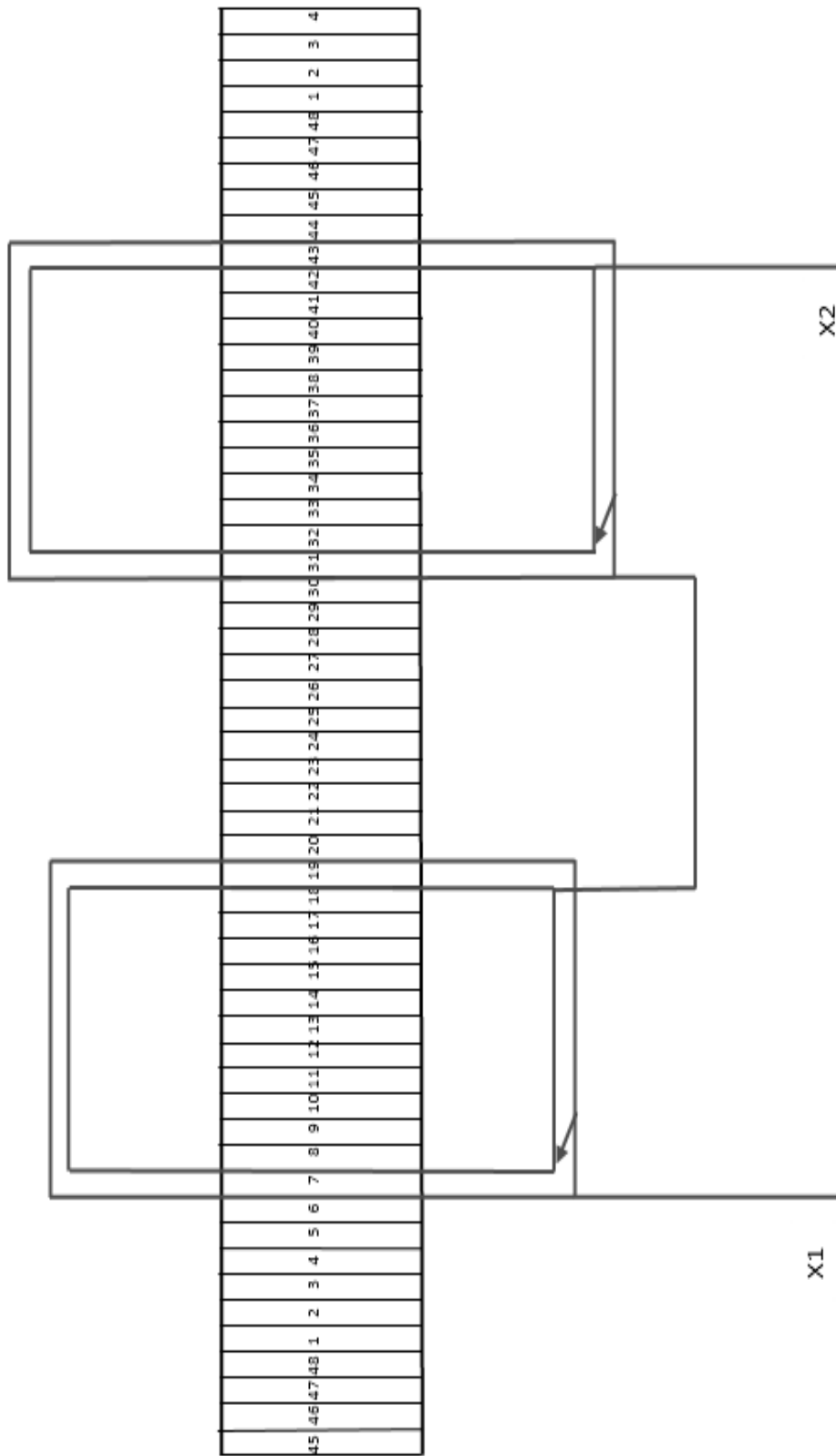
Fig. 3.21 Winding formation of the X phase of the six phase induction motor
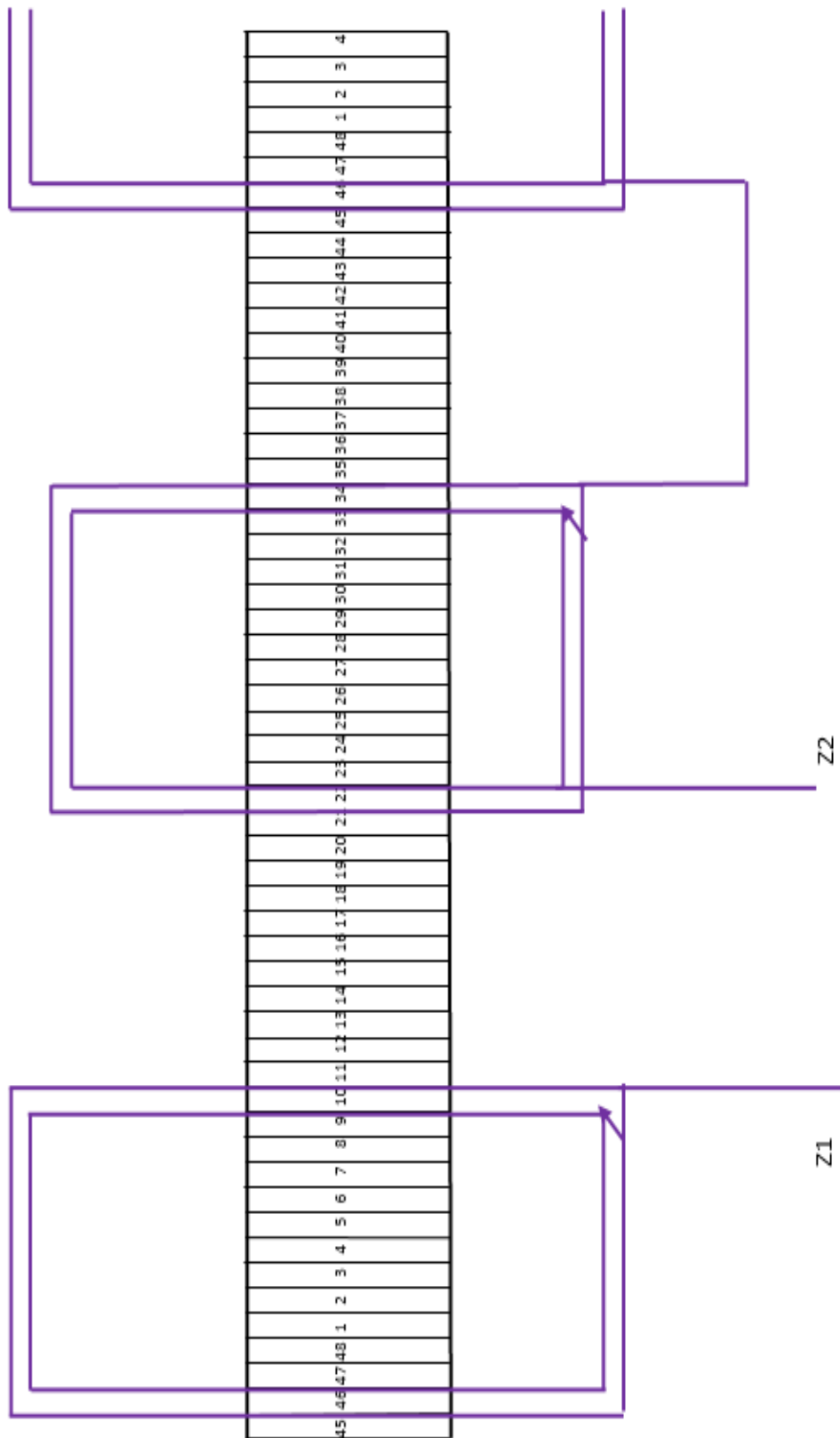
Fig. 3.22 Winding formation of the Z phase of the six phase induction motor
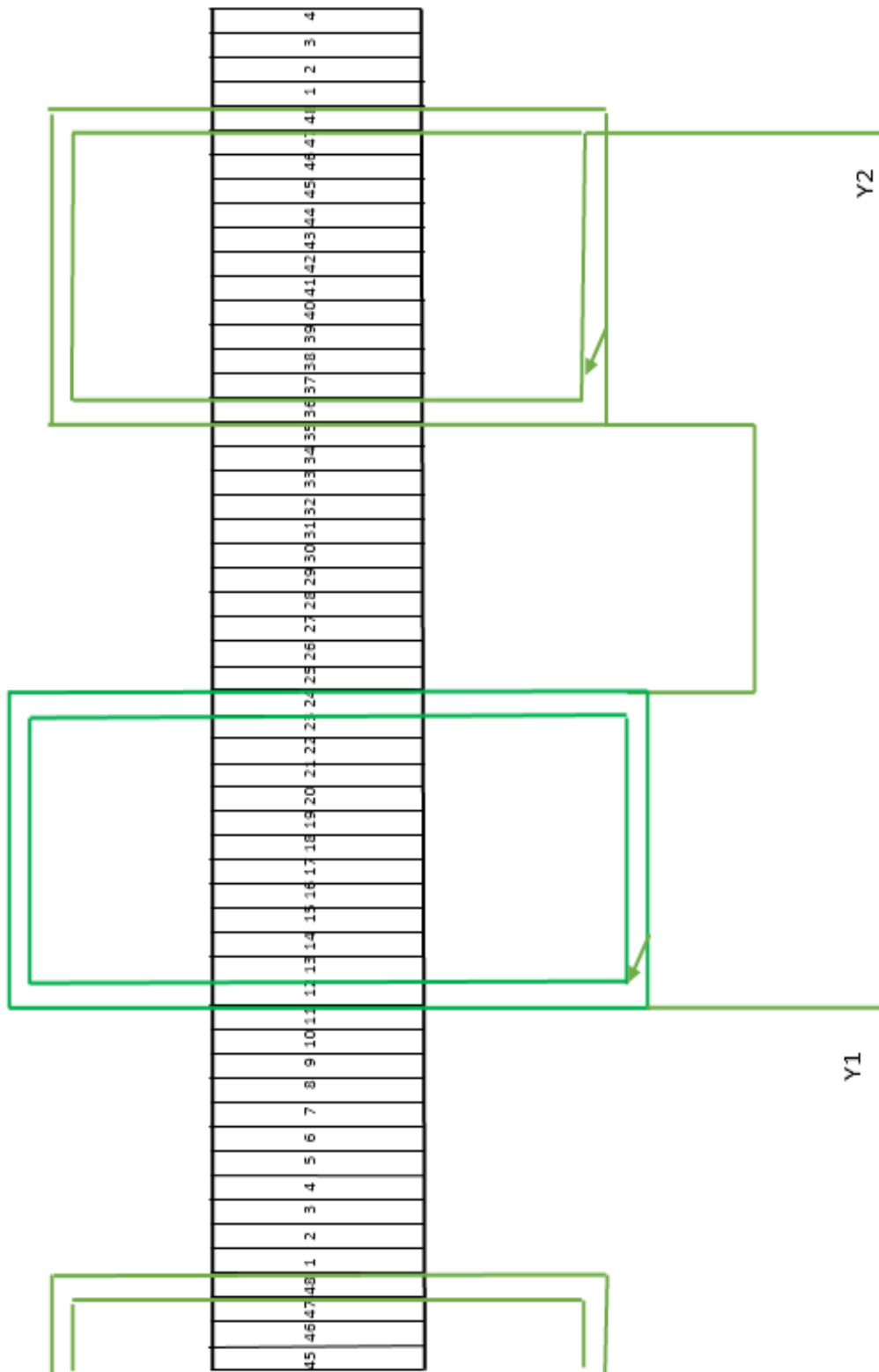
Fig. 3.23 Winding formation of the Y phase of the six phase induction motor
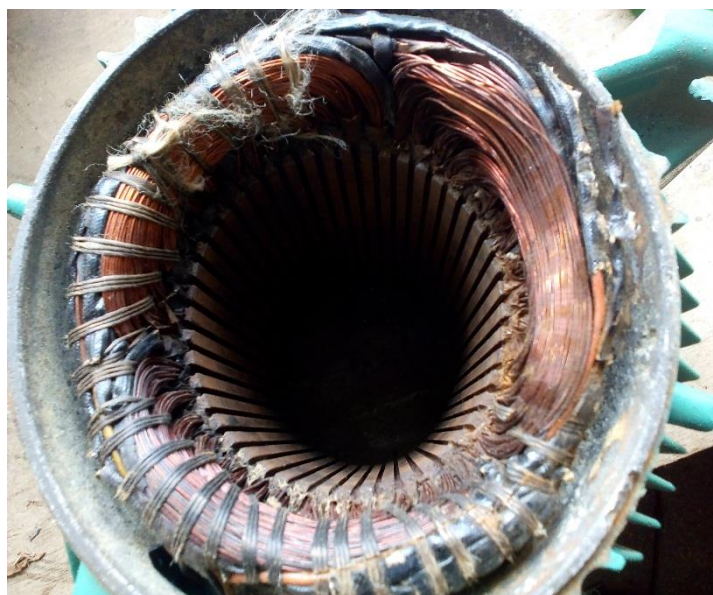
Fig. 3.24 Pictorial view of the original windings of the induction motor

Fig. 3.25 Pictorial view of the stator without the windings

Fig. 3.26 Pictorial view of squirrel cage rotor of the induction motor
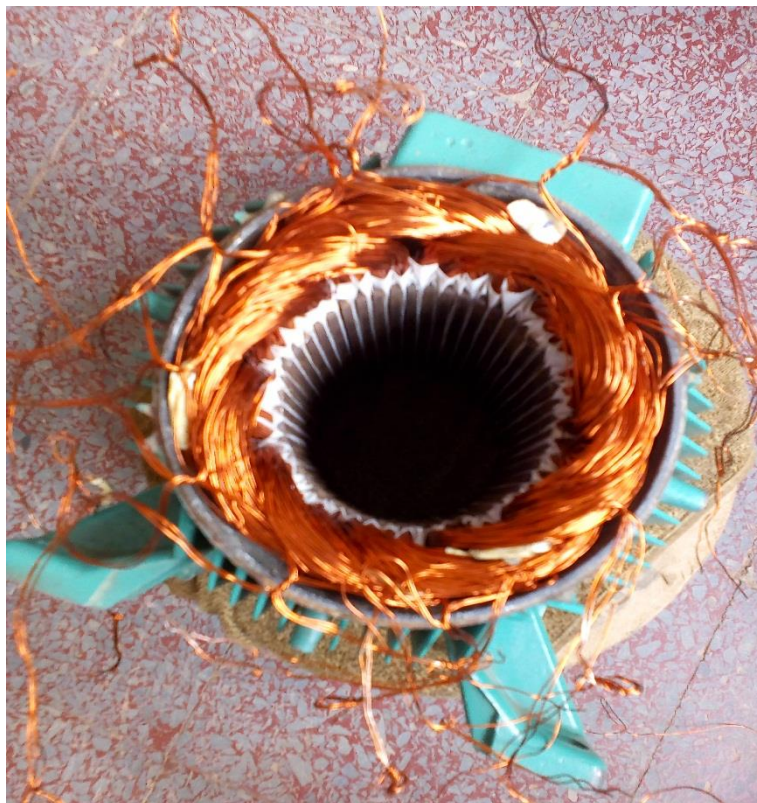
Fig. 3.27 Pictorial view of the stator with re-developed windings
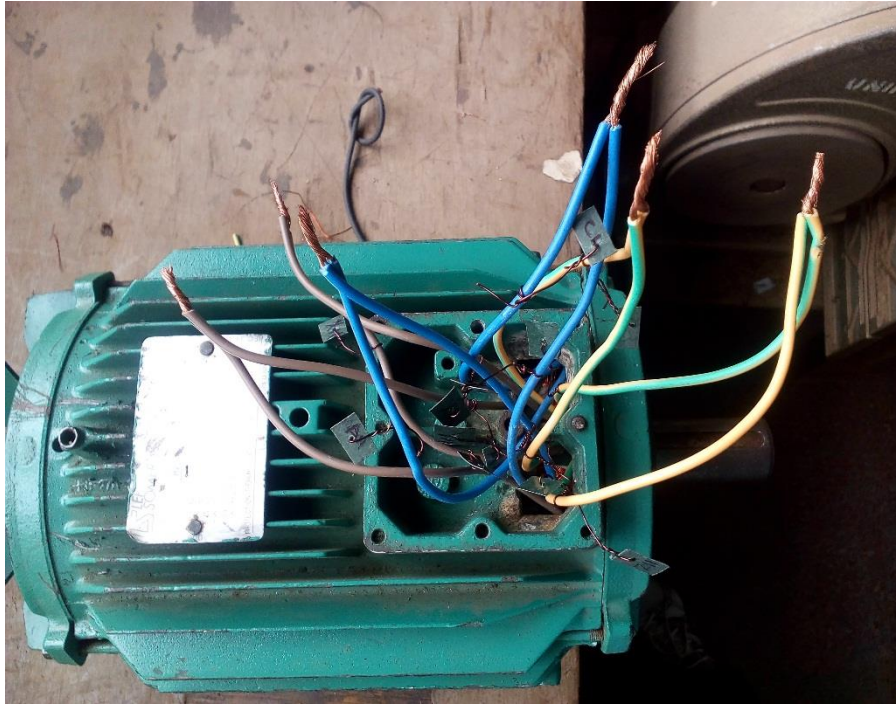
Fig. 3.28 Pictorial view of the completed re-developed induction motor

Fig. 3.29 Pictorial view of the new induction motor with its manufacturer's name

3.11. Dynamic Modeling and Simulation with MATLAB Simulink

The simulation of the developed mathematical model of the SPIM in MATLAB/Simulink is done using *d*- and *q*- reference frames. The multi-phase machine variables are converted into two variables *d*- and *q*- axes. The obtained *d-q* model of the six-phase machine is like that of three-phase machine. The response in terms of stator currents, torque and speed characteristics for the model is also considered (Aher & Thosar, 2016).

3.11.1.   Dynamic Modeling of the SPIM

Among several configurations of multi-phase, a SPIM, whose stator comprises two sets of three-phase coils displaced from each other in an angle, is widely discussed in the literature (Miranda & Gomes, 2012). Fig. 3.30 displays the equivalent circuit model of the asymmetric SPIM. The stator has six-phase split into two sets of symmetrical three-phase winding (with phase shift of 120º) separated by 30º. The rotor being a squirrel cage type can be designed with six or three phases. However, a three-phase equivalent rotor winding is considered in this study.
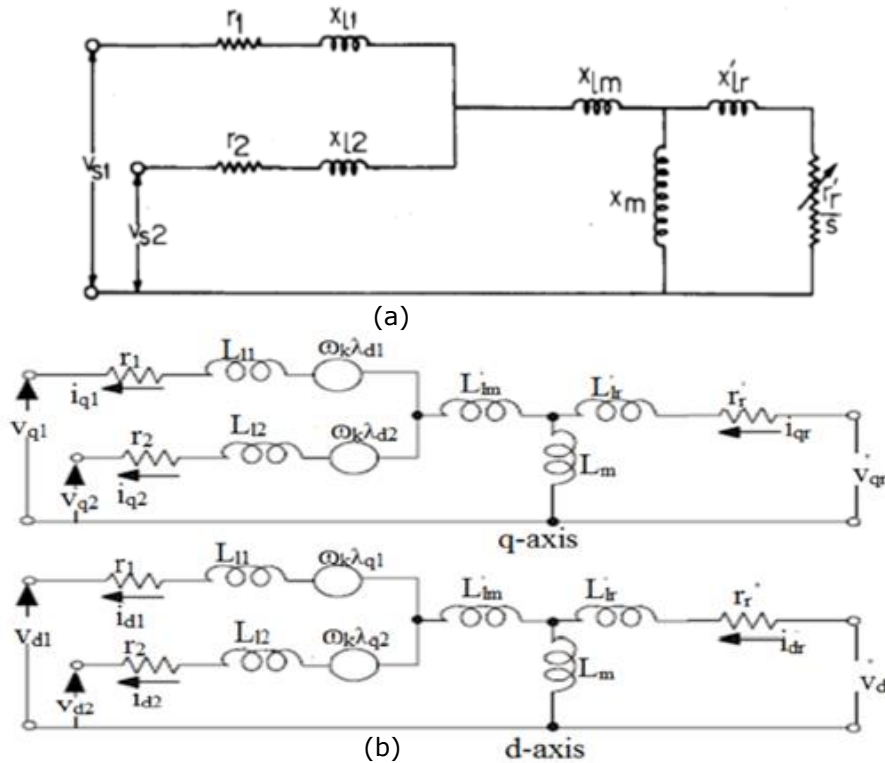
Fig. 3.30 Equivalent circuit model of an asymmetric six phase induction motor

The equivalent circuit diagram of the induction motor considered is shown in Fig. 3.31.
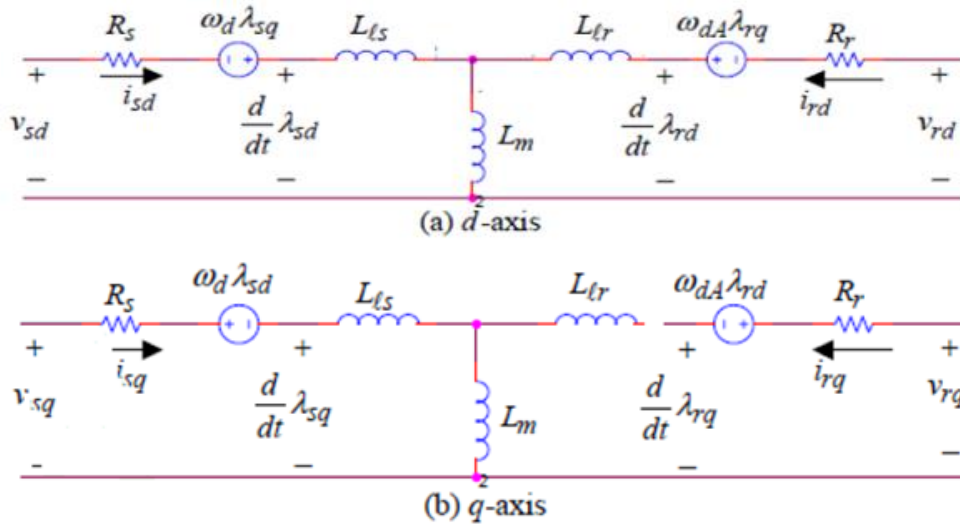
Fig. 3.31 The *d-q* equivalent circuit for an induction motor

The parameters are defined as follow: *d* is the direct axis, *q* is the quadrature axis, *s* is the stator variable, *r* is the rotor variable, λ_{sd}, λ_{sq} are the *d* and *q* axis stator linkage flux, λ_{rd}, λ_{rq} are the *d* and *q* axis rotor linkage flux, V_{sd}, V_{sq} are the *d* and *q* axis stator voltage, V_{rd}, V_{rq} are the *d* and *q* axis rotor voltage, R_s is the stator resistance, R_r is the rotor resistance, X_{Ls} is the stator leakage reactance, X_{Lr} is the rotor leakage reactance, i_{sd}, i_{sq} are *d* and *q* axis stator current, i_{rd}, i_{rq} are *d* and *q* axis rotor current, L_m is the mutual inductance, L_{ls} is the stator leakage inductance, L_{lr} is the rotor leakage inductance, and ω_d, ω_{dA} are the speed of reference frame.

3.11.2.   Mathematical Modeling of the SPIM

The six-phase stator voltage is stated as follows

$$V_a = V_o \cos \omega_o t \tag{3.52}$$

$$V_b = V_o \cos(\omega_o t - \frac{\pi}{3}) \tag{3.53}$$

$$V_c = V_o \cos(\omega_o t - 2 * \frac{\pi}{3}) \tag{3.54}$$

$$V_d = V_o \cos(\omega_o t - 3 * \frac{\pi}{3}) \tag{3.55}$$

$$V_e = V_o \cos(\omega_o t - 4 * \frac{\pi}{3}) \tag{3.56}$$

$$V_f = V_o \cos(\omega_o t - 5 * \frac{\pi}{3}) \tag{3.57}$$

Taking KVL and KCL about Fig. 3.31 (a) & (b) respectively, the mathematical modeling of the machine both for electrical parts and the mechanical parts are presented. The Flux equations are presented as follow:

For Stator

$$\lambda_{sd} = L_s * i_{sd} + L_m * i_{rd} \tag{3.58}$$

$$\lambda_{sq} = L_s * i_{sq} + L_m * i_{rq} \tag{3.59}$$

For Rotor

$$\lambda_{rd} = L_r * i_{rd} + L_m * i_{sd} \tag{3.60}$$

$$\lambda_{rq} = L_r * i_{rq} + L_m * i_{sq} \tag{3.61}$$

The current equations are presented as follow:

For Stator

$$i_{sq} = \frac{1}{X_{Ls}}(\lambda_{sd} - \lambda_{md}) \tag{3.62}$$

$$i_{sq} = \frac{1}{X_{Ls}}(\lambda_{sq} - \lambda_{md}) \tag{3.63}$$

For Rotor

$$i_{rd} = \frac{1}{X_{Lr}}(\lambda_{rd} - \lambda_{md}) \tag{3.64}$$

$$i_{rq} = \frac{1}{X_{Lr}}(\lambda_{rq} - \lambda_{md}) \tag{3.65}$$

The voltage equations are presented as follow:

For Stator

$$V_{sd} = R_s * i_{sd} + \frac{d(\lambda_{sd})}{dt} - \omega_d * \lambda_{sq} \tag{3.66}$$

$$V_{sq} = R_s * i_{sq} + \frac{d(\lambda_{sq})}{dt} - \omega_d * \lambda_{sd} \tag{3.67}$$

For Rotor

$$V_{rd} = R_r * i_{rd} + \frac{d(\lambda_{rd})}{dt} - \omega_{dA} * \lambda_{rq} \tag{3.68}$$

$$V_{rq} = R_r * i_{rq} + \frac{d(\lambda_{rq})}{dt} - \omega_{dA} * \lambda_{rd} \tag{3.69}$$

The Electromagnetic Torque is given as:

$$T_{em} = \frac{p}{2} * L_m(i_{sq} * i_{rd} - i_{sd} * i_{rq}) \tag{3.70}$$

Where, *d* is the direct axis, *q* is the quadrature axis, *s* is the stator variable, *r* is the rotor variable, λ is the flux linkage, V_{sd}, V_{sq} are the *d* and *q* axis stator voltage respectively, V_{rd}, V_{rq} are the *d* and *q* axis rotor voltage respectively, R_s is the stator resistance, R_r is the rotor resistance, X_{Ls} is the stator leakage reactance, X_{Lr} is the rotor leakage reactance, i_{sd}, i_{sq} are the *d* and *q* axis stator current respectively, and i_{rd}, i_{rq} are the *d* and *q* axis rotor current.

3.12. MATLAB/Simulink Implementation

The electrical models (blocks) comprise electrical machines, power electronics switches, voltage and current sources, diverse electric elements, conductors as well as sensors for measurement. The voltage, flux, torque equations and transformation matrices are utilized to realize the model of the SPIM in MATLAB/Simulink. The input to the motor is the six-phase sinusoidal voltage supply. The six-phase to two phase conversion block transfers the six phase stator voltages to *d*- and *q*- axis voltages.

Using Clarke's Transform

$$y = K * u \tag{3.71}$$

$$K = \begin{bmatrix} 1 & 1/2 & -1/2 & -1 & -1/2 & 1/2 \\ 0 & \sqrt{3}/2 & \sqrt{3}/2 & 0 & -\sqrt{3}/2 & -\sqrt{3}/2 \end{bmatrix} \tag{3.72}$$

$$u = \begin{bmatrix} V_a \\ V_b \\ V_c \\ V_d \\ V_e \\ V_f \end{bmatrix} \tag{3.73}$$

$$Scalar = \frac{2}{6}$$

6-phase to DQ: Fig. 3.32 shows the transformation from 6 phase to D-Q model.
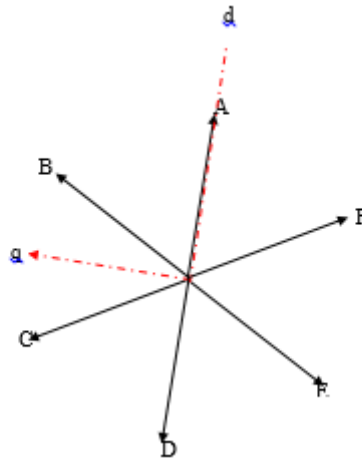
Fig. 3.32 Transformation from 6-phase to D-Q model

Stator flux and rotor flux blocks: The stator flux and rotor flux blocks (Fig. 3.33 and Fig. 3.34) give the flux in direct and quadrature axis using Eq. (3.64) – Eq. (3.69) and implemented in Simulink as Eq. (3.74) – Eq. (3.77) respectively.
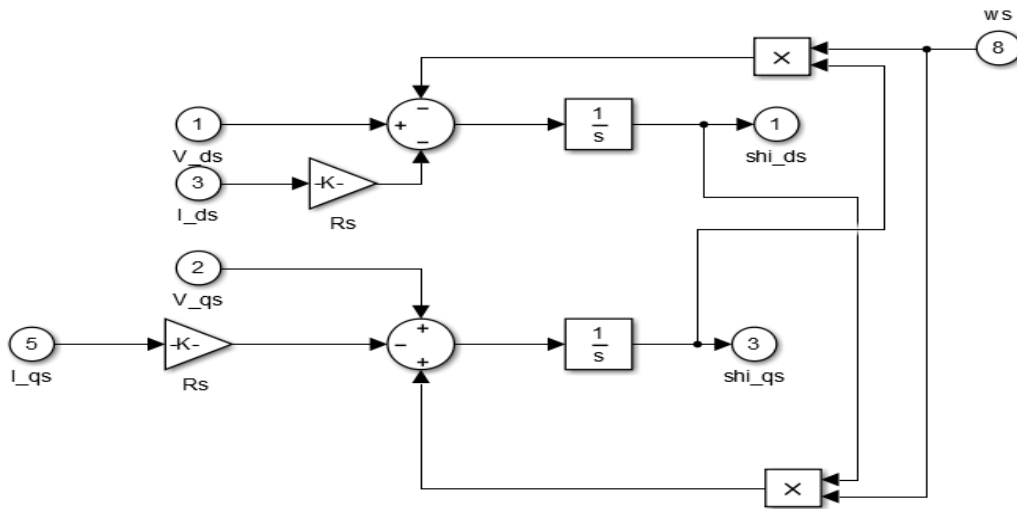
Fig. 3.33 Stator Flux component of the six-phase induction motor simulation

For Stator Flux Block

$$\lambda_{ds} = \int [V_{ds} - I_{ds}.R_s - \omega_d \lambda_{qs}]dt \tag{3.74}$$

$$\lambda_{qs} = \int [V_{qs} - I_{qs}.R_s + \omega_d \lambda_{ds}]dt \tag{3.75}$$

For Rotor Flux Block

$$\lambda_{dr} = \int [-\omega_{dA}.\lambda_{qr} - I_{dr}.R_r]dt \tag{3.76}$$

$$\lambda_{qr} = \int [\omega_{dA}.\lambda_{dr} - I_{qr}.R_r]dt \tag{3.77}$$
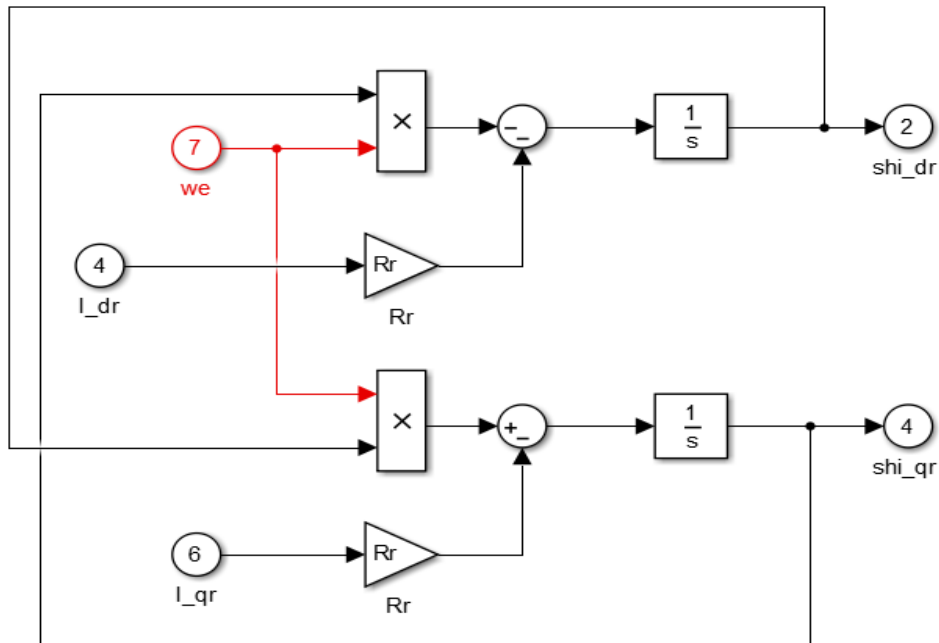
Fig. 3.34 Rotor Flux component of the six-phase induction motor simulation

Mechanical Block: The mechanical components (Fig. 3.35) give the electromagnetic torque and rotor speed using Eq. (3.70) and implemented in Simulink as Eq. (3.78) to Eq. (3.80) respectively.

$$T_e = 3 \times \frac{P}{2} \times L_m \left[I_{qs}.\lambda_{ds} - I_{ds}.\lambda_{qs} \right] \tag{3.78}$$

$$\omega_r = \int \frac{1}{J} [T_e - \tau] \tag{3.79}$$

$$\omega_e = \omega_r \times \frac{P}{2} \tag{3.80}$$

Where, τ is the load torque, T_e is the electromagnetic torque and ω_r is the rotor speed.

(a)

(b)

(c)

Fig. 3.35 Mechanical components of the six-phase induction motor simulation

Flux to d currents: the flux to d current block (Fig. 3.36) gives the d currents using Eq. (3.58) – Eq. (3.61) and implemented in Simulink as Eq. (3.81) and Eq. (3.82).

$$I_{ds} = \frac{1}{\left[L_s - \frac{Lm^2}{Lr}\right]}\left[\lambda_{ds} - \frac{Lm}{Lr}.\lambda_{dr}\right] \qquad (3.81)$$

$$I_{dr} = \frac{1}{\left[L_r - \frac{Lm^2}{Ls}\right]}\left[\lambda_{dr} - \frac{Lm}{Ls}.\lambda_{ds}\right] \qquad (3.82)$$
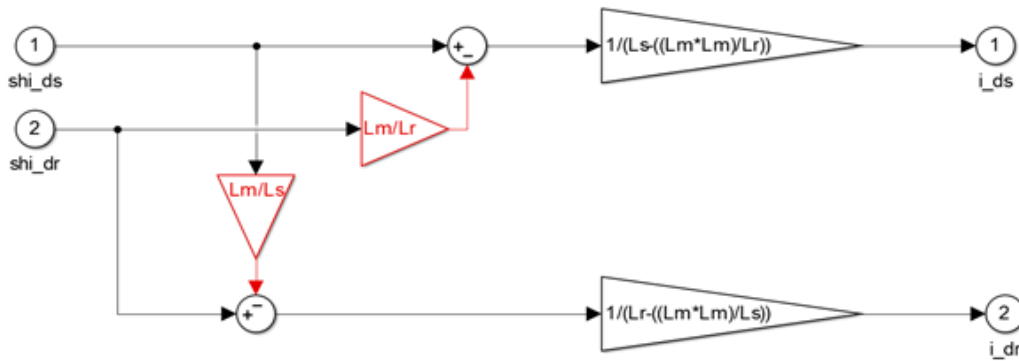
Fig. 3.36 Flux to d-components of the six-phase induction motor simulation

Flux to q currents: the flux to *q* current block (Fig. 3.37) gives the *q* currents using Eq. (3.58) – Eq. (3.61) and implemented in Simulink as Eq. (3.83) and Eq. (3.84).
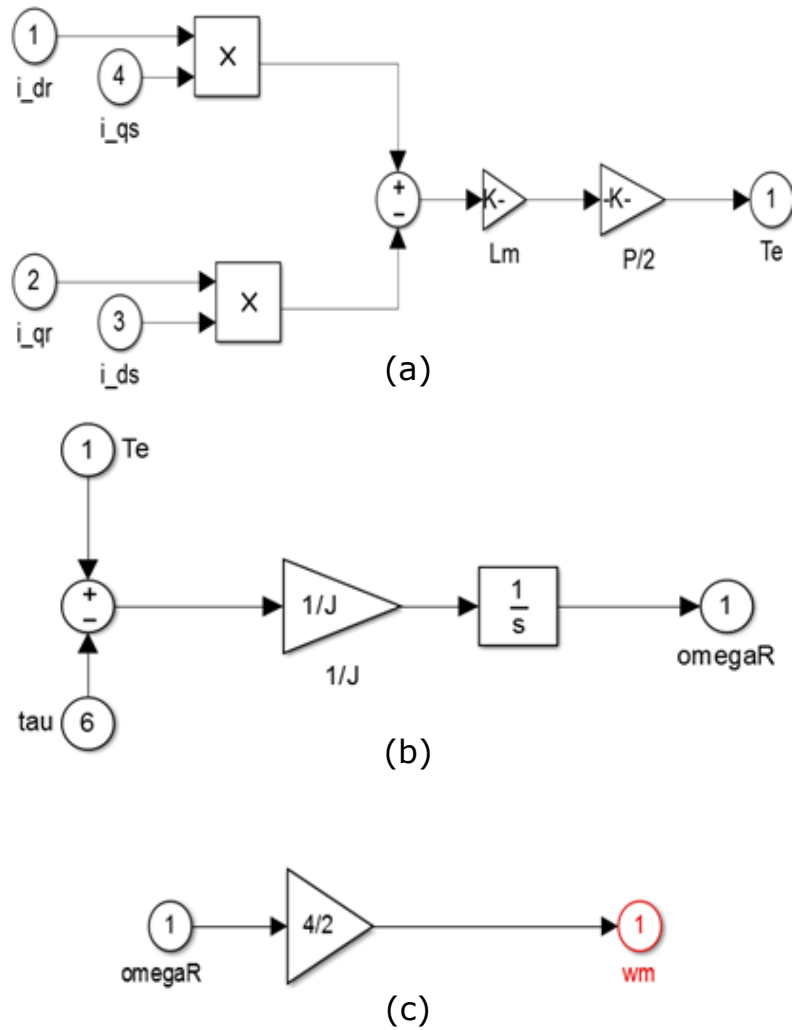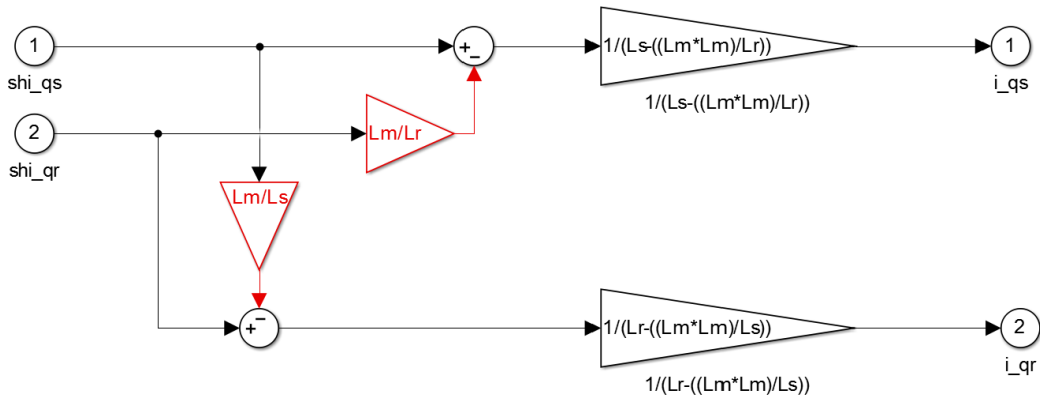

Fig. 3.37 Flux to q-components of the six-phase induction motor simulation

$$I_{qs} = \frac{1}{\left[L_s - \frac{Lm^2}{L_r}\right]}\left[\lambda_{qs} - \frac{L_m}{L_r}.\lambda_{qr}\right] \qquad (3.83)$$

$$I_{qr} = \frac{1}{\left[L_r - \frac{Lm^2}{L_s}\right]}\left[\lambda_{qr} - \frac{L_m}{L_s}.\lambda_{qs}\right] \qquad (3.84)$$

Stator Current dq to abcdef: the stator current block transforms the *d* and *q* component of the stator current back to six phase and it is implemented in Simulink (Fig. 3.38) as Eq. (3.85).
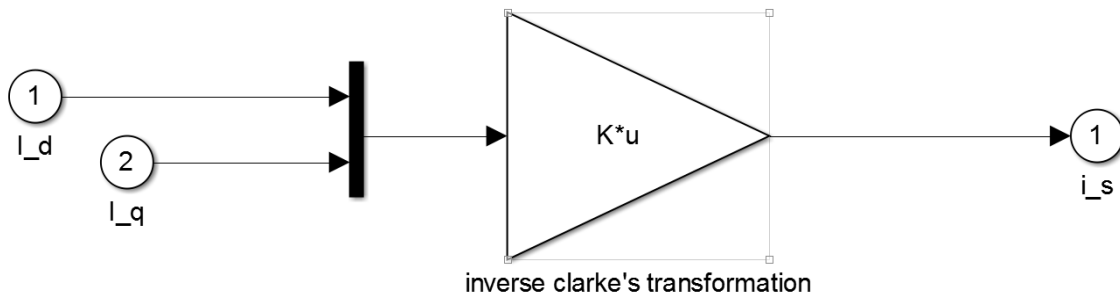
Fig. 3.38 Stator current *dq* to *abcdef* components of the six-phase induction motor simulation model

Applying Inverse Clarke Transform

$$\begin{bmatrix} 1 & 0 \\ 1/2 & \sqrt{3}/2 \\ -1/2 & \sqrt{3}/2 \\ -1 & 0 \\ -1/2 & -\sqrt{3}/2 \\ 1/2 & -\sqrt{3}/2 \end{bmatrix} \begin{bmatrix} I_d \\ I_q \end{bmatrix} = \begin{bmatrix} I_{sa} \\ I_{sb} \\ I_{sc} \\ I_{sd} \\ I_{se} \\ I_{sf} \end{bmatrix} \qquad (3.85)$$

Rotor current dq to abcdef: the rotor current block transforms the *d* and *q* component of the rotor current back to six phase and it is implemented in Simulink (Fig. 3.39) as Eq. (3.86).
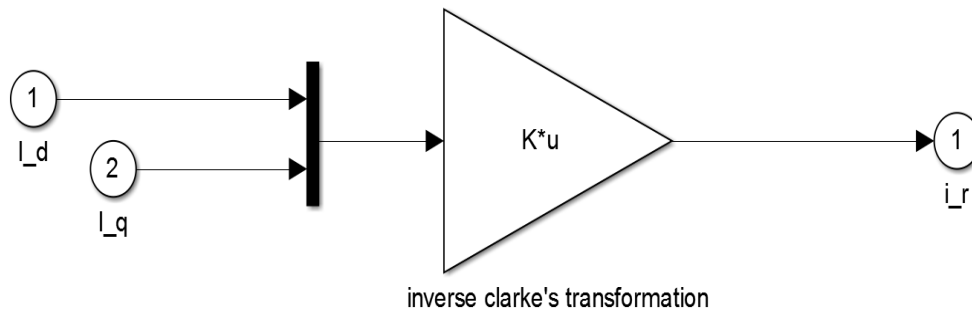
Fig. 3.39 Rotor current *dq* to *abcdef* components of the six-phase induction motor simulation model

$$\begin{bmatrix} 1 & 0 \\ 1/2 & \sqrt{3}/2 \\ -1/2 & \sqrt{3}/2 \\ -1 & 0 \\ -1/2 & -\sqrt{3}/2 \\ 1/2 & -\sqrt{3}/2 \end{bmatrix} \begin{bmatrix} I_d \\ I_q \end{bmatrix} = \begin{bmatrix} I_{ra} \\ I_{rb} \\ I_{rc} \\ I_{rd} \\ I_{re} \\ I_{rf} \end{bmatrix} \qquad (3.86)$$

Fig. 3.40 shows the developed Simulink model of 6-phase induction machine. The assumptions made during the realization and its implementation on MATLAB/Simulink are:

(a) The simulation of the internal structure of six phases induction motor is run assuming no load condition;
(b) The rotor is squirrel caged; and
(c) In the mechanical sub-model of the induction motor considering the torque balance equations, viscous friction was not considered.

Fig. 3.40 Developed Simulink model of SPIM

3.13   Optimization

The quest to optimally design an efficient induction motor gives rise to the use of optimization techniques or algorithms. Optimal design of induction motor suggests the design modification of materials and structure to enhance the efficiency of the motor. An optimization problem involves the establishment of the minimum or maximum value of an objective function, subject to a number of constraints, placed on the variables concerned (Okundamiya, 2015). The optimization methods applied to find an optimal solution to a problem are typically classified as: *deterministic* and *stochastic* methods. Deterministic optimization methods are optimization techniques that converge to a local optimum. The computation of the approximations or derivatives for the derivatives is one of the examples of a deterministic optimization. Stochastic methods use random numbers in addition to certain search strategy to obtain the global optimum. Examples are search algorithm and simulated annealing. The increase in the computational powers of most computers, in modern times, has made it possible to use the stochastic method more effectively in optimization problems especially in machine design.

The design of induction motors is a non-linear optimization problem with non-linear constraint and can be expressed as:

$$\min F(x) \tag{3.87}$$

$$g_i(x) \leq 0, i = 1, \dots I \tag{3.88}$$

x is an *n* dimensional design vector fitting to a feasible domain: $\Omega \subset R^n$. $F(x)$ is the objective function and $g_i(x)$ is called the ith constraint function.

Optimization tries to determine a set of local optimum or global optimum for the problem that would not violate the constraint to a great extent. To maximize the objective function with the same algorithm, only change the sign from $F \rightarrow -F$ is required.

3.13.1. Optimization techniques

Evolutionary Algorithms (EAs): Evolutionary algorithm is a concept that includes a wide group of optimization techniques for the resolution of complex problems through emulating the natural process of evolution. Among the EAs, differential evolution (DE) and genetic algorithm (GA) have been effectively utilized in the design of induction motor. Genetic algorithms and differential evolution have gained ground in solving optimization problems today because they have become an efficient method or technique in finding solutions to nonlinear problems. All these methods are stochastic and they usually require more iterations, but being meta-heuristics, they have a high probability of finding the optimal solution to a problem.

3.13.2.   Optimal Design of the Six-Phase Induction Motor

The mathematical formulation of the weight of material, W_m of the SPIM is similar to that of a 3-phase induction motor. The total weight of iron used is given as (Amayo, 2015):

$$W_{fe} = \rho_{fe}L(\frac{\pi}{4}\left(D_o{}^2 - (D_o - 2d_{sc})^2\right) + S_s w_{st}d_{ss} + \frac{\pi}{4}(D^2 - (D - 2d_{sc})^2) + S_r w_{rt}d_{rs} \qquad (3.89)$$

Where, ρ_{fe} is the resistivity of Iron, L is the length of stator, D is the bore diameter of stator, D_o is the diameter of stator, d_{sc} is the diameter of stator core, is the diameter of stator slot, d_{rs} is the diameter of rotor slot, w_{st} is the width of stator teeth, w_{rt} is the width of rotor teeth, S_s is the number of stator slot, and S_r is the number of rotor slot.

And the total weight of copper, W_{cu} (stator winding and rotor bars including end rings) is given as follows:

$$W_{cu} = \rho_{cu}(\frac{NIm}{J}\left(2L + \frac{2.3\pi D}{p} + 0.24\right) + S_r A_{bar}(L + 2l_{bext}) + 2A_e \pi D_e) \qquad (3.90)$$

Thus, the total weight of the material is:

$$W_T = W_{fe} + W_{cu} \qquad (3.91)$$

$$W_T = \rho_{fe}L(\frac{\pi}{4}\left(D_o{}^2 - (D_o - 2d_{sc})^2\right) + S_s w_{st}d_{ss} + \frac{\pi}{4}(D^2 - (D - 2d_{sc})^2) +$$

$$S_r w_{rt}d_{rs} + \rho_{cu}(\frac{NIm}{J}\left(2L + \frac{2.3\pi D}{p} + 0.24\right) +$$

$$S_r A_{bar}\left(L + 2l_{bar}\right) + \quad 2A_e \pi D_e) \qquad (3.92)$$

Where, ρ_{cu} is the resistivity of copper, D_e is the diameter of end ring of rotor, N is the number of turns, I is the current, m is the number of phase, J is the current density, p is the number of poles, A_{bar} is the cross-sectional area of rotor bar, l_{bar} is the length of rotor bar, and A_e is the area of end ring of rotor.

CHAPTER FOUR
MATLAB/SIMULINK RESULTS AND DISCUSSION

4.1. Induction Motor Model in MATLAB/Simulink

The simplified electrical sub-model of the induction motors, the three-axis to two-axis voltage transformation, achieved using the equations:

$$V_a = V_o \cos \omega_o t \tag{4.1}$$

$$V_b = V_o \cos(\omega_o t - 2 * \tfrac{\pi}{3} \tag{4.2}$$

$$V_c = V_o \cos(\omega_o t - 4 * \tfrac{\pi}{3} \tag{4.3}$$

$$V_{sd} = R_s * i_{sd} + \tfrac{d(\lambda_{sd})}{dt} - \omega_d * \lambda_{sq} \tag{4.4}$$

$$V_{sq} = R_s * i_{sq} + \tfrac{d(\lambda_{sq})}{dt} - \omega_d * \lambda_{sd} \tag{4.5}$$

V_a, V_b and V_c are three-phase stator voltages while V_{sd} and V_{sq} are the two-axis components of the stator voltage vector.

The mathematical model given in this research implemented in MATLAB/Simulink is designed for the machine having the ratings as given in Table 4.1. The machine is 5-hp, 220V, 50Hz, 4-pole squirrel cage induction motor. The machine parameters used for modeling are given in Table 4.2. The stator and rotor resistances in Table 4.2 are for fundamental sequence.

Table 4.1 Machine rating (Name plate)

Parameters	Values
Rated phase voltage	415 V
Rated Phase Current	8.9 A
Rated Power	5 hp
Number of Poles	4
Rated Frequency	50 Hz
Rated Speed	1430 rpm

Table 4.2 Machine parameters

Parameters	Values
Stator Resistance, R_s	7.58 Ω
Rotor Resistance, R_r	6.3 Ω
Mutual Leakage Inductance, L_m	0.0265 mH
Stator Leakage Inductance, L_s	0.5976 mH
Rotor Leakage Inductance, L_r	0.1612 mH
Rotor Inertia, J	0.0054 Kg-m^2

The simulation results obtained from the MATLAB/Simulink are shown in Fig. 4.1 to Fig. 4.8. The typical behavior of the SPIM is observed. The design parameters are:

1   Stator Resistance, R_s (Ohms)
2   Stator Inductance, L_s (Henry)
3   Rotor Resistance, R_r (Ohms)
4   Rotor Inductance, L_r (Henry)
5   Mutual Inductance, L_m (Henry)
6   Rotor Inertia, J (Kg-m^2)
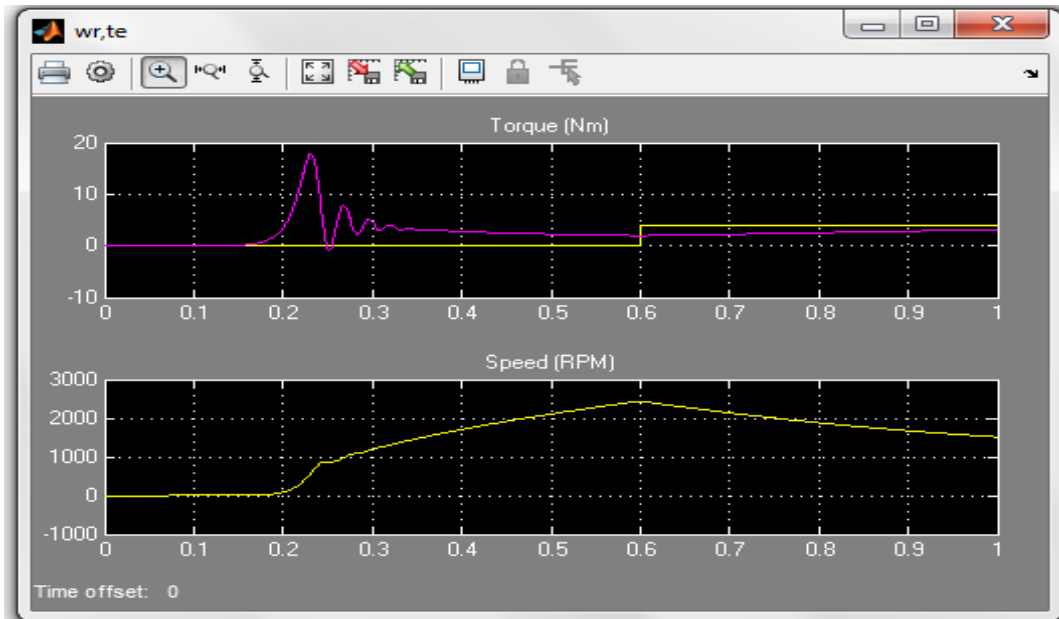7   No of poles

Fig. 4.1 Torque and speed characteristic of the machine
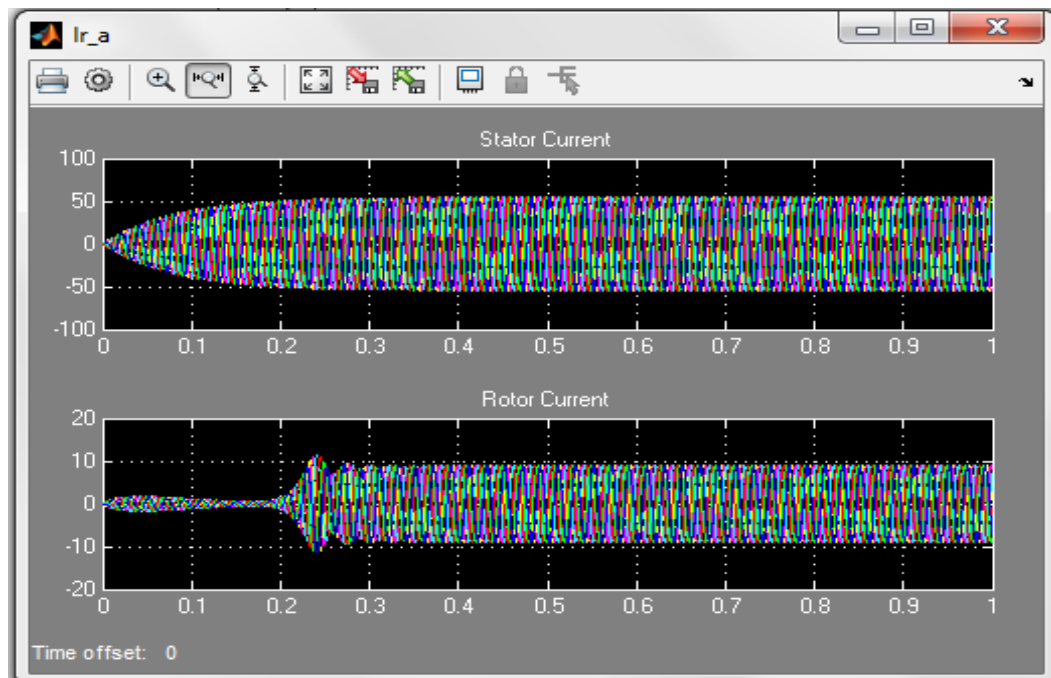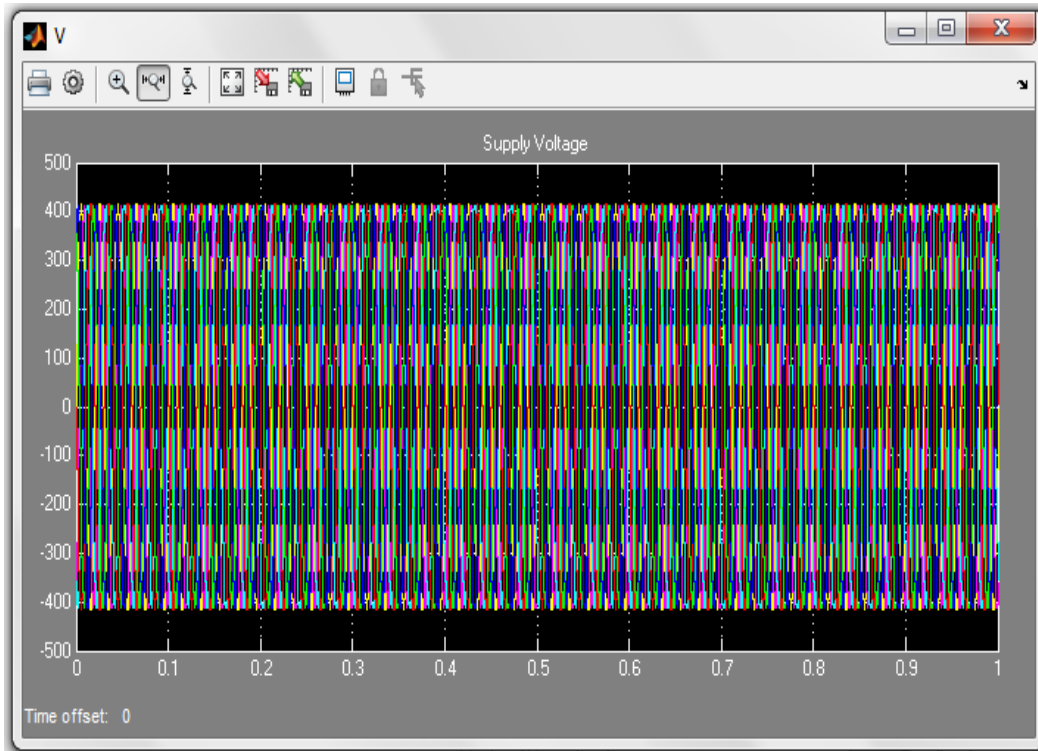

Fig. 4.2 Stator and rotor currents

Fig. 4.3 Six-phase supply voltage

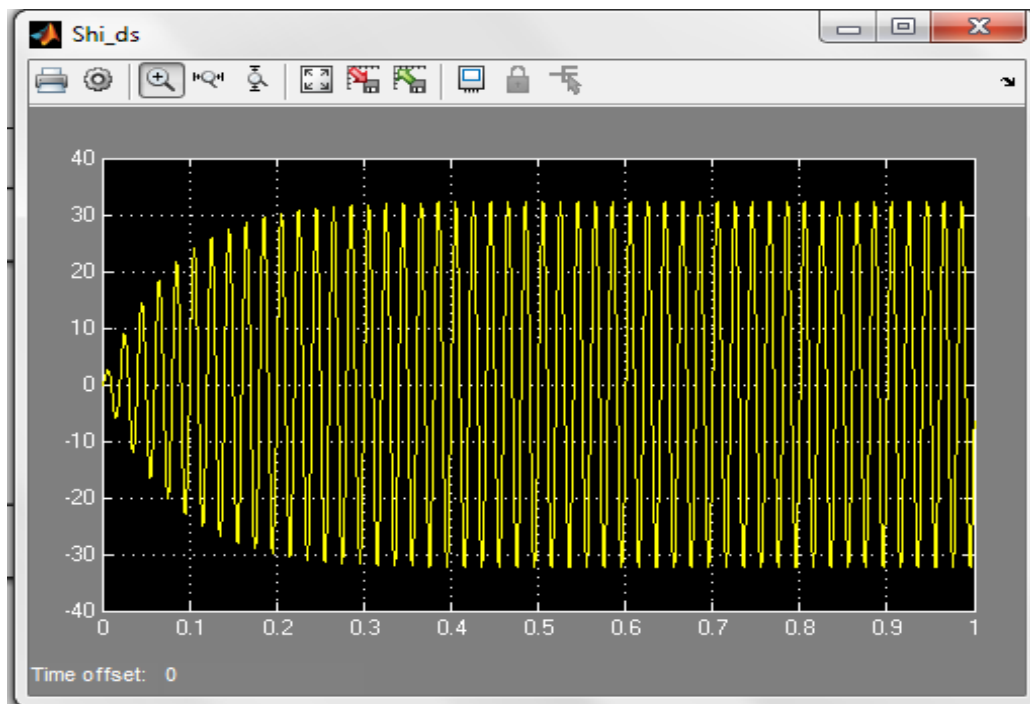**Fig. 4.4** Stator flux in *d* axis
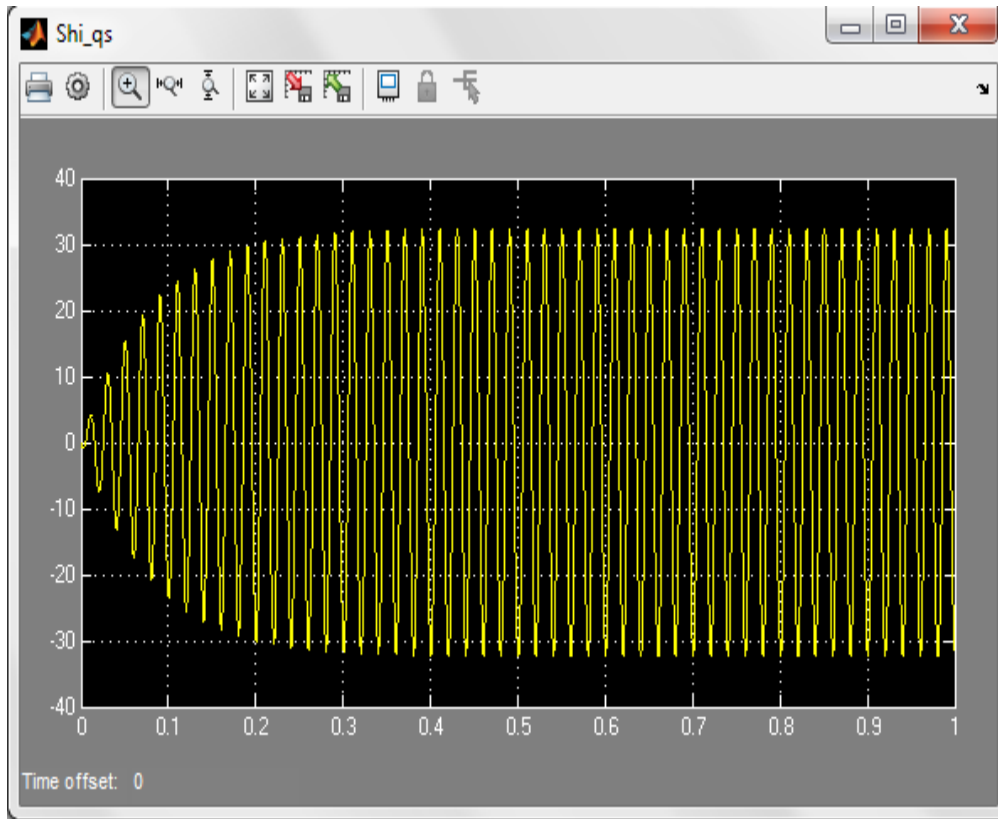
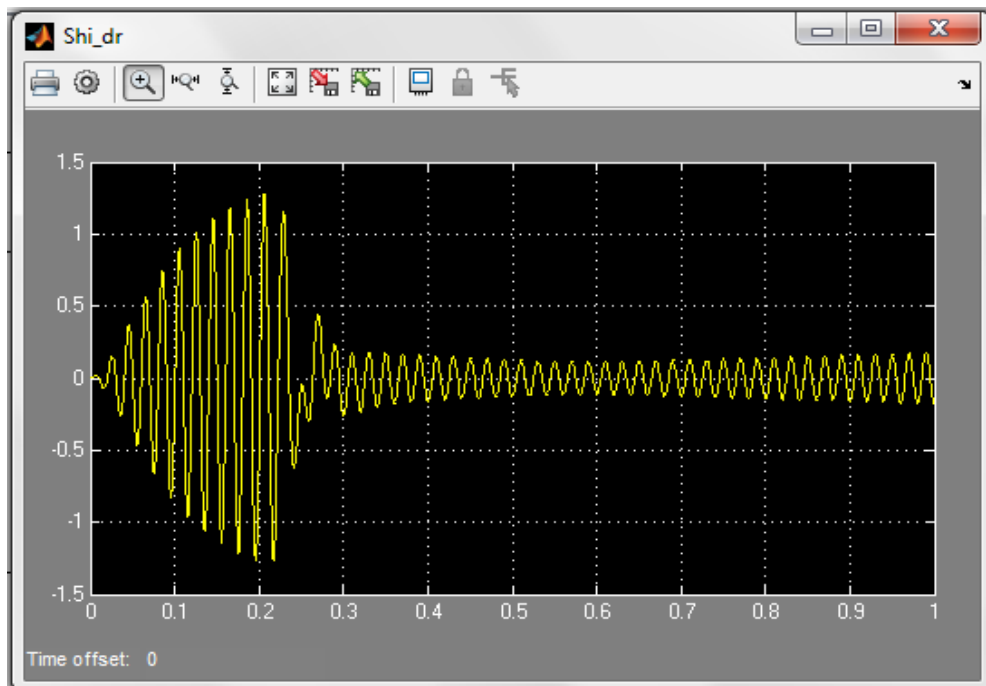**Fig. 4.5** Stator flux in *q* axis

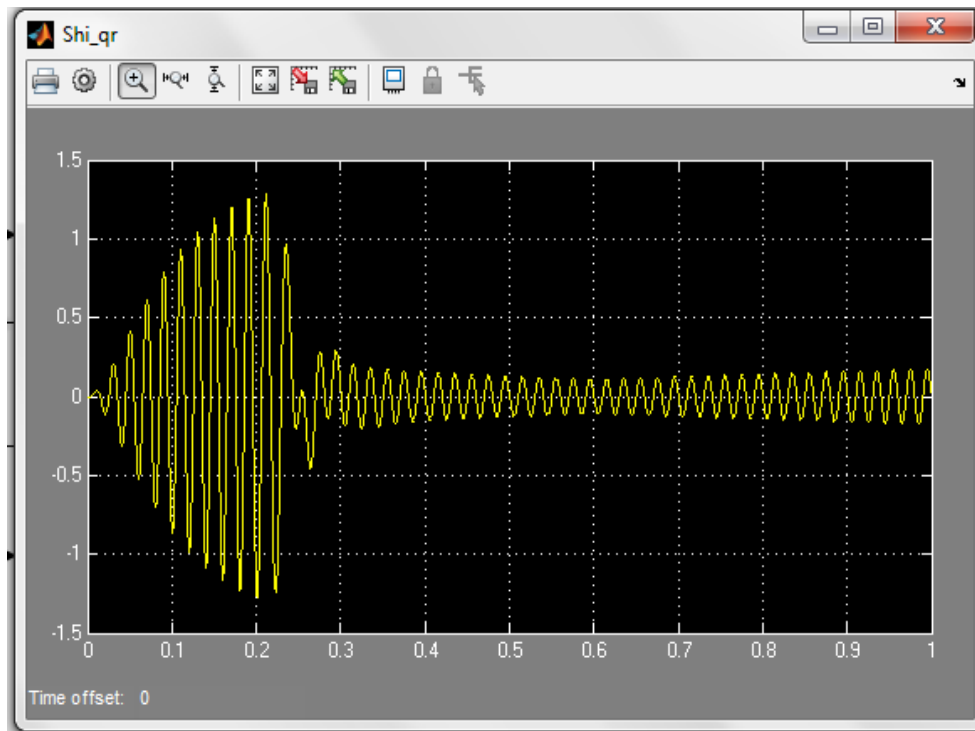**Fig. 4.6** Rotor flux in *d* axis
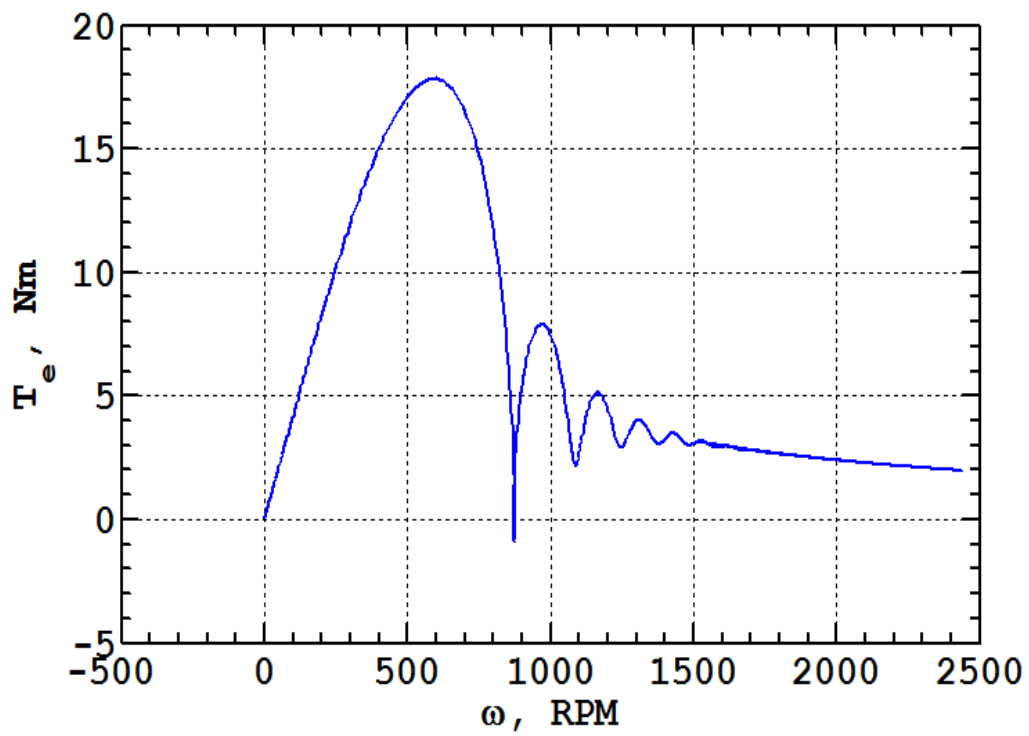
Fig. 4.7 Rotor flux in *q* axis

Fig. 4.8 Torque versus speed characteristics

4.2.   Simulation of SPIM under different Phase Loss Conditions

As shown in Fig. 4.9, the phase loss scenarios in this study are, 3-phase operation with a loss of three phases, 4-phase operation with a loss of two phases and 5-phase operation with a loss of one phase. Besides, the 3-phase and 4-phase operations, in which three or two phases are taken out of service, were investigated under conditions with the loss of adjacent phases or alternately the loss of two or more phases that are non-adjacent to each other.
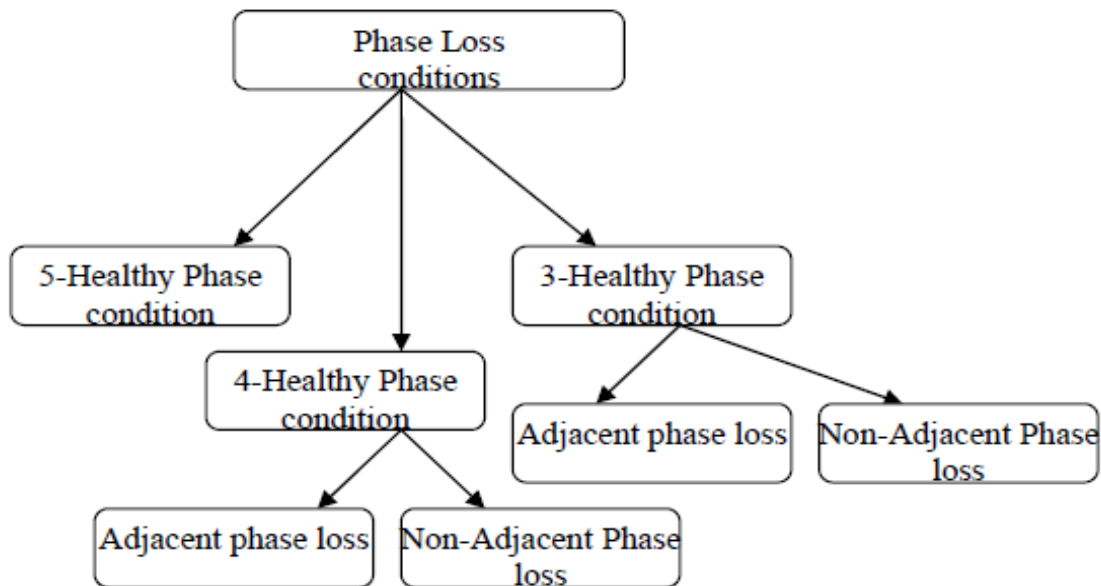

Fig. 4.9 Schematics of phase loss scenarios investigated

Fig. 4.10 displays the Simulink model of the six-phase induction model. The Loss in each phase is modeled by placing a switch on each supply source. The effect on the system torque is measured by the Total Harmonic Distortion (THD) on the torque. This is analyzed using the spectrum analyzer.
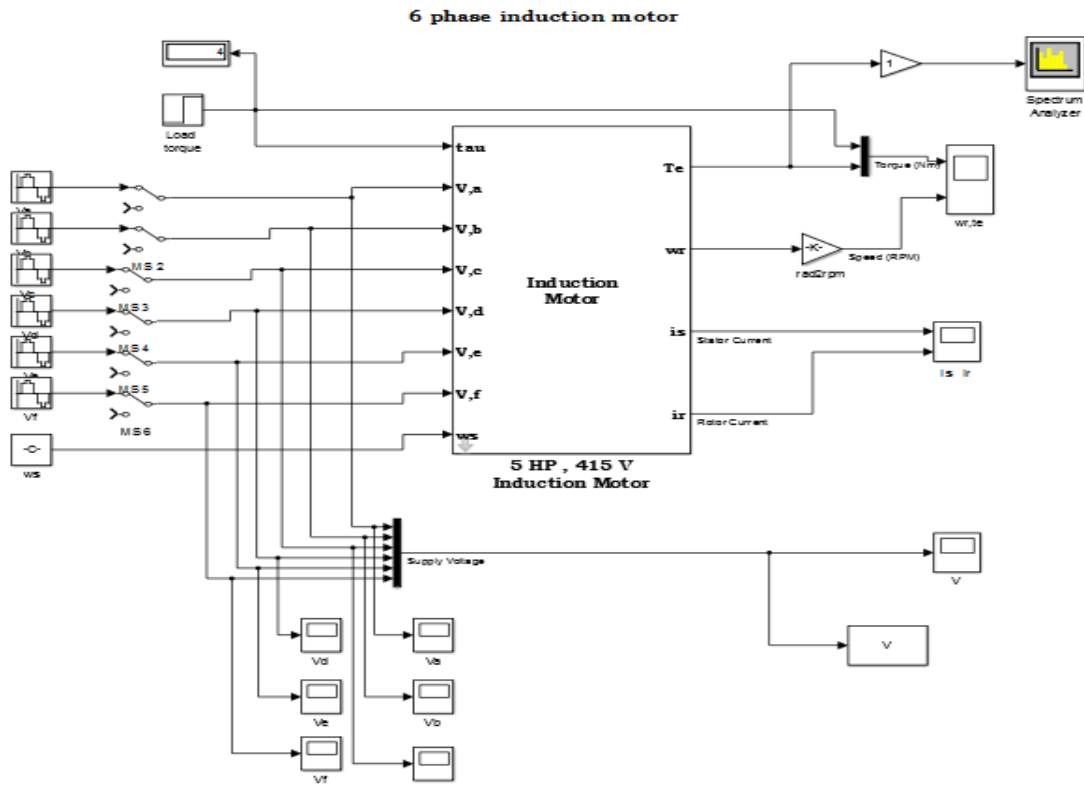
Fig. 4.10 Simulink model of 6 phase induction machine for phase loss operation

4.2.1. Operation of 1-Faulty Phase and 5-Healthy Phase

In this case, the six-phase motor is simulation on Simulink is with the loss of one phase (phase A). Fig. 4.11 and Fig. 4.12 display the phasor voltage diagrams for the different scenarios. The corresponding torque-speed characteristics are compared in Figs. 4.13 and 4.14, respectively. Similarly, the phase currents in the 6-phase healthy and 5-phase healthy with one faulty phase are depicted in Fig. 4.15 and Fig. 4.16 respectively. Fig. 4.17 and Fig. 4.18 also show the distortion measurement of the faulty case as compared with the 6-phase healthy case.
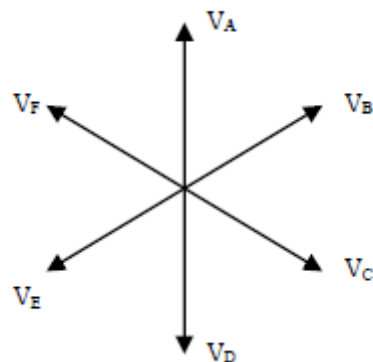

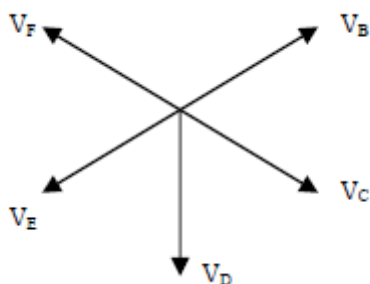**Fig. 4.11** Phasor representation of the voltages in the healthy six-phase operation

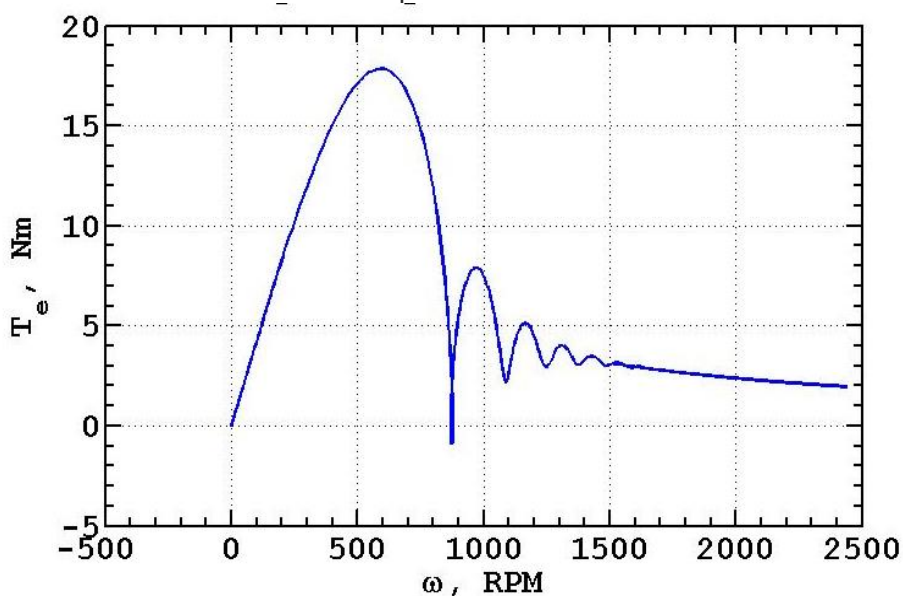**Fig. 4.12** Phasor representation of the voltages in the faulty operation with loss of phase A

Fig. 4.13 Torque versus speed characteristics of healthy six-phase operation
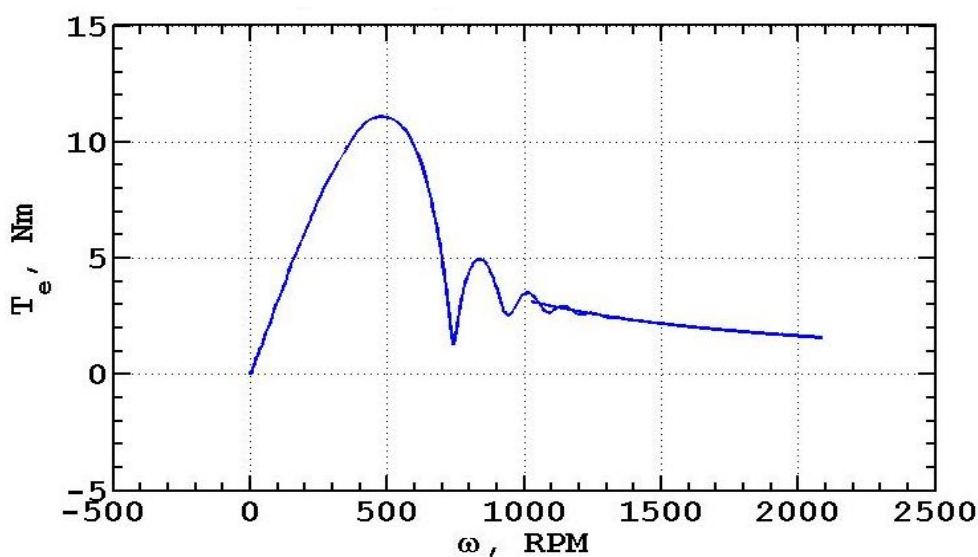

Fig. 4.14 Torque versus speed characteristics of 5-phase operation with loss of phase A
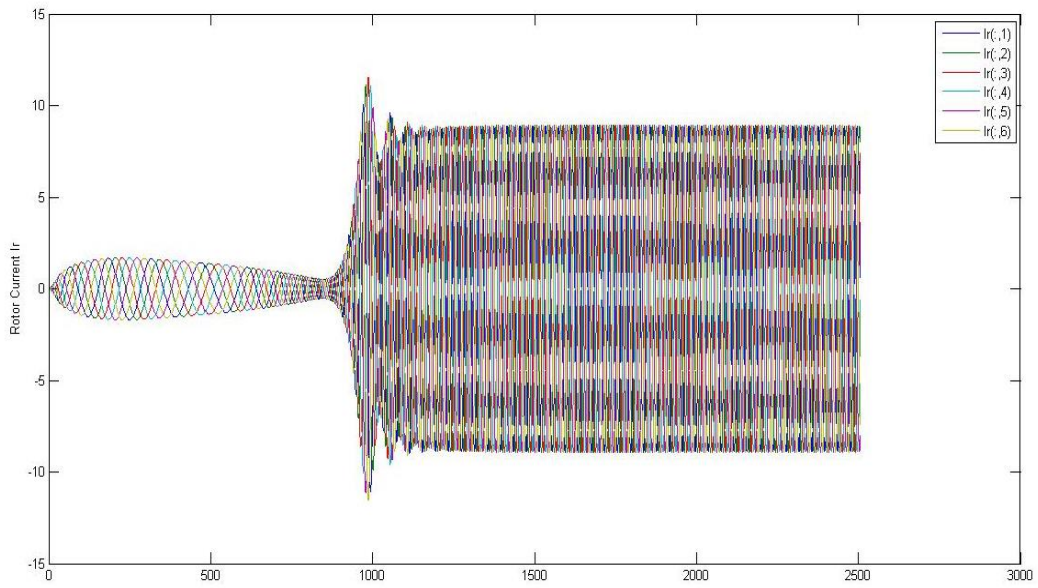
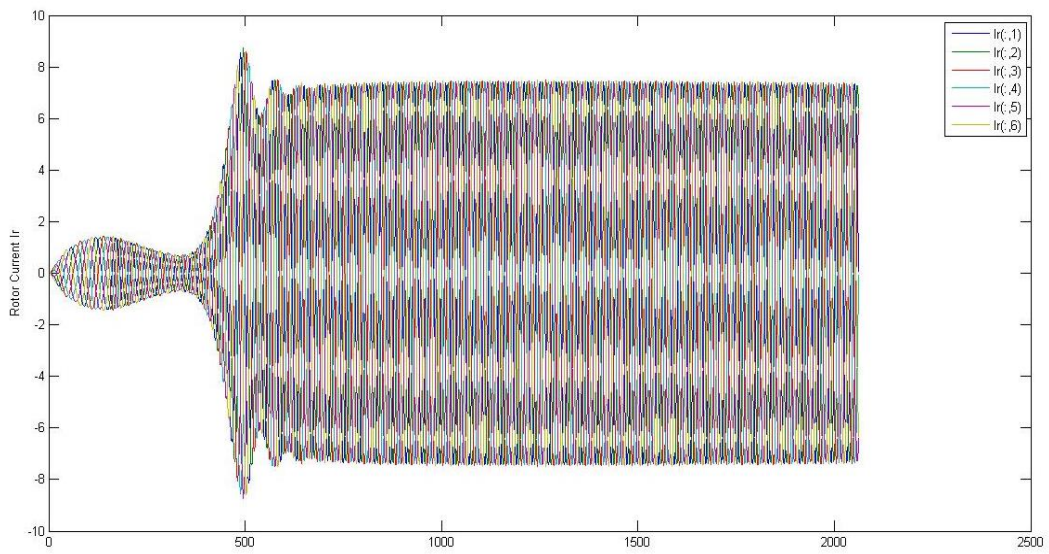**Fig. 4.15** Phase currents of healthy six-phase operation

Fig. 4.16 Phase currents of 5 healthy phase operation with loss of phase A
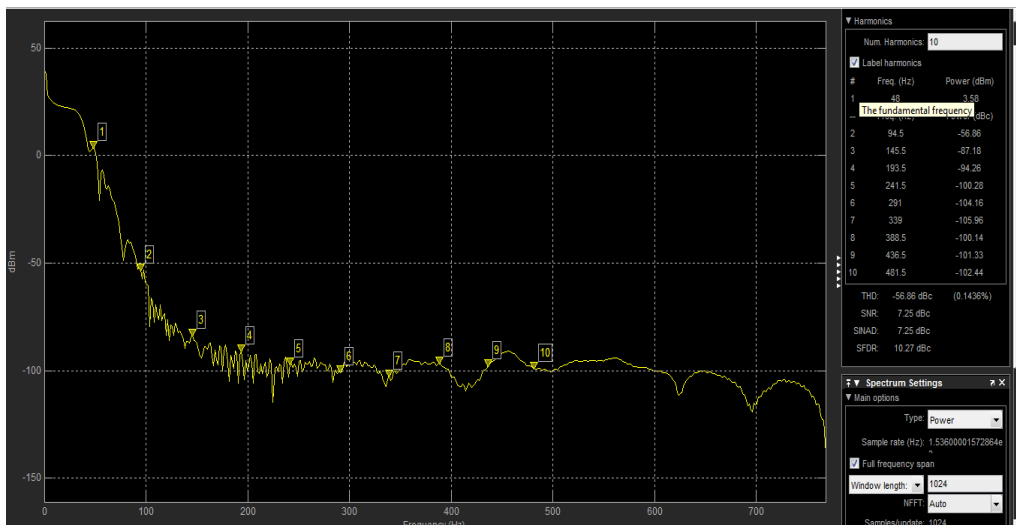
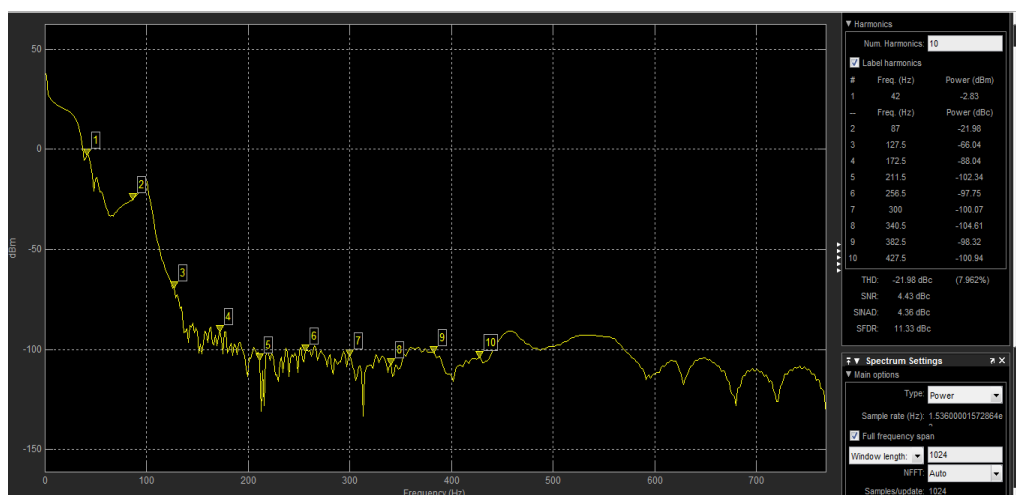**Fig. 4.17** Distortion measurement for healthy six-phase operation

Fig. 4.18 Distortion measurement for 5 healthy phase operation with loss of phase A

The analysis of Fig 4.18, shows the THD content of resulting torque is -21.98dBm with the 5- healthy phases and one faulty phase case as compared with -56.86dBm THD in the healthy six-phase case. Also, there is a slight reduction of the fundamental frequency from 48Hz to 42Hz.

4.2.2. Operation of Two-Faulty Phase and Four-Healthy Phase

Fig. 4.19 summarizes the operation of the two faulty phase and four-healthy phase considered in this study.
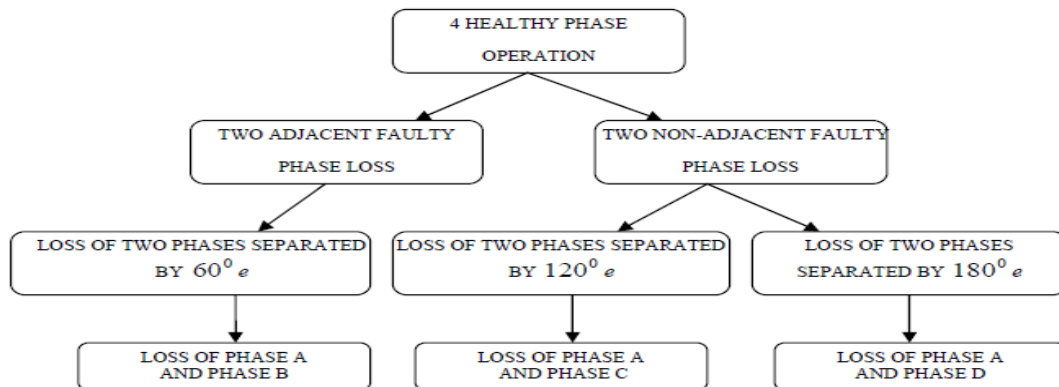
Fig. 4.19 Illustration of different cases of 4-phase operations investigated

Loss of Two Adjacent Phases

Under this scenario, the loss of adjacent phases (A and B) are considered. Figs. 4.20 and 4.21 illustrate the phasor voltages in the healthy and the faulty (with loss of phase A and phase B) cases respectively. The corresponding torque-speed characteristics are compared in Figs. 4.22 and 4.23, respectively. Similarly, the phase currents in the 6-phase healthy and the faulty (with loss of phase A and phase B) are shown Fig. 4.24 and Fig. 4.25 respectively. These figures are accompanied by Figs. 4.26 and 4.27, which show the distortion measurement of the faulty case in comparison with the 6-phase healthy case.
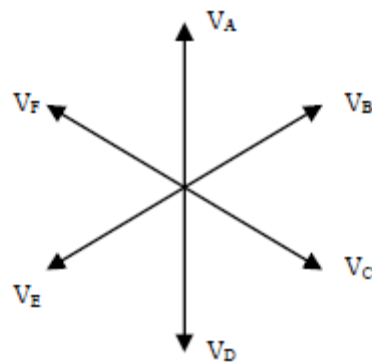

Fig. 4.20 Phasor representation of the voltages in the healthy six-phase case

Fig. 4.21 Phasor representation of the voltages for the faulty case with loss of phases A and B
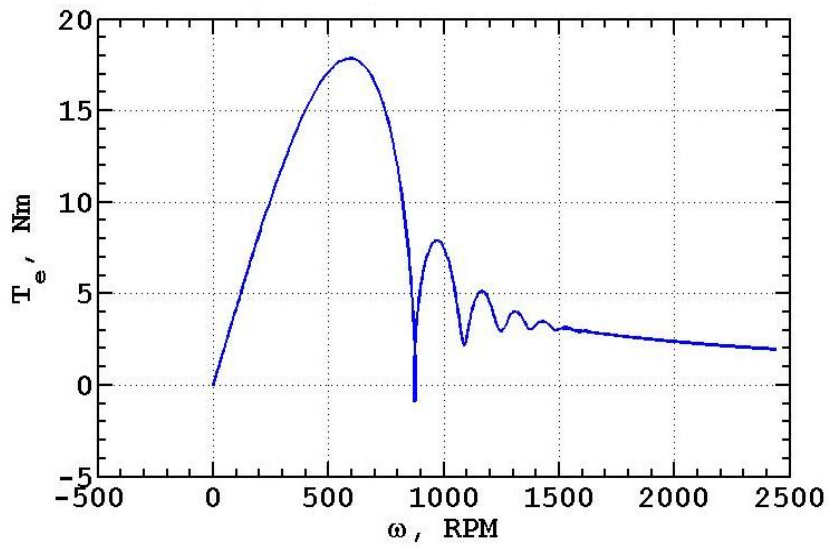
Fig. 4.22 Torque versus speed characteristics of healthy six-phase operation
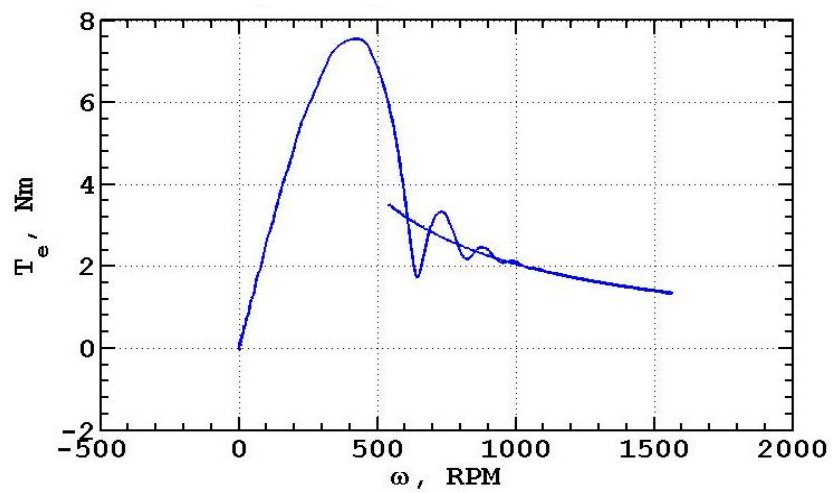
Fig. 4.23 Torque versus speed characteristics of four-phase operation with loss of phases A and B
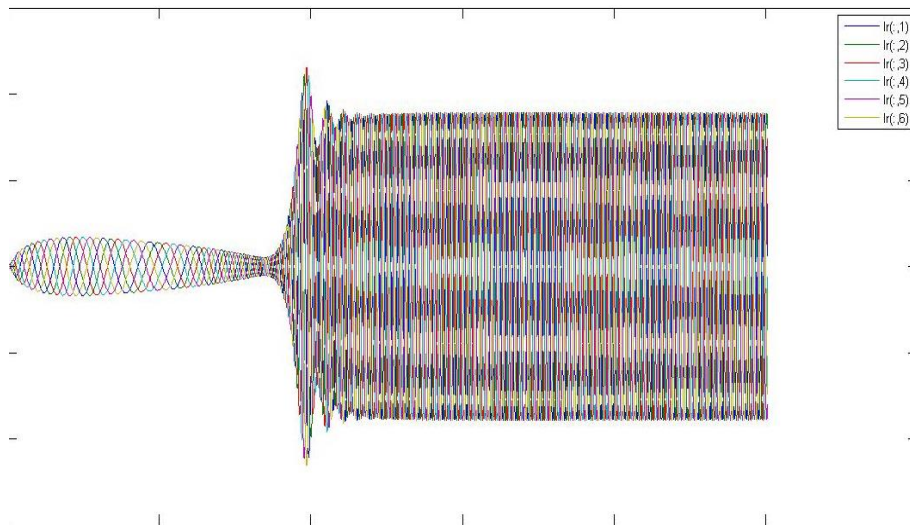
Fig. 4.24 Phase currents of healthy six-phase operation
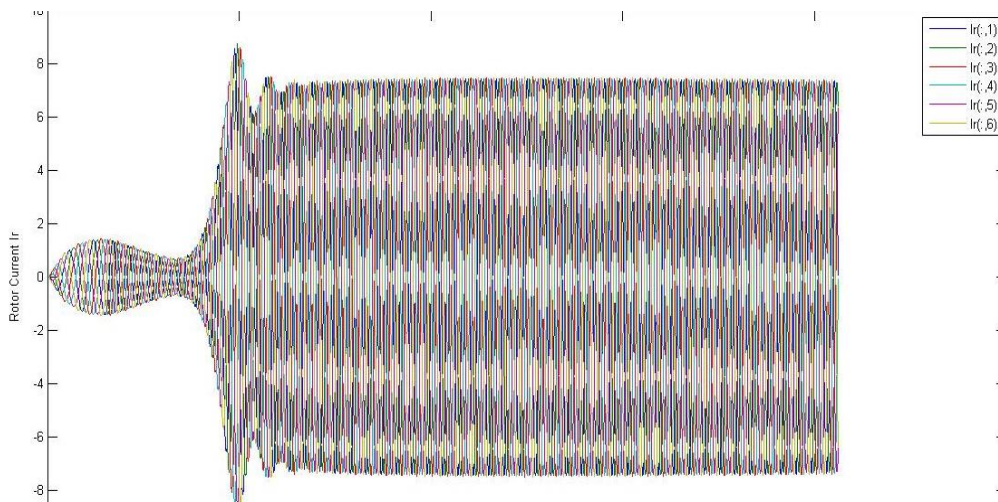
Fig. 4.25 Phase currents of 4 healthy phase operation with loss of phases A and B

Fig. 4.26 Distortion Measurement for healthy six-phase operation
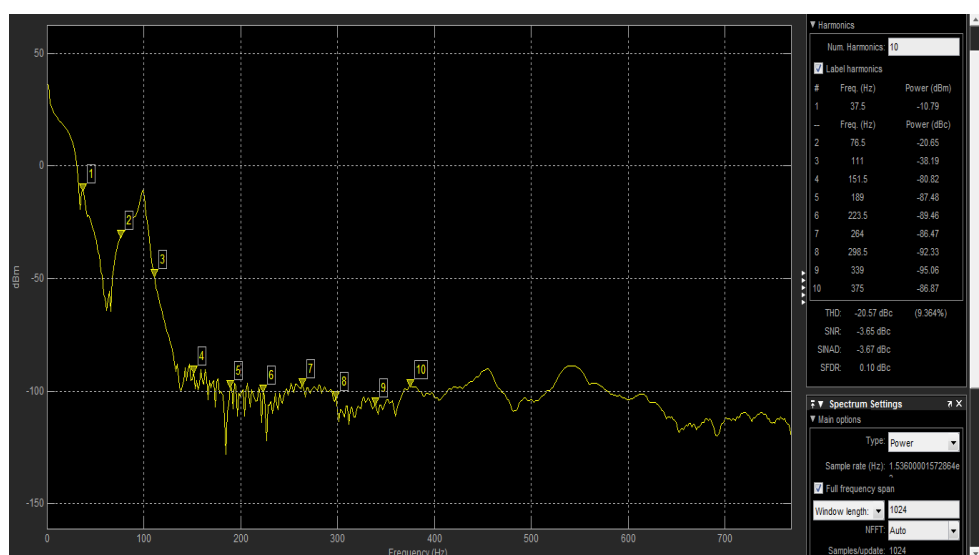
Fig. 4.27 Distortion Measurement for 4 healthy phase condition with loss of phase A and B

Analysis of Fig 4.27 shows the THD content in the torque is -20.57dBm with the 4 healthy phase operation with loss of phases A and B, in comparison with -56.86dBm THD in the healthy six-phase case. Also there is a slight reduction of the fundamental frequency from 48Hz to 37.5Hz

Loss of Two Non-Adjacent Phases

The six-phase motor is first simulated under loss of two non-adjacent phases (phase A and phase C) separated by 120^0e. Figs. 4.28 and 4.29 display the phasor voltages diagram in the six-phase healthy case and the faulty case (with loss of phase A and phase C). The corresponding torque-speed characteristics are compared in Figs. 4.30 and 4.31, respectively. These figures are accompanied by Figs. 4.32 and 4.33, which

show the distortion measurement of the faulty case in comparison with the 6-phase healthy case.
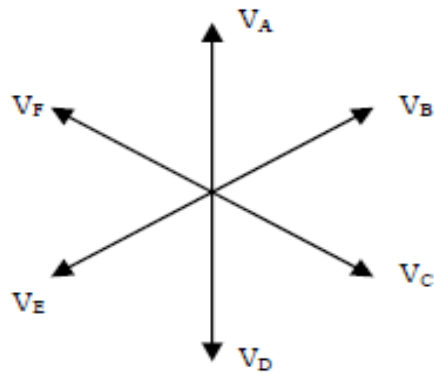
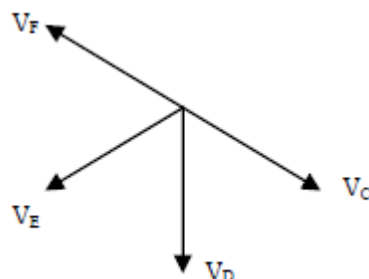**Fig. 4.28** Phasor representation of the voltages in healthy six-phase operation
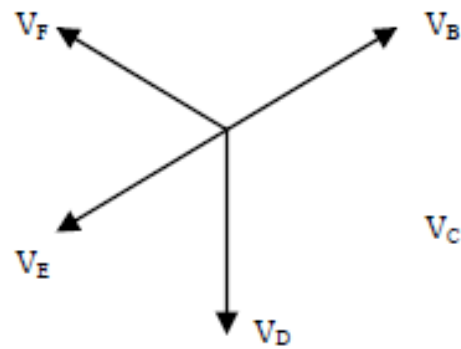
Fig. 4.29 Six-phase motor simulated under faulty case with loss of two non-adjacent phases (A and C) separated by 120^0 *e*

Fig. 4.30 Torque versus speed characteristics of healthy six-phase operation

Fig. 4.31 Torque versus speed characteristics of four-phase operation with loss of phases A and C

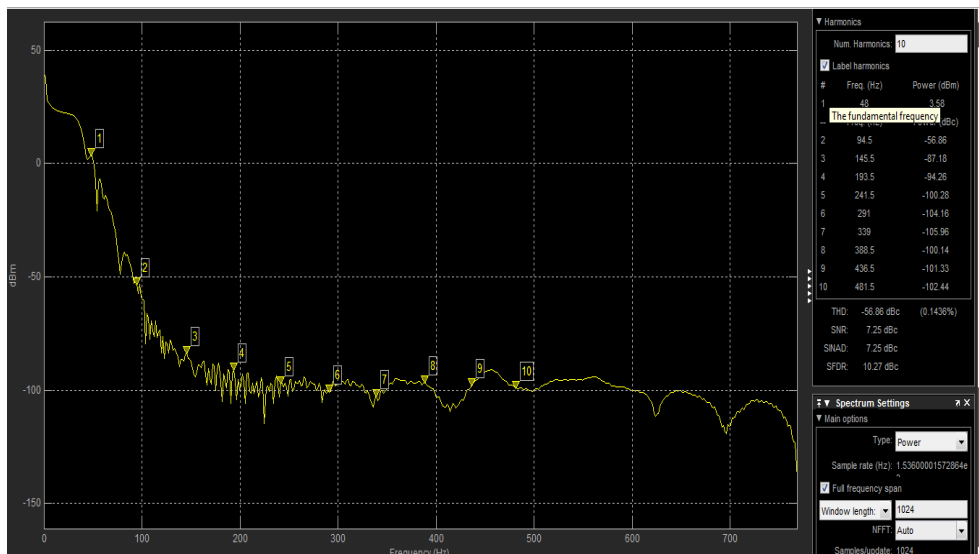**Fig. 4.32** Distortion measurement for healthy six-phase operation

Fig. 4.33 Distortion Measurement for four-phase operation with loss of phases A and C

   From the analysis of Fig 4.33, the THD content in the torque is -20.57 dBm with the 4- healthy phases and loss of Phase A & C, in comparison with -56.86dBm THD in the healthy six-phase case. Also, there is a slight reduction of the fundamental frequency from 48Hz to 37.5Hz.

   The six-phase motor is simulated in the other scenario under the loss of two non-adjacent phases (phase A and phase D) separated by 180^0 *e*. Fig. 4.34 illustrates the phasor voltage representation of the six-phase healthy case while Fig. 4.35 show the faulty case (with loss of phase A and phase D). The corresponding torque-speed characteristics of the health and faulty scenarios are shown in Figs. 4.36 and 4.37, respectively.
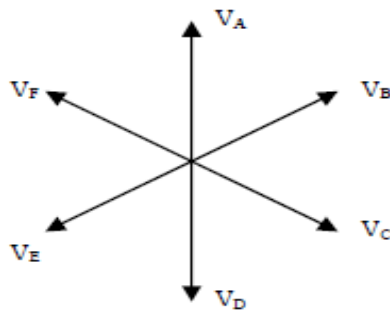
Fig. 4.34 Phasor representation of the voltages in healthy six-phase operation
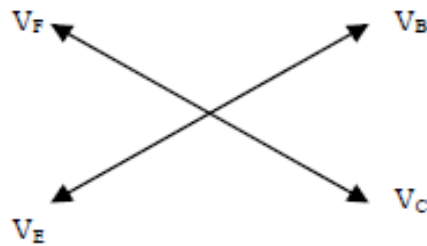
Fig. 4.35 Phasor representation of the voltages in the faulty case with two non-adjacent faulty phases (A and D) separated by 180^0 *e*.
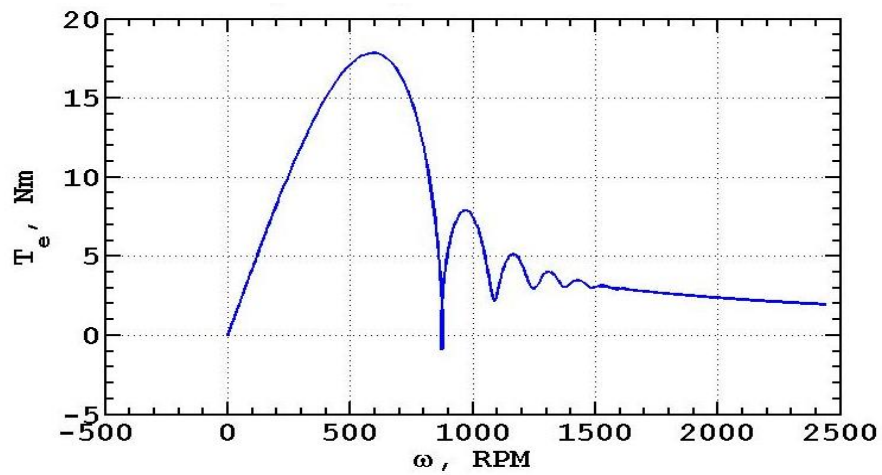

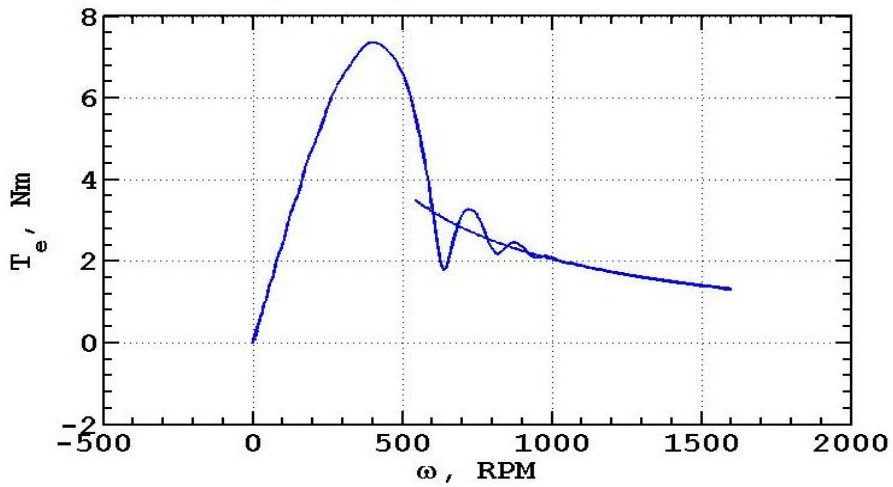**Fig. 4.36** Torque versus speed characteristics of healthy six-phase operation

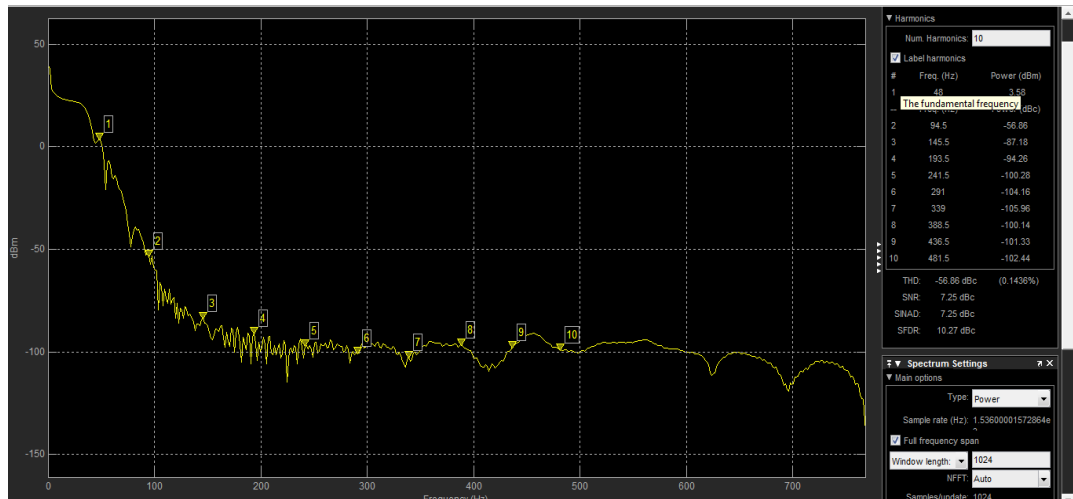**Fig. 4.37** Torque versus speed characteristics of four-phase operation with loss of phases A and D
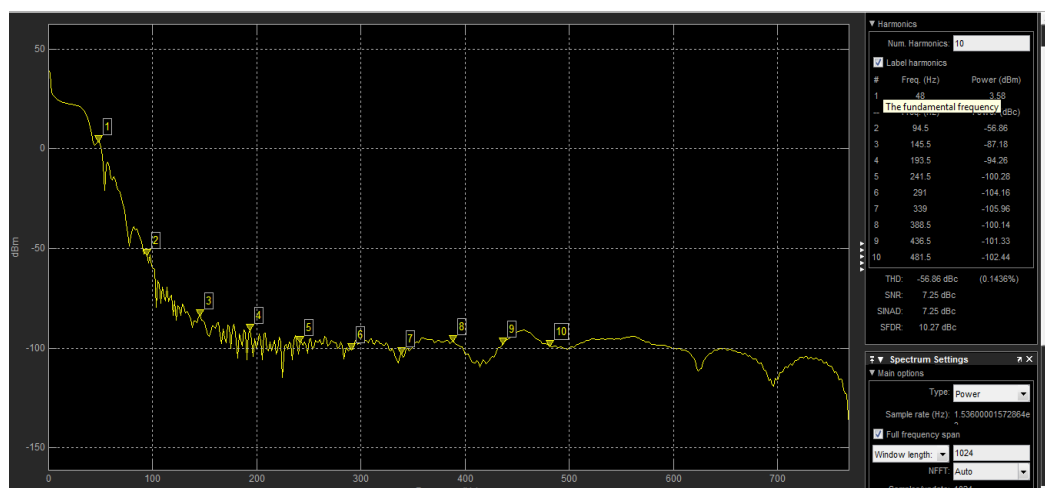
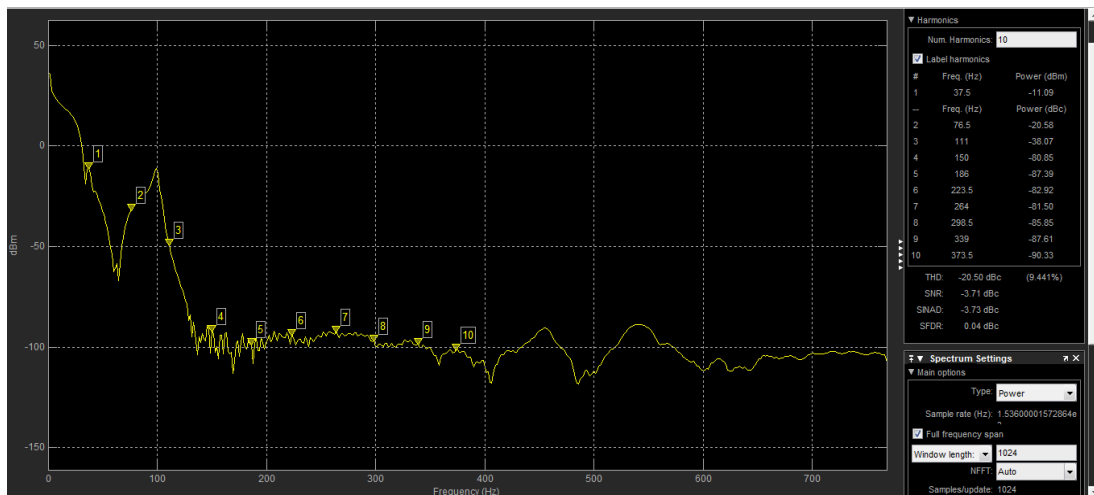**Fig. 4.38** Distortion measurement for healthy six-phase operation

Fig. 4.39 Distortion Measurement for four-phase operation with loss of phases A and D

From the analysis of Fig 4.39, the THD content in the torque is -86.87 dBm with the 4-healthy phases and loss of phases A and D, in comparison with -56.86dBm THD in the healthy six-phase case. Also, there is a great increase in the fundamental frequency from 48Hz to 99Hz. It was observed that there is a clear difference between the two non-adjacent faulty phase cases between the 120^0e separation and the 180^0 e separation cases in so far as the adverse effect on the harmonic distortion in the time-domain of the torque-speed characteristics. The 120^0e separation is far less severe.

4.2.3. Operation of Three-Faulty Phase and Three-Healthy Phase

Fig. 4.40 depicts the phase-loss situations of the three faulty phase and three-healthy phase operations investigated.
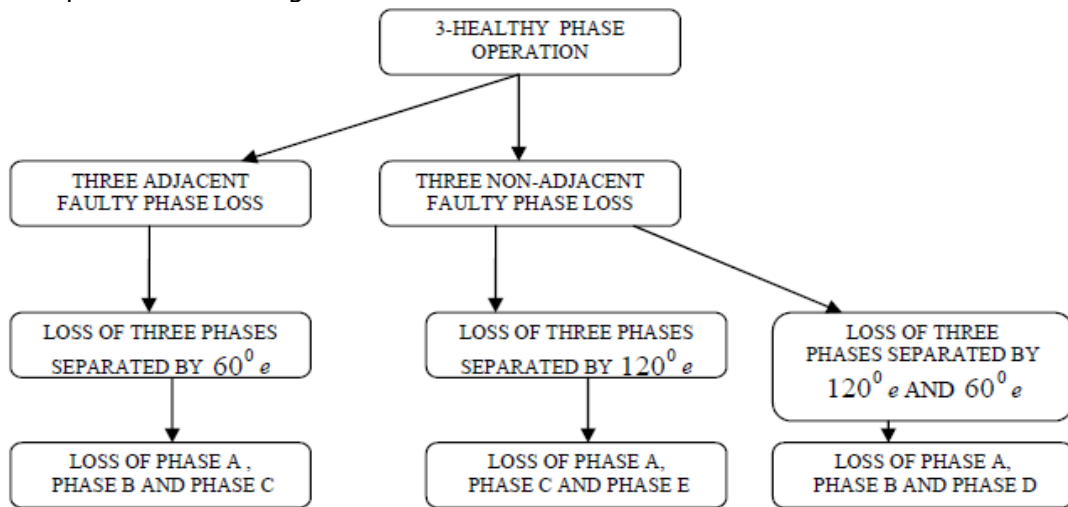
Fig. 4.40 Illustration the different cases of 3-phase operations investigated

Loss of Three Adjacent Phases

The six-phase motor, in this case, is simulated under loss of three phases (A, B and C) adjacent to each when they become faulty and are removed from operation. The six-phase and the loss of three phases (A, B and C) operation phasor is shown in Fig. 4.41 and Fig. 4.42, respectively.
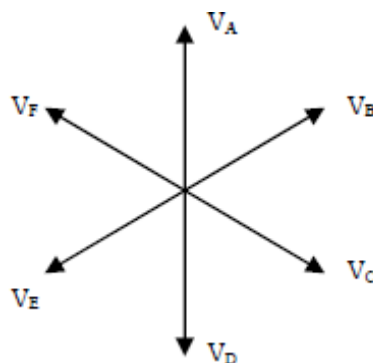
Fig. 4.41 Phasor representation of the voltages in healthy six phase operation
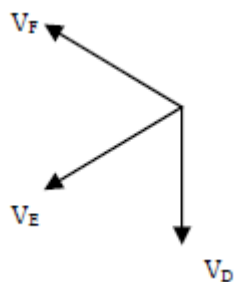
Fig. 4.42 Three-healthy phase and three adjacent faulty phases (A, B and C) loss
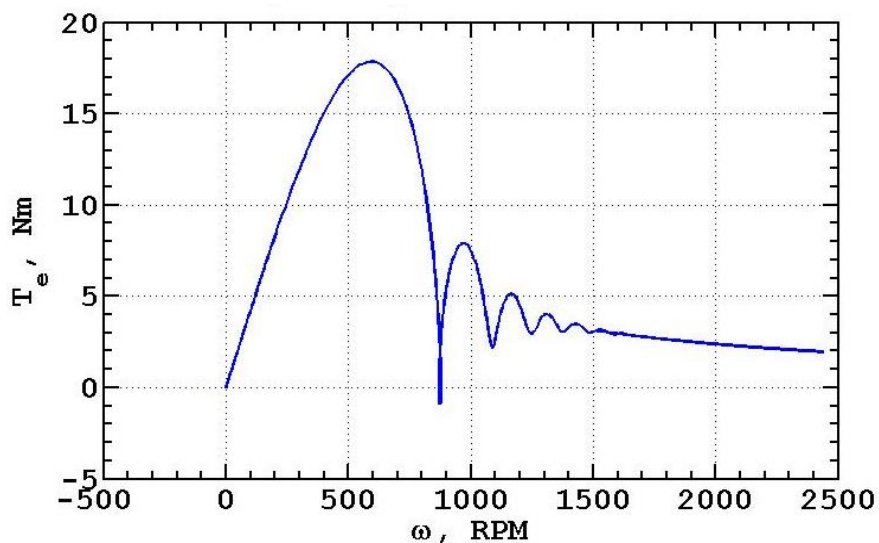
Fig. 4.43 Torque versus speed characteristics of healthy six-phase operation
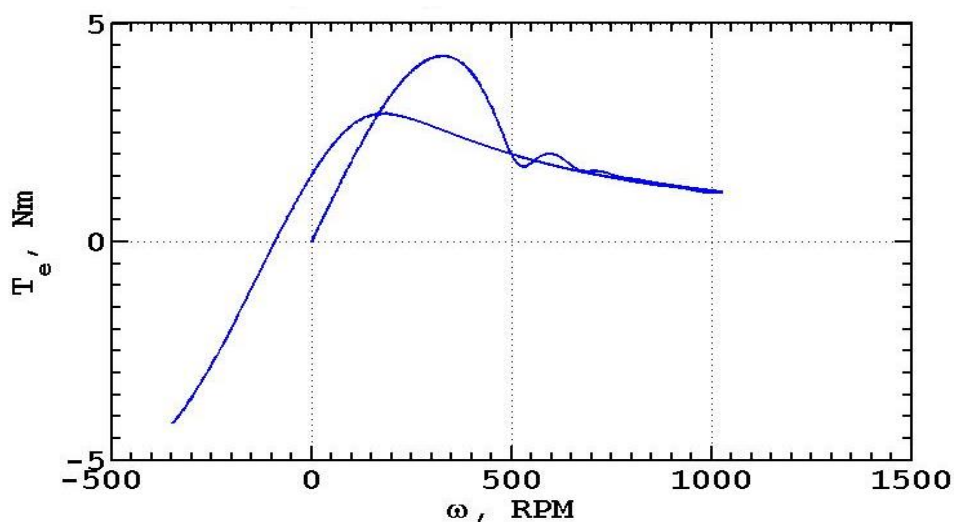
Fig. 4.44 Torque versus speed characteristics of three adjacent faulty phases (A, B and C) loss scenario
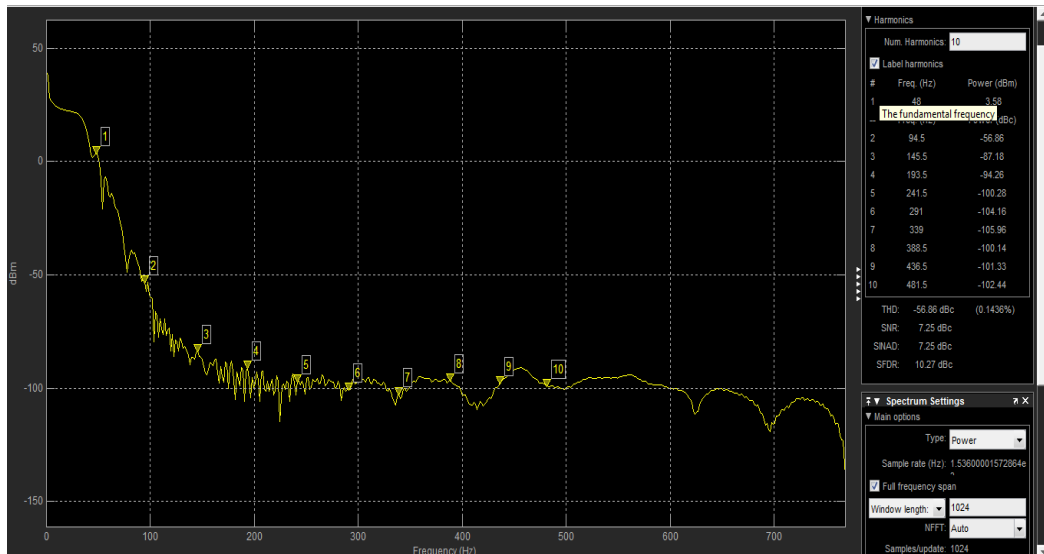
Fig. 4.45 Distortion measurement for healthy six-phase operation.
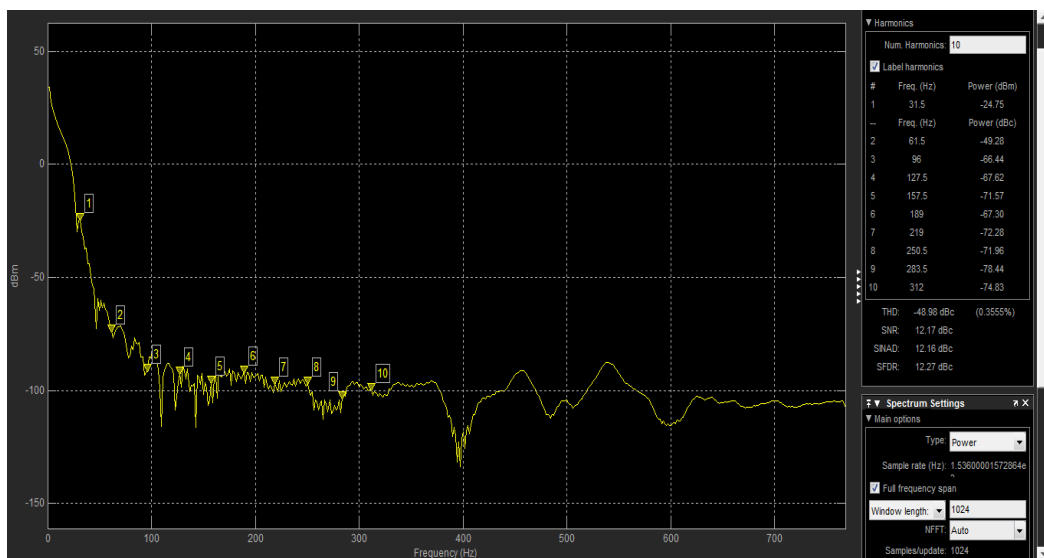
Fig. 4.46 Distortion measurement for three adjacent faulty phases (A, B and C) loss

From assessment of Fig 4.46, the THD content in the torque is -48.98dBm with the 3-healthy phases and loss of phases A, B and C, in comparison with -56.86dBm THD in the healthy six-phase case. Also, there was a reduction in the fundamental frequency from 48Hz to 31.5Hz.

Loss of Three Non-Adjacent Phases

The six-phase motor simulated, in the first case, is considered under loss of three non-adjacent phases (A, C and E) each separated by $120^0 e$. Figs. 4.47 and 4.48 illustrate the phasor voltage representation of the six-phase healthy case and three non-adjacent faulty phases (A, C and E) separated by $120^0 e$, respectively. Figs. 4.49 and 4.50 show their corresponding torque speed characteristics. Fig. 4.51 shows the distortion measurement of the six-phase healthy case in comparison to the faulty case shown in Fig. 4.52.
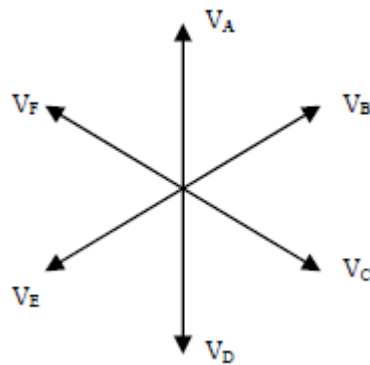
Fig. 4.47 Phasor representation of the voltages in six phase operation
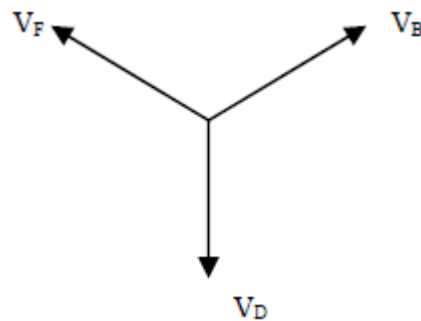
Fig. 4.48 Phasor representation of the voltages in faulty condition with three non-adjacent phases (A, C and E) loss operation separated by120^0e
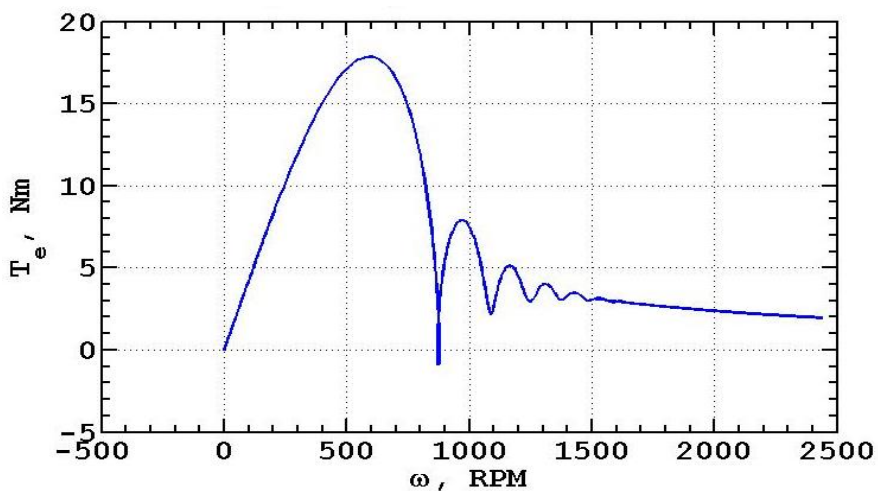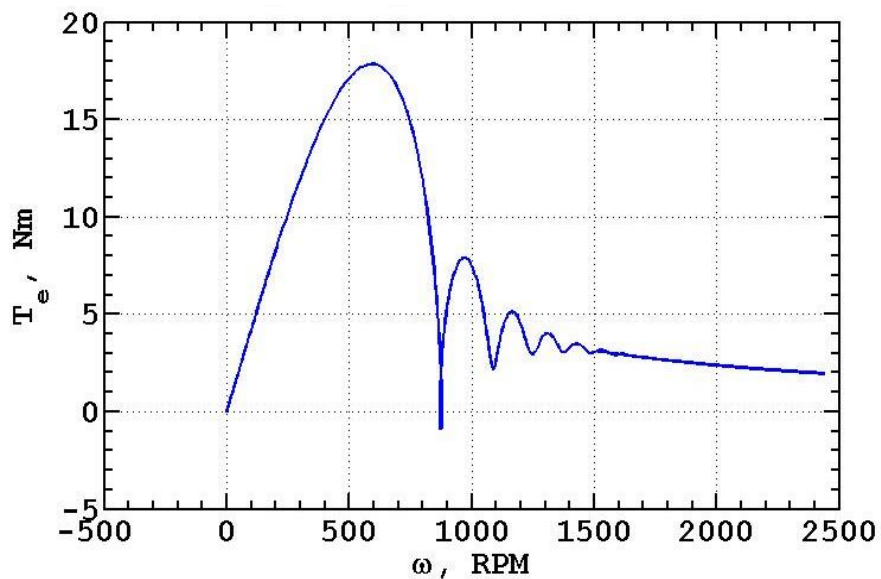

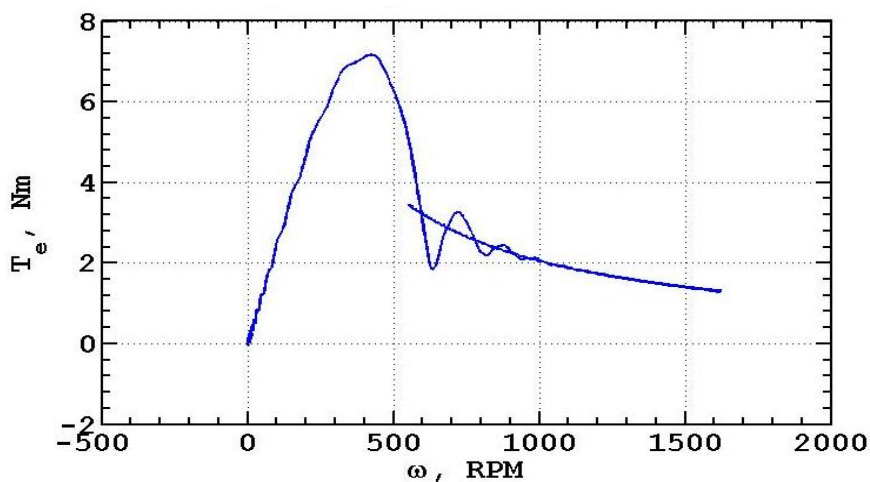**Fig. 4.49** Torque versus speed characteristics of healthy six-phase operation
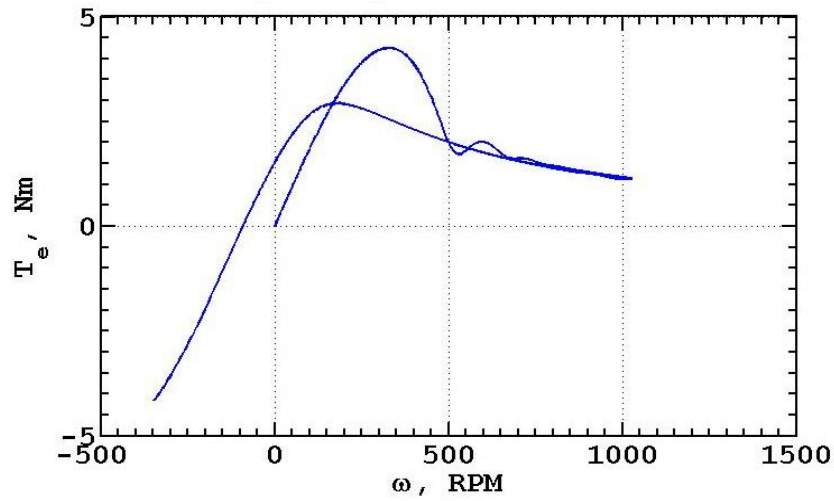
**Fig. 4.50** Torque versus speed characteristics of three-phase operation with the loss of phases A, C and E
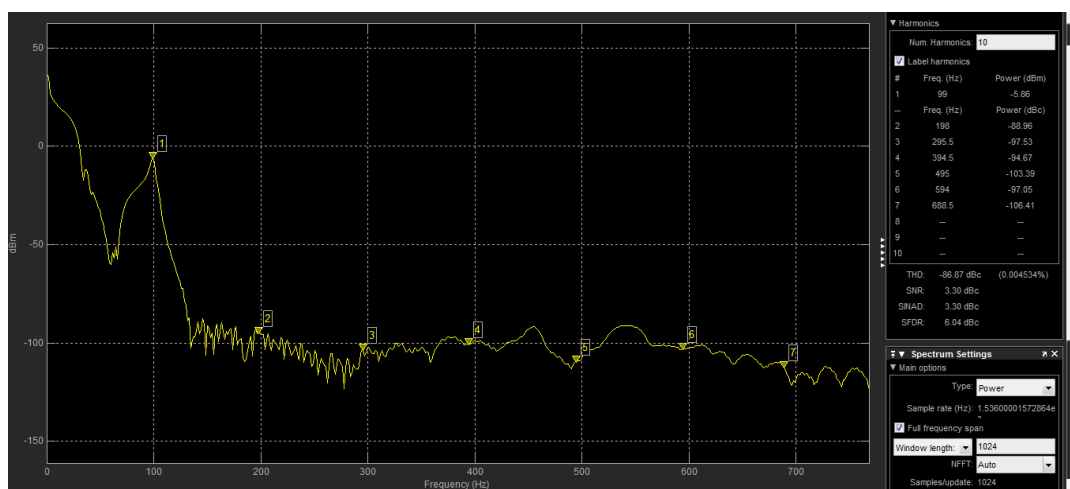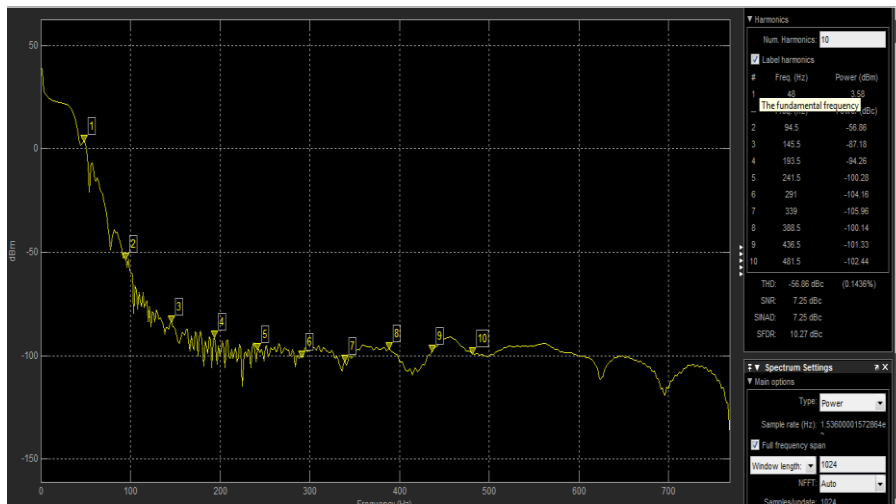

Fig. 4.51 Distortion measurement for healthy six-phase operation
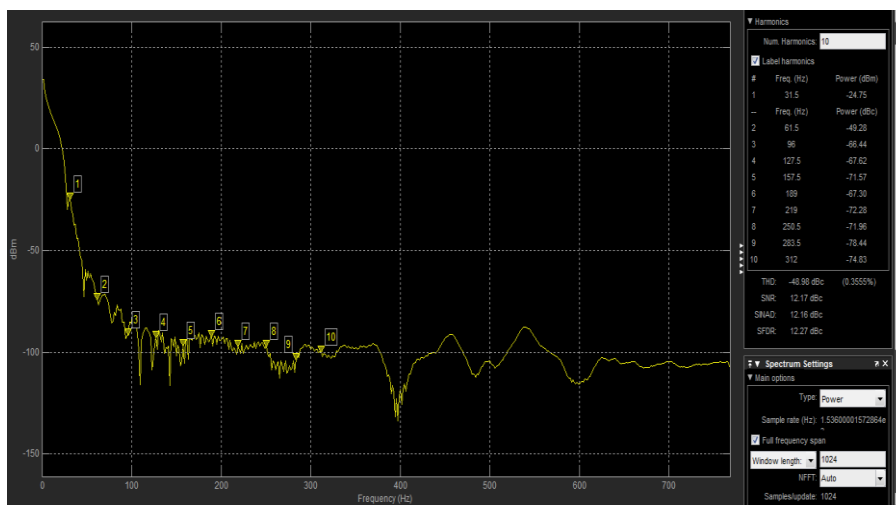
Fig. 4.52 Distortion Measurement for three-phase operation with loss of phases A, C and E

From the analysis of Fig 4.52, the THD content in the torque is -48dBm with the faulty case operation with loss of phases A, C & E, in comparison with -56.86dBm THD in the healthy six-phase case. Also, there was a reduction in the fundamental frequency from 48Hz to 31.5Hz. Figs. 4.53 and 4.54 are the phasor voltage representation in the six-phase healthy case and the three-phase healthy case with three non-adjacent faulty phases (A, B and D) separated by 60^0 e and 120^0 e. In Figs. 4.55 and 4.56, the torque-speed characteristics of the three-phase healthy case with three non-adjacent faulty phases separated by 60^0 e and 120^0 e should be compared with the 6-phase healthy case. Figs. 4.57 and 4.58 show the distortion measurement of the six-phase healthy case and the faulty case, respectively.
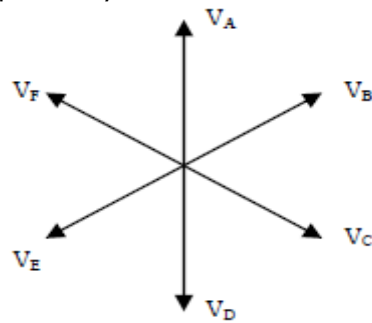
Fig. 4.53 Phasor representation of the voltages in six-phase healthy operation
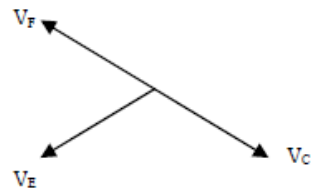
**Fig. 4.54** Phasor representation of the voltages in faulty condition with three non-adjacent phases (A, B and D) loss
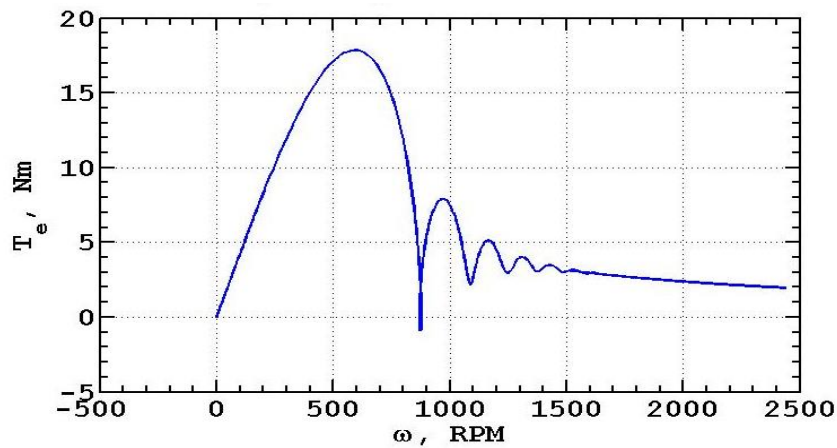
Fig. 4.55 Torque versus speed characteristics of healthy six-phase operation
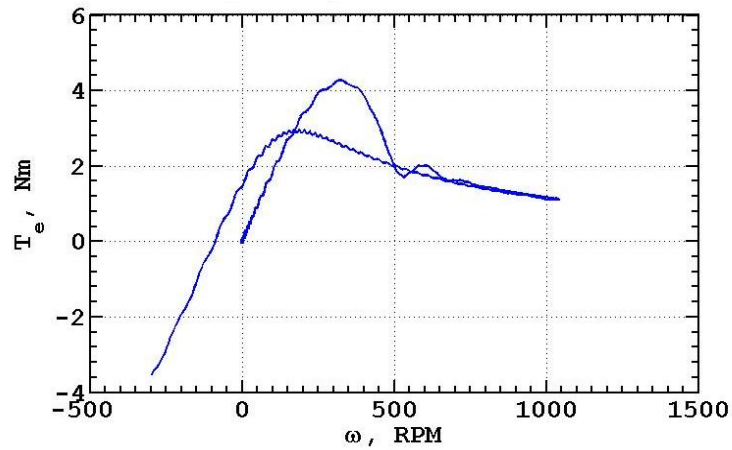
Fig. 4.56 Torque versus speed characteristics of three-phase operation with loss of three phases (A, B and D)
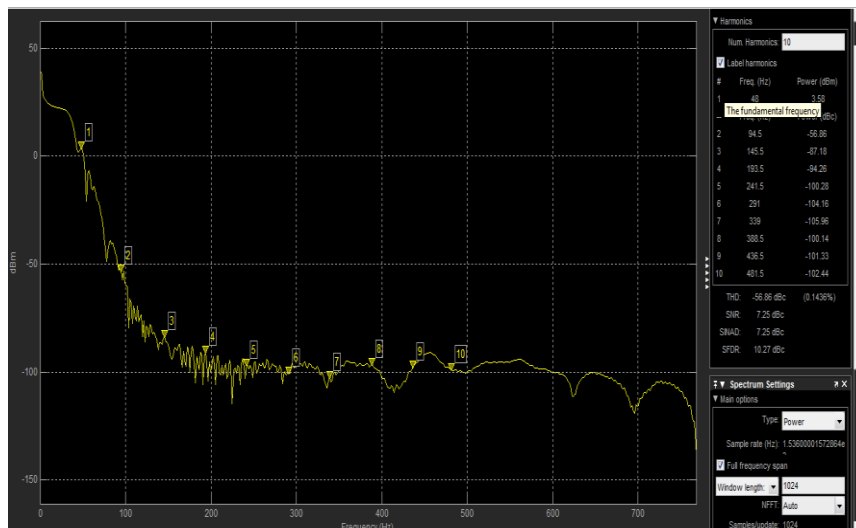
Fig. 4.57 Distortion measurement for healthy six-phase operation
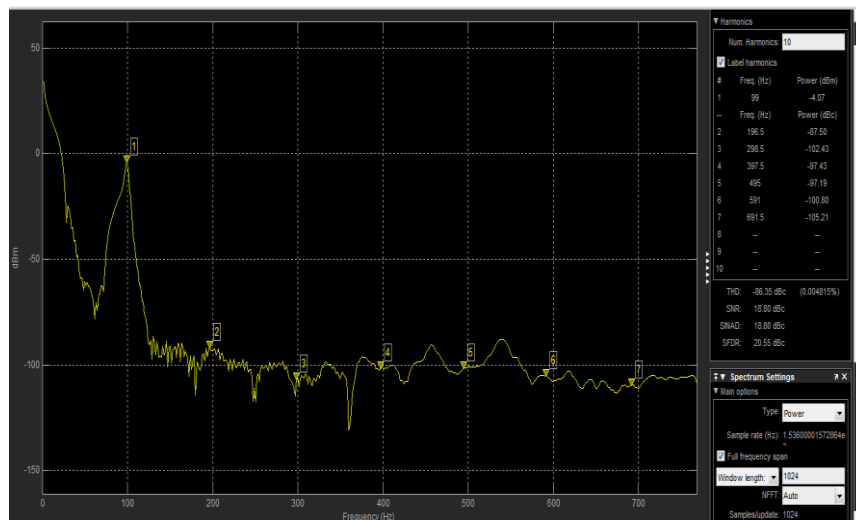
Fig. 4.58 Distortion measurement for three-phase operation with loss of three phases (A, B and D)

From the analysis of Fig 4.58, the total harmonic distortion (THD) content in the resultant torque is -86.35dBm in the operation with loss of phases A, B and D, in comparison with -56.86dBm THD in the six-phase healthy case. Also, there is a great increase in the fundamental frequency from 48Hz to 99Hz.

CHAPTER FIVE
CONCLUSION AND RECOMMENDATIONS

5.1   Conclusion

An exclusive and practical design of a SPIM has been developed in this study. The overall objective was to initiate multiple phases with the aim of enhancing the reliability of the motor under phase(s) loss due to peripheral fault conditions. The design method adopted was to retain the same core or structure of the initial three-phase.

The six-phase motor was simulated using MATLAB/Simulink where the effects of several scenarios of phase-loss on the torque of the motor were investigated. In addition, a comparative assessment of the different phase-loss scenarios with respect to the healthy state was reported and discussed.

Although, the performance of some of the faulty cases were very close to the healthy operations, in general, the best performance of the six-phase motor was observed under the six-phase healthy condition. The result indicated that in most cases the machine can generate the starting torque. Nevertheless, the torque produced when the machine is in healthy operation is more and with fewer oscillations compared to the open-circuit or faulty case of the stator phase.

5.2   Remarkable Achievements

The innovative and remarkable achievements of the designed and developed SPIM are summarized as:
1. There is no decisive factor for sustaining $30°$ phase shift.
2. The continuity of operation is sustained with enhanced reliability; even if one of the inverter fails, the motor continues to operate (but with reduced rating).
3. Harmonic reduction because all harmonics of order $(6n + 1)$, where $n = 1, 3, 5, 7, …$ get canceled because of 30 degrees phase displacement. Reduced torque pulsations because of harmonic reduction.
4. Increased efficiency (with losses reduction) since there is no circulating current due to harmonic reduction.
5. A comparison assessment of the different phase-loss scenarios with respect to the healthy state described.
6. A summary of distortion analysis of the torque under different phase-loss scenarios presented as shown in Table 5.1.

The practical precautions taken during the development of the six-phase motor are as follows;
1. Overheating was experienced even at no load so the applied voltage was kept at the range of 50 volts to 120 volts to avoid burn out of coils.
2. Vibrations due to high voltage supplied was avoided.
3. Due to complication of the windings proper insulation was done to avoid body earth.

Table 5.1 A summary of type of faults scenarios analysis

Types of Fault	Frequency (Hz)	THD (dBm)	HD of 2nd Order (dBm)	HD of 1st Order (dBm)
6 healthy phase	48	-56.86	-56.86	3.58
5 healthy 1 faulty	42	-21.98	-21.98	-2.83
4 healthy + A & B faulty	37.5	-20.57	-20.65	-10.79
4 healthy + A & C faulty	37.5	-20.50	-20.58	-11.09
4 healthy + A & D faulty	99	-86.87	-88.96	-5.86
3 healthy + A, B & C faulty	31.5	-48.98	-49.28	-24.75
3 healthy + A, C & E faulty	31.5	-48.98	-49.28	-24.75
3 healthy + A, B & D faulty	99	-86.35	-87.50	-4.07

HD: Harmonic Distortion

5.3   Limitations of the Study

For higher rated power applications, the size of the motor and inverter becomes very large, and this could increase the total design cost.

5.4   Recommendations for Future Work

The exploration of different winding designs for a 48 slot induction motor for enhanced performance should be explored in order to expand the overall performance with the least amount of harmonic distortion in the steady state torque.

The de-rating of machine under defective conditions should be considered for possible overheating that can damage the motor windings.

Also, the scope of this study can be extended considering multiple of 3-phase (e.g., 9-phase, 12-phase, and 15-phase etc.) motor as per the requirement of torque.

Conflict of Interests

The authors declare that there is no conflict of interests regarding the publication of this paper.

REFERENCES

Aher, K. S., and Thosar, A. G. (2016). Modeling and Simulation of Five Phase Induction Motor using MATLAB/Simulink" Int. Journal of Engineering Research and Applications, 6(5: part 7): 1-8

Amayo, E. B. (2015). Multi objective multi algorithm optimal design of an m-phase induction motor, A Ph.D. Seminar Presented to the Department of Electrical Electronic, University of Benin, Benin City, Nigeria.

Benoît, R., Francois, B., Degobert, P., & Hautier, J. P. (2012). Dynamic modeling of induction machines, Vector Control of Induction Machines, 35-74.

Bojoi I. R., Tenconi, A., Griva, G., & Profumo, F. (2005). Vector control of dual-three phase induction motor drives using two current sensors, IEEE Industry Application Society Conference, Hong Kong, China, 2nd -6th October, 1805-1812.

Dakoju, S. (2016). Dynamic modeling of six phase induction motor, MATLAB Central File Exchange. Retrieved from https://www.mathworks.com/matlabcentral/fileexchange/55654-dynamic-modeling-of-six-phase-induction-motor, (August 1, 2016).

Dejan, D. R., Ostojic, D. B., & Vasic, V. V. (2006). Simple speed sensor less control of induction motor drive, Sixth International Symposium Nikola Tesla, Belgrade, Serbia, 18th – 20th, October, 2006.

Gregor, R., Barrero, F., Toral, S., & Durán, M. J. (2008). Realization of an asynchronous six-phase induction motor drive test-rig, International Conference on Renewable Energies and Power Quality, 12 – 14 March, Santander, Spain.

Hadiouche, D., Razik, H., and Rezzoug, A. (2000). Modeling of a double-star induction motor with an arbitrary shift angle between its three phase windings. Proceedings of 9th International Conference on Power Electronics and Motion Control PEMC, Kosice, Slovakia, pp. 5.125–5.130

Hamdani, S., Touhami, O., & Ibtiouen, R. (2008). a generalized two axes model of a squirrel-cage induction motor for rotor fault diagnosis, Serbian Journal of Electrical Engineering, 5(1): 155-170.

Jimoh, A. A., Appiah, E. K., & Ogunjuyigbe, A. S. O. (2014). Modeling and analysis of higher phase order (hpo) squirrel cage induction machine, Matlab applications for the practical engineer, Kelly Bennett, IntechOpen, doi: 10.5772/57468

Jones, M., Vukosavic, S. N., Emil Levi, E., & Iqbal, A. (2005). A six phase series connected two motor drive with decoupled dynamic control, IEEE Transactions on Industry Applications, 41(4):1056-1066.

Kadaba, A. A. (2008). Design and modeling of a reversible 3-phase to 6-phase induction motor for improved survivability under faulty conditions, M.Sc. thesis, Marquette University, Milwaukee, United States.

Kadaba, A., Suo, S., Sizov, G. Y., Yeh, C., Sayed-Ahmed, A., & Demerdash, N. A. O. (2011). Design and modeling of a reversible 3-phase to 6-phase induction motor for improved survivability, 2011 IEEE Power and Energy Society General Meeting, Detroit, MI, USA, pp. 1-5, doi: 10.1109/PES.2011.6039812.

Kaneyuki, K., & Koyama, M. (1997). Motor-drive control technology for electric vehicles, Mitsubishi Electric Advance -Technical Report.

Karady, G. G., and Holbert, K. E. (2013). Induction Machines, in Electrical Energy Conversion and Transport: an Interactive Computer-Based Approach, second edition, John Wiley & Sons, Inc pp. 541-615.

Krishna, K., Mahopatra, Kanchan, R. S., Baiju, M. R., Tekwani, P. N., & Gopakumar, K. (2005). Independent field oriented control of two split phase induction motors from a single six phase inverter, IEEE Transaction on Industrial Electronics, 52(5):1372-1382.

Levi, E. (2006). Recent developments in high performance variable-speed multiphase induction motor drives, Sixth International Symposium Nikola Tesla, Belgrade, Serbia. 18th – 20th October,

Levi, E., Bojoi, R., Profumo, F., Toliyat, H. A., & Williamson, S. (2007). Multiphase induction motor drives – a technology status review," IET Electr. Power Appl., 1(4): 489–516.

Lipo, T. A. (1980). A d–q model for six-phase induction machine, in: proceedings on International Conference, Electric Machines, Athens, Greece, pp. 860–867.

Lyra, R. O. C., & Lipo, T. A. (2002). Torque density improvement in a six-phase induction motor with third harmonic current injection, IEEE Transactions on Industry Applications, 38(5): 1351-1360.

Mandal, S. (2015). Performance analysis of six-phase induction motor, International Journal of Engineering Research and Technology, 4(2):589-593.

Markadeh, G. R. A., Soltani, J., Abjadi, N. R., & Hajian, M. (2009). Sensor less control of a six-phase induction motors drive using foc in stator flux reference frame, World Academy of Science, Engineering and Technology, 58, 890–896.

Miranda, R. S., & Gomes, E. C. (2012). Analysis and modeling of six-phase induction motor under open phase fault condition, Electrical and Electronics Department, Federal Institute of Education, Science and Technology - IFMA São Luis, Maranhão, Brasil

Mohapatra, K. K., Gopakumar, K., Somasekhar, V. T., and   Umanand, L. (2002). A novel scheme for six phase induction motor with open end windings. In p28th Annual Conference of IEEE Industrial Electronics Society, Spain, 5th - 8th November, 2002

Nanoty, A., & Chudasama, A. R. (2012). Control of designed developed six phase induction motor, International Journal of Electromagnetics and Applications, 2(5): 77-84

Nelson, R. H., & Krause, P. C. (1974). Induction machine analysis for arbitrary displacement between multiple winding sets, IEEE Transaction on power Apparatus and Systems, 93, 841–848.

Nelson, R. H., Lipo, T. A. & Krause, P. C. (1969). Stability analysis of a symmetrical induction machine" IEEE Transactions on Power Apparatus and Systems, Vol. 88, No. 1, 1969.

Okundamiya, M. S. (2015). Modelling and optimization of a hybrid energy system for GSM base transceiver station sites in emerging cities, Ph.D. Thesis, University of Benin, Benin City, Nigeria.

Perng, S-S., Lai, Y-S., & Liu, C-H. (1998). Sensorless vector controller for induction motor drives with parameter identification, Proceedings of the 24th Annual conference of the IEEE Industrial Electronics Society, August 31 –September 4, Aachen, Germany. pp. 1008–1013.

Romeral, L. (2002). Motion control for electric drives, XVI Journal of Conference in Electronics Engineering, November, Terrasa, Spain, 26-30.

Sawhney, A. K. (2001). Electrical Machine Design, Dhanpat Rai & Co (P) Ltd, Delhi.

Shah, S., Rashid, A., & Bhatti, M. K. L. (2010). Direct quadrate (d-q) modeling of 3-phase induction motor using matlab/simulink, COMSATS Institute of Information and Technology, Abbottabad, Pakistan.

Shi, K. L., Chan, T. F., Wong, Y. K., & Ho, S. L. (1999). Modeling and simulation of the three phase induction motor using simulink, International Journal of Electrical Engineering Education, 36, 163 - 172.

Singh, G. K. (2002). Multiphase Induction Machine drive research, Electric Power System Research, 61, 139-147.

Singh, G. K., & Lim, S. K. (2005). A simple indirect field-oriented control scheme for multiphase induction machine, IEEE Transactions on Industrial Electronics, 52(4): 1177-1184

Taheri, A. (2013). Efficiency optimization of six-phase induction motors by fuzzy controller, Department of Electrical Engineering, Faculty of Engineering, University of Zanjan, Zanjan, Iran.

Tir, Z., Malik, O. P., & Eltamaly, A. M. (2016). Fuzzy logic based speed control of indirect field oriented controlled double-star induction motors connected in parallel to a single six-phase inverter supply, Electric power system research, 134, 126-133.

Toliyat, H. A. (1996). Analysis and simulation of multi-phase variable speed induction motor drives under asymmetrical connections, *APEC '96*, 3-7 March, 2, 586 -592.

Tuo, C. (2012). Analysis on the Mathematical Model of the Six-Phase Induction Motor of the Electric Vehicle Pages 303-310 in Future intelligent information systems, Dehuai Zheng, D. (ed.), 1, Springer, Berlin, Germany

White, D. C., and Woodson, H. H. (1959), Electrome-chanical energyconversion, John Wiley and Sons, New York, NY.

Yadav, K. B., Mohanty, A. K., & Kumar, P. (2014). Recent research trend on multi-phase induction motor, Department of Electrical Engineering, National Institute of Technology, Jamshedpur, India, 580-586.

Zhao, Y., & Lipo, T. A. (1995). Space vector PWM control of dual three phase induction machine using vector space decomposition", IEEE Trans. IA-31(5): 1100–1109.

Zhao, Y., & Lipo, T. A. (1996). Modeling and control of multi-phase induction machine with structural unbalance, part I, machine modeling and multi-dimensional current regulation, IEEE Trans. Energy Conversion EC-11(3): 570–577.

APPENDIX
Appendix A. A typical generator data as collected

A1: Objective Function Codes

```
========================================================================================
function weight = weight_obj(x)

% M-file for the six-phase induction machine design.
% The objective function minimize the total weight of Iron and Copper
%% FUNCTION M-FILE OF THE OBJECTIVE FUNCTION OF THE SIX-PHASE INDUCTION MACHINE
% DESIGN PROBLEM TO MINIMIZE THE TOTAL WEIGHT OF IRON AND COPPER
%% WRITTEN BY:
% IDUH, Samuel E
% Matriculation No: PG/ENG9200692
% OMUGBE, Silas Evi
% Matriculation No: PG/ENG1410538
% DATE: 7TH JUNE, 2017.

%% The Six-Phase Induction motor to be optimized has the following parameters;
% No of slots: 48
% No of poles: 4
% Output coefficient Co = 118
% Efficiency = 85%
% Power factor = 0.8
% Specific Electric Coefficient = 23,000
% Axial length per pole pitch k = 0.5
% Magnetic Flux Density Bav = 0.45
% R_Cu = 0.0021 Ohm-m
% Rho_Cu = 8900 kg/m3
% Rho_Fe = 7600 kg/m3
% Input power = 5 Hp
% Frequency f = 50 Hertz
% Phase voltage V = 230 volts
% Winding factor Kw for Six-Phase = 1
% Current Density J = 4 A/mm2
%% Declaration of Design Variables:
% Do = x(1);                % Outer diameter (m)
% dsc = x(2);               % Diameter of stator core
% dss = x(3);               % Diameter of stator slot
% wst = x(4);               % weight of stator tooth
% D = x(5);                 % Innner diameter (m)
% drc = x(6);               % Diameter of rotor core (m)
% dsr = x(7);               % Diameter of (m)
% wrt = x(8);               % weight of rotor tooth
% L = x(9);                 % Axial length

%% Design Paramters
m = 6;
rho_fe = 7600;
V = 230;
p = 4;
Ss = 48;
S_r = Ss-p/2;
Bav = 0.45;
f = 50;
rho_cu = 8900;
kw = 1;
J = 4e6;
Vph = 230;
Pin = 3700;
Iph = Pin/Vph;
========================================================================================
```

```
==============================================================================================
a_cu = Iph/J;
Nph = (V*p)/(4.44*f*pi*x(5)*x(9)*Bav*kw);
I_b = (0.85*m*Nph*Iph)/S_r;
A_b = I_b/J;
Ier = (S_r*I_b)/(pi*p);
Aer = Ier/J;
Der = (x(5)+ x(1))/2;
Lmt = (2*x(1) + (2.3*pi*x(5)))/p + 0.24);
L_b = (x(9) + (2*1.5)/100 + 1/100);

%% Objective Function formulation
% Weight of the stator core
Wsc = rho_fe*x(9)*(pi/4)*(x(1)^2 - (x(1) - 2*x(2))^2);

% Weight of the stator tooth
Wst = rho_fe*x(9)*Ss*x(3)*x(4);

% Weight of rotor core
Wrc = rho_fe*x(9)*(pi/4)*(x(5)^2 - (x(5) - 2*x(6))^2);

% Weigth of the rotor tooth
Wrt = rho_fe*x(9)*S_r*x(7)*x(8);

% Weight of bar
Wbar = rho_cu*A_b*L_b;

% Weight of end ring
Wer = rho_cu*2*pi*Der*Aer;

%Weight of stator winding
Wsw = rho_cu*Nph*Lmt*a_cu;

%total weight which makes up the objective function
weight = Wsc + Wst + Wrc + Wrt + Wbar + Wer + Wsw;
end
==============================================================================================
```

A2: Constraints Function Codes

```
==============================================================================================
function [C, Ceq] = weight_nonlcon(x)

% The non-linear constraint function for six-phase induction motor design
%% Nonlinear inequality constraint:

C = (0.0002 + (0.002*sqrt(x(5)*x(9))) - 0.008);

% Nonlinear equality constraint:
Ceq = [];
end
==============================================================================================
```

A3: Optimization Function Codes

```
==============================================================================================
% M-file to solve the nonlinear constrained optimization of six
% phase induction motor design
%% WRITTEN BY:
% IDUH, Samuel E
% Matriculation No: PG/ENG9200692
% OMUGBE, Silas Evi
% Matriculation No: PG/ENG1410538
==============================================================================================
```

```matlab
========================================================================================
% DATE: 7TH JUNE, 2017.
%%
clc
clear
format shortG

%% number of design variables
nvars = 9;
lb = [0.18 0.028 0.016 0.0045 0.12 0.016  0.028 0.0035 0.14];   % the lower bound for the problem.
ub = [0.22 0.032 0.019 0.0065 0.15 0.0185 0.032 0.005  0.19];    % the upper bound for the problem.

%% Matrix of linear equality constraints (Assuming that Do + 2*dsc + 2*dss = D):
Aeq = [1 -2 -2 0 -1 0 0 0 0;                      % Do - D - 2*dsc - 2*dss = 0
       0 0 0 0 0 0 0 0 0;
       0 0 0 0 0 0 0 0 0;
       0 0 0 0 0 0 0 0 0;
       0 0 0 0 0 0 0 0 0;
       0 0 0 0 0 0 0 0 0;
       0 0 0 0 0 0 0 0 0;
       0 0 0 0 0 0 0 0 0;
       0 0 0 0 0 0 0 0 0];
 Beq = [0;0;0;0;0;0;0;0;0];

%% Display plotting functions while ga minimizes
options = gaoptimset('PlotFcns',...
        {@gaplotbestf,@gaplotbestindiv,@gaplotexpectation,@gaplotstopping});

%% solution of the optimization problem using genetic algorithm
[x,weight,exitflag,output] = ga(@weight_obj,nvars,[],[],Aeq,Beq,lb,ub,@weight_nonlcon);

%% Table of optimal results
X = [num2str(x(1)),' ', num2str(x(2)), ' ', num2str(x(3)),' ', num2str(x(4)),' ',
num2str(x(5)),' ', num2str(x(6)),' ', num2str(x(7)),' ',...
    num2str(x(8)),' ', num2str(x(9)),' ', num2str(weight)];
disp(X)
========================================================================================
```